

Loop corrections in the separate universe picture

Laura Iacconi,^{1,2} David Mulryne,¹ David Seery³

¹Astronomy Unit, Queen Mary University of London,
Mile End Road, London, E1 4NS, UK

²Institute of Cosmology and Gravitation, University of Portsmouth,
Burnaby Road, Portsmouth, PO1 3FX, UK

³Astronomy Centre, University of Sussex,
Falmer, Brighton, BN1 9QH, UK

E-mail: l.iacconi@qmul.ac.uk, d.mulryne@qmul.ac.uk, D.Seery@sussex.ac.uk

Abstract. In inflationary models that produce a spike of power on short scales, back-reaction of small-scale substructure onto large-scale modes is enhanced. Loop corrections that quantify this back-reaction have been evaluated by a number of authors. We argue that the separate universe framework provides a highly convenient tool for such computations. Each loop of interest is characterized by large hierarchies in wavenumber and horizon exit time. The separate universe framework highlights important factorizations involving these hierarchies. We interpret each loop correction in terms of a simple, classical, back-reaction model, and clarify the meaning of the different volume scalings that have been reported in the literature. We argue that significant back-reaction requires *both* short-scale nonlinearities and long-short couplings that modulate the short-scale power spectrum. In the absence of long-short couplings, only incoherent “shot noise”-like effects are present, which are volume-suppressed. Dropping the shot noise, back-reaction from a particular scale is controlled by a product of f_{NL} -like parameters: an equilateral configuration measuring the nonlinearity of the short-scale modes, and a squeezed configuration measuring the long-short coupling. These may carry important scale dependence controlling the behaviour of the loop in the decoupling limit where the hierarchy of scales becomes large. In single-field models the long-short coupling may be controlled by this hierarchy, in which case the net back-reaction would be safely suppressed. We illustrate our framework using explicit computations in a 3-phase ultra-slow-roll scenario. Our analysis differs from earlier treatments of this model, which did not consistently include the effect of small-scale modes. Finally, we discuss different choices for the smoothing scale used in the separate universe framework and argue the effect can be absorbed into a renormalization of local operators. This complicates interpretation of the loop, because the analytic part of each loop integral is degenerate with unknown, ultraviolet-sensitive contributions.

Contents

1	Introduction	2
1.1	A classical, stochastic back-reaction model	4
1.2	Outline and summary	9
2	The separate universe framework and the δN formula	11
2.1	Review: the δN formula in phase space	11
2.2	The δN formula with back-reaction	13
2.2.1	Inflationary particle creation at the horizon	15
2.2.2	Energy exchange between quasiparticles and condensate	17
2.2.3	Loops in δN perturbation theory	20
3	The 3-phase ultra-slow-roll model	25
3.1	CMB scales based at horizon exit	27
3.2	Peak scales based at horizon exit	30
3.3	CMB scales based at exit time for peak scales	33
4	Case study: δN loops in the 3-phase ultra-slow-roll model	34
4.1	12-loop	34
4.2	22-loop	40
4.3	13-loop	41
5	The smoothing scale as a Wilsonian cutoff	44
5.1	The separate universe framework as an effective field theory	44
5.2	12- and 13-loop counterterms	47
5.3	22-loop counterterm	49
6	Discussion	49
6.1	Advantages of the separate universe framework	49
6.2	The role of nonlinear couplings	51
6.3	The Wilsonian EFT description	53
6.4	Degeneracy with UV counterterms	53
A	Numerical results for a 3-phase ultra-slow-roll model	55

1 Introduction

It is a longstanding proposal that the primordial power spectrum might grow significantly on small scales relative to its value on CMB or galaxy scales. Several independent lines of evidence have recently repopularized this idea. First, despite advances in detector technology, the lack of clear evidence for a WIMP-like dark matter particle has encouraged consideration of alternative scenarios. Several possibilities exist, but one option is that (at least some of) the dark matter is locked into small-scale collapsed objects, perhaps primordial black holes formed from direct collapse of high peaks in the inflationary density perturbation [1–3]. To produce an appreciable population of these objects would require enhancement of the power spectrum by roughly seven orders of magnitude at the relevant wavenumber k .

Second, the LIGO/Virgo/KAGRA collaboration continues to detect significant numbers of black-hole merger events via their gravitational radiation. The inferred mass and spin distribution of the progenitor objects is not easy to reconcile with an interpretation in which all such objects form at the endpoint of stellar evolutionary pathways [4]. In particular, the presence of significant numbers of low-spin progenitors may suggest the existence of a population of primordial black holes. Modelling the evolution of the spin distribution for such a population is extremely challenging, due to (among other issues) uncertainties in the accretion physics. These details are currently a topic of active debate. While there are reasons to believe that the entire population of progenitor objects is unlikely to be primordial in origin [5], it remains possible that there is a primordial component [6]. This would again require an enhancement of power.

Back-reaction and mode-coupling.—In either of these scenarios, and similar ones, we must take seriously the possibility that back-reaction from a spike of power at some high wavenumber k might spoil the successful prediction of a roughly Gaussian, scale-invariant perturbation at low wavenumbers $p \ll k$ that seed galaxy formation or the cosmic microwave background anisotropy [7]. This is because, whatever its origin, a realistic model for the primordial density field must predict *some* coupling between Fourier modes. This coupling enables short-wavelength power to spill over into the distribution of long-wavelength field values.

There are standard tools to measure this leakage of power. Recently, Kristiano & Yokoyama [8] used the methods of nonequilibrium field theory to compute a “one-loop” correction to the usual tree-level power spectrum. The terminology of the loop expansion is most familiar from perturbative field theory based on the equilibrium vacuum state, in which the loops are dominated by vacuum fluctuations and can be regarded as capturing the effect of quantum corrections. At least in their ultraviolet part, such loops measure the way that a bath of short-wavelength fluctuations influences the behaviour of long-wavelength modes. This applies whether the modes in the bath evolve according to classical or quantum laws. The conclusion is that loop-level terms such as those computed by Kristiano & Yokoyama can be regarded as a measure of back-reaction.

In an inflationary model there are two types of contribution to the short-wavelength bath. Superhorizon modes (but still shortward of the modes of interest) arising from the inflationary density perturbation sometimes have long-lived coherent behaviour because the

field operators and their canonical momenta approximately commute.¹ In this regime we can model their behaviour as stochastic fields with classical time dependence. Meanwhile, subhorizon modes (and possibly others) supply a bath of short-scale oscillators that must be treated quantum-mechanically. The loop correction must aggregate the influence from fluctuations of both types. An analogous situation occurs in finite temperature field theory, where loops measure the aggregate effect of thermal *and* vacuum fluctuations [9]. For example, it is well-known that when coupled to a spin-0 field, the effect of thermal fluctuations is to generate a confining potential that drives the spin-0 vev to zero at sufficiently high temperature. This is a form of back-reaction in which the cold, highly ordered, long-wavelength spin-0 condensate is disordered by incoherent, short-wavelength thermal effects. It is possible that the CMB-scale density field could be similarly disordered due to short-scale fluctuations. Related examples in a cosmological context are the loop corrections that appear in the effective field theory of large scale structure [10–13].

The conclusion drawn by Kristiano & Yokoyama was that one-loop back-reaction may be significant, and possibly already large enough (even without higher loop orders) to invalidate the tree-level analysis [8]. Their calculation primarily depended on approximate analytical estimates, and it is not yet entirely clear whether these adequately capture the relevant physics. As a result, the calculations of Ref. [8] were soon refined by many other authors [14–33].² This literature is already too extensive to review in detail here. However, the current position can be summarized by saying there is not yet agreement on the size of the one-loop effect. Neither is there agreement on the way regularization and renormalization of the divergent answer should be handled. We discuss some of these issues in §6.

In this paper we revisit the calculation of one-loop corrections. Our primary tool is the separate universe framework [37–39]. Many previous analyses have used the *in-in* (or ‘Schwinger–Keldysh’) formulation of nonequilibrium quantum field theory, beginning with the early analyses of Inomata *et al.* and Kristiano & Yokoyama [8, 34]. Once calculations progressed beyond linear order, it was soon established that both approaches yielded identical results for the tree-level ζ three-point function [39, 40]. A more general demonstration of the equivalence appeared in Refs. [41, 42], although still restricted to tree-level. At loop-level, the precise relationship between these two approaches does not yet appear to be settled.

In particular, Kristiano & Yokoyama focused on a loop-level contribution proportional to the commutator $[\zeta, \zeta']$, which temporarily grows during ultra-slow-roll inflation. This growth signals amplification of a previously decaying mode. Kristiano & Yokoyama characterized this effect as intrinsically quantum-mechanical. Once the ultra-slow-roll stage has passed, the $[\zeta, \zeta']$ commutator decays normally. We expect that this effect will change the statistics of particle creation around the horizon scale, where the $[\zeta, \zeta']$ commutator is not yet strongly suppressed. This would be relevant for modes near the peak of the power spectrum. On the other hand, once particle creation is complete and the $[\zeta, \zeta']$ commutator begins to decay, we expect that the subsequent evolution of these modes can be described classically. Hence, for

¹This property can be disrupted by ultra-slow-roll effects, so we generally assume modes are in this regime only when all ultra-slow-roll phases have ended.

²For an analysis of the contribution of enhanced small-scale modes to the one-loop power spectrum evaluated at the peak scales and at near infrared scales, see Refs. [34, 35] and Ref. [36] respectively.

scales near the peak, the separate universe framework would then apply in the usual way.

Meanwhile, on large scales where we wish to estimate the one-loop back-reaction effect, the commutator $[\zeta, \zeta']$ is strongly suppressed outside the horizon, even if it does receive a small amplification during the ultra-slow-roll period. (This argument parallels the discussion of the decaying mode during ultra-slow-roll; see §3.1 and §3.3.) We therefore conclude, on physical grounds, that the separate universe framework should provide an adequate description of the time dependence of modes between the peak scale and the CMB scale, provided we wait until all inflationary particle production effects have ceased and relevant commutators $[\zeta, \zeta']$ have begun to be suppressed. This is not very different to the usual stipulation that we must wait until all relevant scales are outside the horizon before invoking the separate universe framework.

Accepting this approach, we argue that the separate universe framework has at least two concrete advantages. First, on the basis of what has already been said, the back-reaction effect to be computed involves only modes that can be modelled by a stochastic field with classical time dependence. This is a considerable simplification compared to the full in-in approach, and makes it easier to separate important aspects of the physics. It yields a relatively transparent physical interpretation that can be framed in terms of a classical back-reaction model. We introduce this model in §1.1.

Second, the loop effects under discussion involve a large hierarchy of scales—between the early horizon-exit time of the CMB modes, and the late horizon-exit time of the enhanced peak scales. Inflationary correlation functions (just like correlation functions that appear in many other applications of quantum field theory) develop a very rich structure in the presence of such hierarchies [43, 44]. In many cases, the separate universe framework explains how large effects associated with these hierarchies may be factorized into products of lower-order correlation functions [43, 45]. Maldacena’s famous consistency condition is one example of a factorization result of this type [46]. Another is the squeezed limit of the three-point correlation function in phase space studied by Kenton & Mulryne [45]. Clearly, it must be possible to obtain these factorization formulae within the framework of in-in perturbation theory. However, experience has shown that the factorization results require considerably more work to derive there. The separate universe framework encodes these results in a technically simple way.

The separate universe framework (in the context of the δN formula for the curvature perturbation, ζ , on uniform density slices) has already been used to compute loop corrections by Firouzjahi & Riotto [23]. While our implementation is similar to theirs, they differ in the application of the framework. We give a more detailed discussion in §2.2.

1.1 A classical, stochastic back-reaction model

As explained above, in this paper our primary focus is the contribution from outside-the-horizon modes that can be treated as a stochastic source. We will return to the question of vacuum contributions in §6.3.

Correlation function between patches.—To calibrate our expectations, suppose that we divide some region of the universe into large superhorizon-sized patches of characteristic size

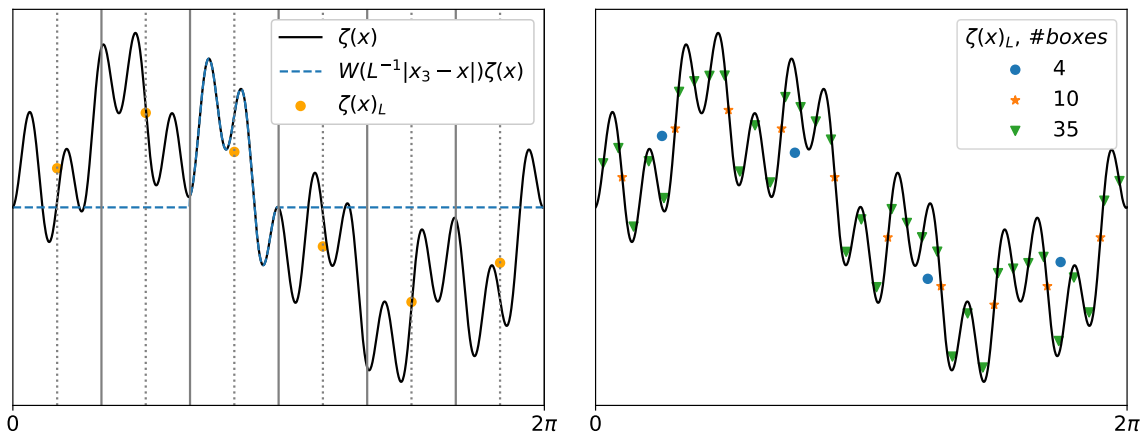


Figure 1: **Left panel:** Spatial averaging of a one-dimensional signal, $\zeta(x)$ with $x \in [0, 2\pi]$, over patches with size $L = 2\pi/6$. **Right panel:** Effect of changing the size of the L -patches, where $L = 2\pi/(\#\text{boxes})$.

$L \sim 2\pi/k_L$. We spatially average over these regions to produce a smoothed value for each perturbation. To keep the discussion simple, we usually work only with the curvature perturbation on a uniform density slicing, ζ , and denote its smoothed value by ζ_L . (However, our methods are general and will apply to other species of perturbation.) It is obtained from the spatial average

$$\zeta_L(\mathbf{x}) = \frac{1}{V} \int d^3x' W(L^{-1}|\mathbf{x} - \mathbf{x}'|)\zeta(\mathbf{x}'), \quad (1.1)$$

where $W(z)$ is a window function that falls to zero rapidly when $z \gtrsim 1$, and V is its volume. The coarse-grained coordinate \mathbf{x} labels the spatial position of each L -sized box. The familiar mechanism of inflationary perturbations will disorder the field, so that ζ_L takes a different value in each patch. Its distribution over the ensemble of patches will be almost Gaussian.

[For comparison, we show an example of spatial averaging in Fig. 1. We apply Eq. (1.1) to a one-dimensional signal, and demonstrate the effect of changing the size of the L -patch. As L decreases, an increasing number of high-wavenumber modes are retained after smoothing.]

Using Eq. (1.1) we find the correlation of the smoothed field between patches satisfies

$$\langle \zeta_L(\mathbf{x})\zeta_L(\mathbf{x} + \mathbf{r}) \rangle = \int_0^\infty \frac{dk}{k} \left[L^3 W(2\pi k/k_L) \right]^2 \mathcal{P}(k) \text{sinc } kr, \quad (1.2)$$

where \mathbf{r} is the coarse-grained displacement between patches and $W(k)$ is the Fourier transform of the normalized window function $W(z)/V$. Notice that ζ_L and $\mathcal{P}(k)$ may each be time dependent, although we suppress this in the notation.

For $r \lesssim L$, the locations \mathbf{x} and $\mathbf{x} + \mathbf{r}$ label the same coarse-grained volume. The integral in (1.2) receives contributions from k smaller than the window-function cutoff $\sim k_L$. For these wavenumbers we can roughly approximate $\text{sinc } kr \approx 1$, and therefore $\langle \zeta_L(\mathbf{x})\zeta_L(\mathbf{x} + \mathbf{r}) \rangle \approx \langle \zeta_L(\mathbf{x})^2 \rangle = \sigma_L^2$, where³

$$\sigma_L^2 \approx \int_0^{k_L} \frac{dk}{k} \mathcal{P}(k). \quad (1.3)$$

³Here and in the remainder of this paper we ignore questions of convergence in the infrared limit $k \rightarrow 0$,

We identify σ_L^2 as the variance of the smoothed field ζ_L among the L -sized patches.

If instead $r \gg L$, the oscillations of $\text{sinc } kr$ effectively cut off the integral at $k \sim 1/r \ll k_L$. In this region the window function satisfies $W \approx 1$. On these scales we have $\langle \zeta_L(\mathbf{x})\zeta_L(\mathbf{x} + \mathbf{r}) \rangle \approx \sigma_r^2$. If the power spectrum is scale invariant, or grows towards low wavenumbers, then spatial correlations persist between patches. On the other hand, if the power spectrum drops significantly for $k \lesssim k_L$ then the correlation function behaves like a smoothed δ -function. If the drop is sufficiently sharp then it may be a good approximation to neglect correlations over scales larger than a few L patches.⁴

Smoothing over substructure.—Now suppose that at some later stage, fluctuations associated with a much smaller physical scale $\ell \sim 2\pi/k_\ell$ exit the horizon. To describe these fluctuations we subdivide each L -patch into smoothed regions of characteristic size $\ell \ll L$, and suppose that each region is populated by one or more perturbations S_ℓ that contribute additively to ζ .⁵ We will sometimes describe these regions as ‘boxes’. Each S_ℓ is a random variable, but we are not yet being specific about its distribution. We apply this analysis to explicit examples below.⁶

The net effect is to overlay each L -patch with a mosaic of many ℓ -patches; see Fig. 2. In many realizations the mosaic will contain roughly equal positive and negative fluctuations, and its spatial average will be nearly zero.⁷

For these realizations the long wavelength field ζ_L will be almost unaffected. However, for some realizations the spatial average over the mosaic will not be zero. This may happen by chance, but is more likely where non-Gaussianity systematically skews the distribution to produce more positive or negative regions. In this case, the spatial average over the mosaic may significantly shift ζ_L . This is the back-reaction effect we wish to analyse.

Now focus on a single L -patch. It contains roughly $N = (L/\ell)^3$ independent small

which concern the distribution of field values on unobservably large scales and do not significantly affect the discussion of back-reaction on the scale L . For example, if $\mathcal{P}(k)$ is red-tilted we assume an infrared cutoff is implicitly present by computing conditional expectations within our locally observable region, which has a defined value of the ultra-large scale background. See, e.g., Lyth [47] and also Ref. [48].

⁴To make a more precise statement one can develop asymptotics for the sinc integral (1.2) using the Barnes representation

$$\text{sinc } x = \frac{1}{2\pi i} \int_{c-i\infty}^{c+i\infty} \Gamma(s) x^{-s-1} \sin \frac{\pi s}{2} ds, \quad (1.4)$$

for $x > 0$ and $0 < \text{Re}(s) < 1/2$. Using (1.4), it is possible to evaluate Eq. (1.2) for a prescribed functional form of $\mathcal{P}(k)$. The large r behaviour can be extracted using standard asymptotic methods for Mellin–Barnes integrals, which have been widely deployed in the analysis of Feynman diagrams [49–51]. However, for blue spectra with suitable growth to represent a spike, the conclusion agrees with the simpler analysis presented here. A similar procedure can be used to estimate gradient corrections, discussed below, to the approximation of independent, identically distributed small-scale realizations S_i .

⁵By ‘additive’, we mean that when $S_\ell \rightarrow S_\ell + \Delta$, we also have $\zeta_\ell \rightarrow \zeta_\ell + \Delta$.

⁶In §3 we introduce a 3-phase ultra-slow-roll model, and evaluate its loop corrections in §4. For this example, S_ℓ might be the quadratic operator $\delta\phi^2$. However, we emphasize that the discussion presented here is general, and applies beyond this scenario.

⁷Notice that this discussion applies regardless of the statistical distribution of the random variable S_ℓ . Indeed, if S_ℓ has a non-zero average, μ , this will be independent of the L -patch and therefore can be subtracted by redefining $\zeta_L \rightarrow \zeta_L - \mu$. On the other hand, the contribution to $\bar{\sigma}_L^2$ due to correlations with the long mode ζ_L cannot be subtracted, as $\langle \zeta_L S_\ell \rangle$ depends on the value of ζ_L , which changes across different L -patches.

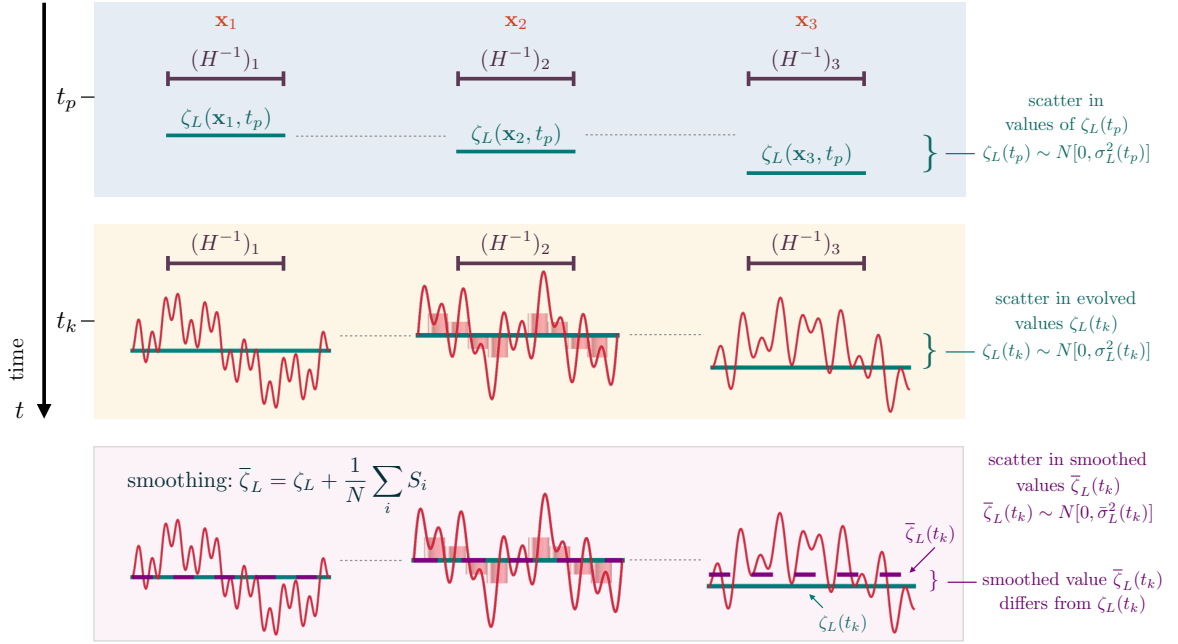


Figure 2: Evolution of superhorizon regions. **Top row:** Three regions of size $L \sim 2\pi/p$ just after horizon exit at time t_p . At this time, each region has no coherent substructure. The average value of ζ in each patch is $\zeta_L(\mathbf{x}_i, t_p)$. The distribution of ζ_L has variance $\sigma_L^2(t_p)$. **Middle row:** At a much later time, the scale $\ell \sim 2\pi/k$ exits the horizon. At this time, the value of $\zeta_L(\mathbf{x}_i, t_k)$ may have evolved due to isocurvature effects between t_p and t_k , yielding a modified variance $\sigma_L^2(t_k)$. Long-lived coherent substructure associated with the scale ℓ is now present. **Bottom row:** In many regions (here $\mathbf{x}_1, \mathbf{x}_2$), averaging over the substructure does not appreciably alter the long-wavelength field. But in some patches (here \mathbf{x}_3) the substructure does not average to zero. The spatial average $\bar{\zeta}_L(t_k)$ therefore differs from $\zeta_L(t_k)$ and may have differing variance $\bar{\sigma}_L^2(t_k)$.

boxes in the overlaid mosaic. We label the S_ℓ perturbation in each small box by S_i , where $i \in \{1, 2, \dots, N\}$. The autocorrelation of the S_i is the variance $\langle S_i S_i \rangle = \sigma_\ell^2$, whereas the cross-correlation between different boxes is $\langle S_i S_j \rangle$. If the spectrum used to generate the perturbation within each small box is sufficiently steep, the discussion above shows that we can take the S_i to be approximately independent, identically distributed (‘IID’) random variables. The leading corrections to this picture will be gradient suppressed of order $\sim (\ell/r)^2$. Here, r is the displacement appearing in Eq. (1.2).

Each S_i contributes additively to the curvature perturbation, so the corrected long-wavelength field in the L -patch, denoted $\bar{\zeta}_L$, can be written

$$\zeta_L(\mathbf{x}) = \zeta_L + \sum_i S_i \mathbf{1}_i(\mathbf{x}). \quad (1.5)$$

where $\mathbf{1}_i(\mathbf{x})$ is an indicator function that is unity when \mathbf{x} is within the i^{th} box and zero otherwise. The field $\zeta_L(\mathbf{x})$ traces the original background field ζ_L (which is constant over the

L -patch), but is dressed by the small-scale fluctuations. Its volume-weighted average over the L -patch can be written

$$\bar{\zeta}_L = \zeta_L + \frac{1}{N} \sum_i S_i. \quad (1.6)$$

Eq. (1.6) is our desired formula for the back-reaction of small-scale fluctuations on the long-wavelength mode, with the factor $1/N$ accounting for the volume average over the mosaic. The realization of both the long-wavelength field ζ_L and the short-wavelength fluctuations S_i vary between L -sized regions. They can therefore be regarded as stochastic variables. Meanwhile, the effect of the short-wavelength fluctuations can be regarded as a sort of shot noise: they arise from a discreteness effect, because we can fit only $\sim N$ independent samples into each L -patch. They formally disappear in the limit $N \rightarrow \infty$, corresponding to an infinite hierarchy of scale L/ℓ . A similar discussion was already given by Riotto [14].

We now ask how the short-scale fluctuations contribute to the variance $\langle \bar{\zeta}_L \bar{\zeta}_L \rangle \approx \bar{\sigma}_L^2$. The simplest situation occurs when the short-scale fluctuations do not correlate with the long-wavelength mode ζ_L . In this case only correlations among the S_i are present, generating a contribution

$$\bar{\sigma}_L^2 \supseteq \frac{1}{N^2} \left(\sum_i \sum_j \delta_{ij} \langle S_i S_j \rangle + \sum_i \sum_{j \neq i} \langle S_i S_j \rangle \right) = \frac{1}{N} \sigma_\ell^2 + \frac{1}{N^2} \sum_i \sum_{j \neq i} \langle S_i S_j \rangle. \quad (1.7)$$

The symbol ‘ \supseteq ’ is used to indicate that $\langle \bar{\zeta}_L \bar{\zeta}_L \rangle$ contains this contribution among others. For independent fluctuations, Eq. (1.7) reduces to

$$\bar{\sigma}_L^2 \supseteq \frac{1}{N} \sigma_\ell^2 \sim \frac{\ell^3}{L^3} \sigma_\ell^2. \quad (1.8)$$

The physical picture is that, although short-scale power is distributed evenly throughout the entire L -patch, the realization in each ℓ -patch is an independent sample. Therefore, the contributions from distinct ℓ -patches cannot add up coherently. Although there are N small patches, the absence of correlation means that their cumulative effect is insufficient to overcome the $1/N$ suppression from spatial averaging over the L -patch. This is simply the usual argument that leads to the central limit theorem. Riotto had earlier made the same observation, that this scaling should be associated with incoherent addition of small volumes populated by a Poisson process [14].

Corrections to the IID scenario.—If the fluctuations in each ℓ -patch are not independent then we should expect this conclusion to be modified. We have seen that this will happen if the spectrum populating the ℓ -patches is not sufficiently steep, which would allow long-range cross-correlation between patches. In this case the second contribution in Eq. (1.7) is not zero.

Alternatively, the ℓ -patches could correlate with the long-wavelength ζ_L mode. We then find

$$\bar{\sigma}_L^2 \supseteq \left\langle \zeta_L \left(\frac{1}{N} \sum_i S_i \right) \right\rangle = \langle \zeta_L S_\ell \rangle \equiv \sigma_\ell \sigma_L R(S_\ell, \zeta_L), \quad (1.9)$$

where we have assumed that all S_i correlate with ζ_L in the same way. In the last step we have introduced the correlation coefficient $R(S_\ell, \zeta_L)$ between S_ℓ and ζ_L . Notice there is no

longer a volume suppression factor $1/N$. This happens because—although each ℓ -patch is still an independent sample of the short-scale noise—each patch now correlates with the *same* long-wavelength mode ζ_L and therefore can add up coherently over the L -patch. Whether this effect is more or less important than the S autocorrelation (1.8) depends on a balance between the amplitudes σ_ℓ, σ_L , the scale hierarchy ℓ/L and the long–short coupling $R(S_\ell, \zeta_L)$. In some cases, we will see that R can be interpreted as the reduced bispectrum f_{NL} evaluated on a squeezed momentum configuration with sides $\sim 1/\ell, 1/L$ [14, 18, 32].

Note that the form of (1.9) does not require that back-reaction persists even in the limit of an infinite scale hierarchy $\ell/L \rightarrow 0$, which would be difficult to interpret physically. In practice the correlation coefficient R will typically become negligible (at least formally) in this limit. In cases where R can be associated with the reduced bispectrum, this corresponds to f_{NL} approaching zero in the ultra-squeezed limit.

1.2 Outline and summary

In this paper our primary aim is to develop a more sophisticated version of the toy model described in §1.1, suitable for the accurate evaluation of cosmological correlation functions. Our main tool is the separate universe framework. We carefully demonstrate how this should be deployed to capture back-reaction from small-scale substructure. Along the way, we introduce simplified models that help clarify the meaning of each loop, and the physical processes that contribute to it.

In §2 we briefly introduce and review the separate universe framework. This is a very general tool. It is most familiar when applied to the curvature perturbation ζ , where it leads to the ‘ δN ’ formula. This is widely used to evaluate inflationary correlation functions on superhorizon scales. In §2.1 we summarize the main ideas. In §2.2 we carefully explain how to set up the separate universe framework to be used for calculations of back-reaction. This does not require the introduction of new elements, but the necessary scales and times must be carefully distinguished. We relate the δN formula to the toy model of §1, which provides an extremely useful framework in which to build geometrical intuition. In particular, the key features of volume-suppressed auto-correlation, as in Eq. (1.8), and unsuppressed cross-correlation, as in Eq. (1.9), emerge naturally from the more detailed δN picture.

In §§2.2.1–2.2.2 we discuss the different physical processes that drive back-reaction in the separate universe framework. In §2.2.1 we discuss the effect of incoherent particle creation at the horizon scale. One approach would be to account for this using a stochastic framework, such as the original Starobinsky model [52]. In such frameworks the aim is usually to compute the one-point probability distribution of the fields smoothed on the horizon scale. (For a more general discussion, see Ref. [53].) In our application we require the fields smoothed on much larger scales, so the stochastic formalism cannot be applied directly. In §2.2.2 we discuss a different effect, caused by a cascade of power towards the infrared. This is driven by nonlinear interactions among the different particle species that contribute to ζ . To interpret the contributing processes, and relate them to S-matrix elements describing spacetime scattering processes, we draw an analogy with a system consisting of a Bose–Einstein condensate interacting with a cloud of quasiparticles.

Up to this point our argument is very general. In §3 we introduce a 3-phase ultra-slow-roll model, which is used in §4 to illustrate our framework by explicit calculations. The 3-phase model is very similar to models previously introduced by Cai *et al.* [54] and (especially) Firouzjahi & Riotto [23]. Readers familiar with the discussion given by Firouzjahi & Riotto will find no new material in this section and may wish to skip directly to §4. However, we discuss the model carefully because (as explained above) there are differences of detail in our application of the framework. Although our model is the same, our final expressions for the δN coefficients needed in the back-reaction calculation differ from those reported in Ref. [23].

In §4 we evaluate the 12-, 22- and 13-type loops in the 3-phase ultra-slow-roll model. We report values for both instantaneous and smooth transitions between the ultra-slow-roll phase and the second slow-roll phase, and emphasize the role of different types of nonlinear coupling. We also emphasize that loop contributions that are *not* volume-suppressed generally depend on soft limits of correlation functions. These limits can frequently be evaluated by another application of the separate universe framework, but they may have gauge ambiguities, and suitable subtractions may be needed to isolate the *physical* correlations. In this paper we do not pursue these subtractions in detail. Taken together, our detailed outcomes differ from previously published results. We find that—even if taken at face value, without subtractions—the 13-type loop vanishes, and the 12- and 22-type loops are too small to invalidate the tree-level prediction. This applies no matter how the we choose to transition between the different slow-roll and ultra-slow-roll phases. In comparison with the results of Firouzjahi & Riotto [23], these differences can be attributed partly to differences in our application of the separate universe framework.

In §5 we consider the effect of changing the separate universe smoothing scale. We argue that this functions exactly like a Wilsonian cutoff. As the cutoff changes, quanta are included or excluded from the loop, depending whether the cutoff is increased or decreased, respectively. This procedure is simply a reorganization of the calculation, and can not change the outcome for any correlation function. To absorb changes from the cutoff-dependence of the loop integrals will require counterterms, as in any application of effective field theory methods. In this section we show explicitly that the 12- and 13-type loops can be absorbed into a renormalization of local operators in the ζ Lagrangian. We argue that the necessity to introduce counterterms means that contributions to the loops of §4 that are analytic in the CMB-scale wavenumber must be combined with unknown ultraviolet-sensitive terms before they are be used to evaluate observables. We comment briefly on the prospects for finding measures of the loop contribution that are not sensitive to the unknown ultraviolet completion.

In §6 we conclude with an extended discussion. Appendix A collects a number of numerical results for the ultra-slow-roll model of §3.

Conventions.—We work in natural units where $c = \hbar = 1$. The reduced Planck mass is defined by $M_{\text{P}} = (8\pi G)^{-1/2}$, where G is Newton’s gravitational constant. Numerically, $M_{\text{P}} = 2.435 \times 10^{18}$ GeV. Latin indices I, J, \dots , label the coordinates needed to cover the phase-space manifold of fields. In the N -field model, they run from 1 up to $2N$. For the single-field models considered in detail below, they range over a field fluctuation $\delta\phi$ and a

momentum fluctuation $\delta\pi$. These fluctuations are defined in Section 2.1.

Our Fourier transform convention is

$$f(\mathbf{k}) = \int d^3x f(\mathbf{x})e^{-i\mathbf{k}\cdot\mathbf{x}} \quad \text{and} \quad f(\mathbf{x}) = \int \frac{d^3k}{(2\pi)^3} f(\mathbf{k})e^{i\mathbf{k}\cdot\mathbf{x}},$$

where $f(\mathbf{x})$ and $f(\mathbf{k})$ represent an arbitrary function and its Fourier transform, respectively. We sometimes use the shorter notation $f_{\mathbf{k}} = f(\mathbf{k})$, or $[\mathcal{O}]_{\mathbf{k}}$ for the Fourier mode of a composite quantity \mathcal{O} .

We use the notation $\langle \dots \rangle'$ to indicate a correlation function with removal of the momentum-conservation δ -function and the accompany factor of $(2\pi)^3$.

2 The separate universe framework and the δN formula

The separate universe framework is a tool used to compute the nonlinear evolution of perturbations on superhorizon scales. Let \mathbf{p} be a comoving wavenumber associated with some perturbation whose evolution we wish to compute. Outside the horizon, if $p = |\mathbf{p}|$ and H are the only relevant scales, spatial gradients of this Fourier mode will typically be suppressed by at least $(p/a)/H = p/(aH) \ll 1$ in any local model.⁸ Where this estimate is valid, a smoothed patch of the universe of size $L \sim 1/p$ will evolve like a ‘‘separate’’ unperturbed universe up to corrections of order $p^2/(aH)^2$.

2.1 Review: the δN formula in phase space

Trajectory description.—Dropping gradients, each smoothed patch evolves along an available trajectory in the *background* phase space M . This trajectory is selected (at least in the absence of back-reaction) by its initial conditions, which identify a particular point in M . To be concrete, let us suppose that the background model is described by some number of scalar fields, although our discussion is more general than this scenario. We assume the corresponding phase space to be labelled by the value and conjugate momentum for each field, which can be collected into a set of coordinates X^I .

To build statistical quantities we require an ensemble of smoothed patches. The time evolution of this ensemble can be expressed in terms of the trajectories followed by its members. Consider two regions whose initial conditions (specified at some early time t_*) differ by an amount $\delta X^I(t_*)$. We should regard $\delta X^I(t)$, for $t > t_*$, as a connecting vector linking the distinct trajectories followed by these regions. At some later time t this connecting vector can be written

$$\begin{aligned} \{\{\delta X^I(t, \mathbf{x})\}\}_L &= \frac{\delta X^I(t)}{\delta X^J(t_*)} \{\{\delta X^J(t_*, \mathbf{x})\}\}_L \\ &+ \frac{1}{2} \frac{\delta^2 X^I(t)}{\delta X^J(t_*) \delta X^K(t_*)} \{\{\delta X^J(t_*, \mathbf{x})\}\}_L \{\{\delta X^K(t_*, \mathbf{x})\}\}_L + \dots \end{aligned} \quad (2.1)$$

⁸We use the term ‘local’ to mean that the model remains finite when all wavenumbers go to zero together. Although suppression of gradients by the horizon scale $1/H$ is usually assumed in presentations of the separate universe technique, this situation can be different in models with more than one relevant scale [55]. In our scenario, this manifests as gradient corrections that are suppressed by $\sim \ell/L$. In §5 and §6.3 we show that this can be usefully interpreted in the context of an effective field theory description.

The brackets $\{\!\!\{\dots\}\!\!\}_L$ represent smoothing by spatial averaging over the scale L , and we have added a label \mathbf{x} to distinguish the regions linked by $\delta X^I(t)$.⁹ In the quadratic term—and its higher-order counterparts, not written here—it follows from the discussion of initial conditions above that each factor δX^I is smoothed *before* forming the product. As a point of principle the operations of multiplication and smoothing do not commute.

The variational derivatives $\delta X^I(t)/\delta X^J(t_*)$, $\delta^2 X^I(t)/\delta X^J(t_*)\delta X^K(t_*)$, and their higher-order analogues, measure changes in the background trajectory $X^I(t)$ due to changes in its initial conditions. They are the essential building blocks of the separate universe method. Each derivative can be computed from explicit knowledge of the trajectories $X^I = X^I[t, X^J(t_*)]$ as functions of their initial conditions [37, 39], or by integrating a Jacobi-like equation along the phase-space flow [42].

For typical models in which isocurvature modes decay by the time initial conditions are set for the CMB anisotropy, the primary quantity of interest is the curvature perturbation ζ . This represents a locally defined scale factor $a(t, \mathbf{x}) = a_0(t)e^{\zeta(t, \mathbf{x})}$ for each smoothed region. It can be shown that $\zeta(t, \mathbf{x})$ satisfies a separate-universe equation analogous to (2.1),

$$\begin{aligned} \{\!\!\{\zeta(t, \mathbf{x})\}\!\!\}_L &= \frac{\delta N(t)}{\delta X^J(t_*)} \{\!\!\{\delta X^J(t_*, \mathbf{x})\}\!\!\}_L \\ &+ \frac{1}{2} \frac{\delta^2 N(t)}{\delta X^J(t_*)\delta X^K(t_*)} \{\!\!\{\delta X^J(t_*, \mathbf{x})\}\!\!\}_L \{\!\!\{\delta X^K(t_*, \mathbf{x})\}\!\!\}_L + \dots, \end{aligned} \quad (2.2)$$

where $N(t)$ represents the number of e-folds elapsed along a given trajectory between a spatially flat hypersurface at time t_* with initial conditions set by $\delta X^I(t_*)$, and a uniform-density hypersurface at time t . As before, $\{\!\!\{\dots\}\!\!\}_L$ indicates smoothing on the scale L . For details, see Refs. [56, 57]. Eq. (2.2) is the ‘ δN formula’, introduced by Starobinsky [37] and extended nonlinearly by Lyth & Rodríguez [39].

In practical calculations we typically wish to work in Fourier space and extract a superhorizon mode \mathbf{p} from (2.1) or (2.2). For this purpose we can (almost) neglect the window function W , which is nearly unity if $1/p$ is at least a little larger than the smoothing scale. It has negligible effect except to specify how the convolution integrals implied by the quadratic term in (2.2), and higher-order terms, should be handled. Accordingly, when working in Fourier space, we will often drop an explicit smoothing label on the field. Notwithstanding this notational convenience, however, we will see that in a back-reaction calculation—which involves averaging over small-scale structure—the cutoff on each convolution integral must be treated with due care.

Low-order correlation functions of ζ .—In the later discussion we will need explicit forms for some ζ correlation functions. The main quantities of interest are the 2-, 3- and 4-point functions,

$$\langle \zeta_{\mathbf{k}_1} \zeta_{\mathbf{k}_2} \rangle \equiv (2\pi)^3 \delta(\mathbf{k}_1 + \mathbf{k}_2) P_\zeta(k_1), \quad (2.3a)$$

$$\langle \zeta_{\mathbf{k}_1} \zeta_{\mathbf{k}_2} \zeta_{\mathbf{k}_3} \rangle \equiv (2\pi)^3 \delta(\mathbf{k}_1 + \mathbf{k}_2 + \mathbf{k}_3) B_\zeta(k_1, k_2, k_3), \quad (2.3b)$$

$$\langle \zeta_{\mathbf{k}_1} \zeta_{\mathbf{k}_2} \zeta_{\mathbf{k}_3} \zeta_{\mathbf{k}_4} \rangle \equiv (2\pi)^3 \delta(\mathbf{k}_1 + \mathbf{k}_2 + \mathbf{k}_3 + \mathbf{k}_4) T_\zeta(\mathbf{k}_1, \mathbf{k}_2, \mathbf{k}_3, \mathbf{k}_4). \quad (2.3c)$$

⁹The coordinate label \mathbf{x} identifies only one of these regions. The other is taken to be a fixed fiducial region. The choice of fiducial region drops out of connected correlation functions.

The functions P_ζ , B_ζ and T_ζ are the power spectrum, bispectrum, and trispectrum, respectively. In order to deal with dimensionless amplitudes it is often preferable to work with the dimensionless power spectrum $\mathcal{P}_\zeta(k)$ and the reduced bispectrum $f_{\text{NL}}(k_1, k_2, k_3)$, which are defined to satisfy

$$P_\zeta(k) \equiv \frac{2\pi^2}{k^3} \mathcal{P}(k), \quad (2.4a)$$

$$B_\zeta(k_1, k_2, k_3) \equiv \frac{6}{5} f_{\text{NL}}(k_1, k_2, k_3) \left[P_\zeta(k_1) P_\zeta(k_2) + 2 \text{ perms} \right]. \quad (2.4b)$$

Note that f_{NL} defined in this way depends on the momentum configuration $\{k_1, k_2, k_3\}$, and therefore can vary as a function of both its scale (measured by the perimeter $k_t = k_1 + k_2 + k_3$) and shape (measured by the ratios k_i/k_t).

There is no simple parametrization for the amplitude of the trispectrum, but it is conventional to recognize two distinct ‘shapes’ with amplitude τ_{NL} and g_{NL} ,

$$T_\zeta(\mathbf{k}_1, \mathbf{k}_2, \mathbf{k}_3, \mathbf{k}_4) \equiv \tau_{\text{NL}} \left[P_\zeta(k_{13}) P_\zeta(k_3) P_\zeta(k_4) + 11 \text{ perms} \right] \\ + \frac{54}{25} g_{\text{NL}} \left[P_\zeta(k_2) P_\zeta(k_3) P_\zeta(k_4) + 3 \text{ perms} \right], \quad (2.5)$$

where $\mathbf{k}_{ij} = \mathbf{k}_i + \mathbf{k}_j$ and $k_{ij} = |\mathbf{k}_{ij}|$. Eq. (2.5) is exact within the local model, in which the nonlinear ζ is *defined* to satisfy

$$\zeta(t, \mathbf{x}) = \zeta_g(t, \mathbf{x}) + \frac{3}{5} f_{\text{NL}}^{\text{loc}} \left(\zeta_g(t, \mathbf{x})^2 - \langle \zeta_g(t, \mathbf{x})^2 \rangle \right) + \frac{9}{25} g_{\text{NL}}^{\text{loc}} \zeta_g(t, \mathbf{x})^3, \quad (2.6)$$

where $\tau_{\text{NL}} = (6f_{\text{NL}}^{\text{loc}}/5)^2$ and $g_{\text{NL}}^{\text{loc}}$ are constant, and ζ_g is a Gaussian random field. In a realistic model τ_{NL} and g_{NL} will develop scale- and shape-dependence, but it is then difficult to separate them unambiguously.

2.2 The δN formula with back-reaction

Separate universe expressions such as Eqs. (2.1) and (2.2) invoke a Taylor expansion in the initial conditions for each patch. This yields a correct result only when the time evolution can be predicted uniquely from knowledge of the initial conditions $\delta X^I(t_*)$. If back-reaction is sufficiently strong it will spoil the critical property of uniquely predictable evolution.

In this situation the picture becomes more complicated. At one extreme, the trajectories followed by smoothed regions within the ensemble may be disturbed continuously. For example, this is the case if we repeatedly adjust the size of the smoothed patches to follow the horizon scale. In any time interval, the value of ζ within each (adjusted) patch is coherently disturbed due to inflationary particle creation at the horizon. Eqs. (2.1) and (2.2) are then invalidated, with the outcome that $\delta X^I(t)$ and $N(t)$ should be replaced by a statistical distribution representing the range of phase space coordinates accessible from a given starting position $X^I(t_*)$. This approach leads to the Starobinsky formulation of stochastic inflation [37], and more recent variants including the ‘stochastic δN ’ method (see, e.g. Ref. [58]). Our analysis will not apply to this regime.

At the other extreme, each patch may be disturbed just once during its evolution. This is the scenario needed to study back-reaction from a relatively narrow spike over a

well-defined range of wavenumbers, and is the main focus of the analysis in this paper. It is somewhat different to the conventional stochastic formalism. First, the intention is to follow the evolution of an ensemble of patches of *fixed* scale as they are inflated far beyond the horizon. Second, when the back-reaction event occurs, it involves the eruption of substructure in many comparatively small horizon-scale patches, which add incoherently as explained in §1. For both these reasons we cannot immediately compute the back-reaction using a Starobinsky-type approach.

A δN formula for back-reaction.—Instead, we now aim to use Eq. (2.2) to build an analogue of the toy model (1.5) and its smoothed counterpart (1.6). To fix ideas, we let \mathbf{p} label a soft mode with $p = |\mathbf{p}| \sim L^{-1}$. In our later applications this will represent a typical CMB scale. As explained in §1 we are primarily interested in models where the short-scale modes $\sim \ell^{-1}$ receive an enhanced amplitude. We use \mathbf{k} to label typical Fourier modes in this enhanced region. There will now be three types of gradient correction to the separate universe formula—those suppressed by $p/(aH)$, $k/(aH)$, and those suppressed by $\ell/L \sim p/k$.

Allow the ensemble of large L -sized patches to exit the horizon. Up to the point where the smaller ℓ -sized boxes emerge from the horizon, the field value distribution within each patch can be evolved using any convenient method, including the δN formula (2.2). However, once the ℓ -boxes have emerged, we re-apply (2.2) *with smoothing scale set by ℓ* . The result is $\{\{\zeta(\mathbf{x})\}\}_\ell$. It represents the full spatial dependence of the ζ field, smoothed on the scale of the ℓ -sized patches, and is the exact analogue of the field $\zeta_L(\mathbf{x})$ in the toy model (1.5). Specifically, $\{\{\zeta(\mathbf{x})\}\}_\ell$ traces the distribution of field values over the large L -patches, but is dressed by small ℓ -scale fluctuations. In Fourier space, this dressing includes contributions from enhanced peak-scale modes $k \sim \ell^{-1}$.

The necessity to re-apply the formula (2.2) after the ℓ -scale boxes emerge is a restatement of the well-known requirement that, to apply separate-universe arguments, one must wait until *all* relevant scales have left the horizon. As explained in §1 we must also wait until the subsequent time evolution is classical. The necessary conditions in this case are $p/(aH) \ll 1$ and $k/(aH) \ll 1$. The natural time at which to base the δN calculation is therefore (a few e-folds after) the horizon-crossing time of the peak scales, t_k .

In §4 we specialize the general treatment developed here to a 3-phase model with ultra-slow-roll, to be introduced in §3. This is the same scenario described by Firouzjahi & Riotto in Ref. [23]. However, in their calculation, the δN formula was applied from the horizon exit time t_p for the large-scale mode \mathbf{p} . We argue that this approach does not correctly account for the influence of the short-scale modes, which are still deep inside the horizon at t_p .¹⁰

¹⁰In principle, there is another reason why it is necessary to restart the calculation at t_k . After the short-scale boxes exit the horizon, it is possible for their aggregate effect to displace larger smoothed regions onto a new trajectory in the background phase space. See Eq. (2.8). Therefore, if the δN calculation is based at t_p , to account for this effect there must be a step in which we re-evaluate the initial condition for each smoothed region in light of our knowledge of the newly-emerged short-scale modes. This is exactly how stochastic approaches work, and is needed here for the same reason. We estimate this effect in §2.2.1 and find it to be negligible when there is appreciable separation of scales, because the small-scale boxes add incoherently. There is a possible coherent effect that may be less suppressed by the scale hierarchy, and which is not included in §2.2.1. This is model-dependent. It would be interesting to obtain a more accurate estimate of its possible importance.

In the prescription given above, we choose to smooth over the scale ℓ when the δN calculation is restarted at t_k . However, one might instead consider smoothing immediately on the scale L . In comparison with our prescription, this choice represents a different way to organize the calculation, but must give a compatible outcome. We comment on the relation between these two computational schemes, and their respective merits, in §5 below.

Because we assume there is only one back-reaction event, Eq. (2.2) (with the replacement $L \rightarrow \ell$) can be used to evaluate $\{\{\zeta(\mathbf{x})\}\}_\ell$ at any late time of interest, t . Once we have arrived at this time, the next step conceptually is to smooth on the scale L associated with the original large patches. In practice, however, we simply extract a Fourier mode \mathbf{p} . As explained above, this effectively entails a spatial average. The resulting expression for $\zeta_{\mathbf{p}}$ is

$$\zeta_{\mathbf{p}}(t) = \frac{\delta N(t)}{\delta X^J(t_*)} \left[\{\{\delta X^J(\mathbf{x}, t_*)\}\}_\ell \right]_{\mathbf{p}} + \frac{1}{2} \frac{\delta^2 N(t)}{\delta X^J(t_*) \delta X^K(t_*)} \int_{q \lesssim \ell^{-1}} \frac{d^3 q}{(2\pi)^3} \left[\{\{\delta X^J(\mathbf{x}, t_*)\}\}_\ell \right]_{\mathbf{p}-\mathbf{q}} \left[\{\{\delta X^K(\mathbf{x}, t_*)\}\}_\ell \right]_{\mathbf{q}} + \dots, \quad (2.7)$$

where ‘...’ denotes terms of cubic order and higher in $\{\{\delta X\}\}_\ell$ that we have not written explicitly.

We could obtain equivalent results by choosing any smoothing lengthscale smaller than ℓ . Whichever time we pick, the base time t_* can be chosen at any time after horizon exit of the smoothing scale. The particular choice we are making here, i.e. $t_* = t_k$, is simply the most convenient for our purpose. There is no advantage in choosing a base time t_* significantly later than horizon exit of modes with wavelength comparable to the smoothing scale, because one must then account for the time evolution of the ℓ -size boxes between their horizon exit and t_* . Likewise, there is no advantage in choosing a smoothing scale that is significantly smaller than ℓ , because one must then wait for it to exit the horizon.

As explained above, we have dropped the smoothing label on $\zeta_{\mathbf{p}}$. However, it appears on the right-hand side in two locations. First, we have written $[\{\{\delta X^J(\mathbf{x}, t_*)\}\}_\ell]_{\mathbf{p}}$ to denote the \mathbf{p}^{th} Fourier mode of the field $\{\{\delta X^J\}\}_\ell$. Since $p \ll \ell^{-1} \sim k$ it must be remembered that many ℓ -size patches will fit within a box of size $L \sim 1/p$. Therefore one must include the scatter among these boxes when performing the Fourier transform, as in the toy model Eq. (1.6). This effect is discussed in §2.2.1 below. Second, the smoothing scale appears in the cutoff $q \lesssim \ell^{-1}$ applied to the convolution integral. Since $p \lesssim L^{-1} \ll \ell^{-1}$, both Fourier modes in the convolution lie approximately below the cutoff. Back-reaction from the convolution is discussed in §2.2.2.

2.2.1 Inflationary particle creation at the horizon

Our first task is to estimate the Fourier transform $[\{\{\delta X^J(\mathbf{x}, t_*)\}\}_\ell]_{\mathbf{p}}$ when $p \sim L^{-1} \ll \ell^{-1}$. This is needed in the linear term of Eq. (2.7). In contrast, for our scenario, the convolution integral is dominated by Fourier modes close to the peak in short-scale power. We do not need to include back-reaction from particle creation when evaluating these convolution modes. When included in a one loop correction to the power spectrum its effect would be higher order in the peak amplitude than the contributions that we keep.

As we have explained, once the ℓ -size boxes have exited the horizon, $[\{\delta X^J(\mathbf{x}, t_*)\}]_{\mathbf{p}}$ differs from the background Fourier mode $\delta X_{\mathbf{p}}^J$ because of the stochastic ℓ -scale modes. The effect can be estimated using Eq. (1.6). After translation to the present context, this would suggest

$$[\{\delta X^J(\mathbf{x}, t_*)\}]_{\mathbf{p}} \approx \delta X_{\mathbf{p}}^J(t_*) + \frac{1}{N} \sum_i S_i^J, \quad (2.8)$$

where $\delta X_{\mathbf{p}}^J(t_*)$ is the original background Fourier mode. To specify S_i^J , take $(\sigma^2)_{\ell}^{IJ}$ to be the variance in $\delta X^I(t_*)$, computed over the narrow band of wavenumbers that support the peak,

$$(\sigma^2)_{\ell}^{IJ} \approx \int_{\text{peak scales}} \frac{dq}{q} \mathcal{P}^{IJ}(q). \quad (2.9)$$

The (cross-)power spectrum $\mathcal{P}^{IJ}(q) = q^3 P^{IJ}(q)/(2\pi^2)$ is determined by the correlator

$$\langle \delta X_{\mathbf{k}_1}^I(t_*) \delta X_{\mathbf{k}_2}^J(t_*) \rangle = (2\pi)^3 \delta(\mathbf{k}_1 + \mathbf{k}_2) P^{IJ}(k; t_*), \quad \text{where } |\mathbf{k}_1| = |\mathbf{k}_2| = k. \quad (2.10)$$

Then S_i^J is a random variable whose covariance should be chosen to satisfy

$$\langle S_i^I S_j^J \rangle \approx (\sigma^2)_{\ell}^{IJ} \delta_{ij}. \quad (2.11)$$

The correlation (2.10) is evaluated just after horizon exit for the ℓ -scale modes and can be estimated using the usual methods of in–in quantum field theory.

The contribution of Eq. (2.8) to the two-point correlation function of $\zeta_{\mathbf{p}}$ is

$$\langle \zeta_{\mathbf{p}} \zeta_{-\mathbf{p}} \rangle \supseteq \frac{\delta N(t)}{\delta X^I(t_*)} \frac{\delta N(t)}{\delta X^J(t_*)} \left[\langle \delta X_{\mathbf{p}}^I(t_*) \delta X_{-\mathbf{p}}^J(t_*) \rangle + \frac{1}{N} (\sigma^2)_{\ell}^{IJ} + \langle \delta X_{\mathbf{p}}^I(t_*) S_{\ell}^J \rangle \right], \quad (2.12)$$

where the first term encodes the linear piece (that is, without back-reaction).

In a naïve estimate where one counts only powers of the short-scale amplitude $(\sigma^2)_{\ell}^{IJ}$, the second term in Eq. (2.12) would be the *leading* contribution to the back-reaction. It involves only a single power of $(\sigma^2)_{\ell}^{IJ}$. In practice, Eq. (2.8) shows that the effect is suppressed by a central-limit-like volume factor $N^{-1} \sim (\ell/L)^3$. For applications to formation of primordial black holes, L is a CMB scale and ℓ might be a scale associated with formation of solar-mass objects or smaller. This makes N^{-1} exponentially small, and the correction (2.8) is negligible. The outcome is that other sources of back-reaction can dominate, if they are not similarly volume-suppressed, even if they are formally higher order in the power spectrum amplitude.

Although it is the leading contribution when counting powers of the amplitude, the effect described by (2.8) has not previously been considered (in this context). One reason is that it is not visible directly from Eq. (2.7) when this is used to construct a loop expansion for correlation functions, of the form to be described in §2.2.2. Nor is it visible directly from the loop expansion in the in–in formalism, because any such loop must involve at least one n -point vertex for $n \geq 3$. In contrast, Eq. (2.8) depends only on particle creation from coupling to the background geometry and is present even for a massless free field.

Instead, to compute this type of back-reaction within the in–in formalism, one should coarse-grain the fields in the Wilsonian sense by integrating out fluctuations in momentum

modes $k \gtrsim \ell^{-1}$. This approach was used by Gell-Mann & Hartle to obtain effective equations of motion for the coarse-grained field [59], generalizing earlier work by Feynman & Vernon [60, 61] and Caldeira & Leggett [62, 63]. Their analysis was reformulated in terms of the in-in path integral by Calzetta & Hu, who emphasized the application to effective field theories [64, 65]. After coarse-graining, the path integral yields an influence functional of Feynman–Vernon type that describes energy exchange between the high- and low-energy sectors in terms of noise and dissipation kernels [60]. An analysis of this type could be used, if required, to provide a more precise estimate of the back-reaction effect (2.8).

Long–short correlations.—This discussion leaves open the question of what happens when the short-scale amplitude $(\sigma^2)_\ell^{IJ}$ correlates with the L -scale mode $\delta X_{\mathbf{p}}^J$. This effect is encoded in the third term in Eq. (2.12). The outcome in that case depends on the long–short correlation, but is not *explicitly* suppressed by the central-limit volume factor $N^{-1} = (\ell/L)^3$. In practice it will typically inherit at least mild dependence on the ratio ℓ/L from the scaling of the long–short correlation.

In this situation the magnitude of the back-reaction requires a detailed evaluation in each model of interest. Here, we assume that the physics of the spike is sufficiently insensitive to the background that long–short correlations are suppressed. Under this assumption the loops to be described in §2.2.2 would remain the dominant source of back-reaction. However, this should clearly be checked. It certainly appears possible to imagine scenarios in which the long–short correlation from inflationary particle creation contributes significantly.

2.2.2 Energy exchange between quasiparticles and condensate

The conclusion of §2.2.1 is that, under our assumptions, L -scale modes $[\{\delta X^J(\mathbf{x}, t_*)\}]_{\ell, \mathbf{p}}$ with $p \sim L^{-1}$ are undisturbed by the effect of particle creation at the (much smaller) horizon scale. The physical reason is that an exponentially large number of horizon volumes fit within each L -sized box, allowing their fluctuations to balance each other statistically to very high accuracy. Hence, at lowest order and in typical regions, the corresponding ζ mode $\zeta_{\mathbf{p}}$ will inherit its amplitude from the background Fourier mode $\delta X_{\mathbf{p}}^J(t_*)$ with negligible back-reaction. However, it is still possible for $\zeta_{\mathbf{p}}$ to be corrected by the convolution term in (2.7) and its higher-order analogues.

The convolution integral is dominated by modes with enhanced amplitude.¹¹ These occur near the spike in short-scale power and have wavenumbers $k \sim \ell^{-1}$. Let \mathbf{k} label a Fourier mode near the peak scale with $k = |\mathbf{k}| \sim \ell^{-1}$, and let \mathbf{p} label a soft mode with $p = |\mathbf{p}| \sim L^{-1}$. The convolution allows a pair of excitations with wavenumbers \mathbf{k} , $\mathbf{p} - \mathbf{k}$ to combine, producing a disturbance in the long-wavelength mode \mathbf{p} .

Noise from short-scale interactions.—What physical processes are described by such combinations? The particle content of an inflating patch of spacetime can be described as a dense condensate of zero-momentum particles with a comparatively dilute cloud of excitations scattering over it. These excitations are described as *quasiparticles* in the condensed matter literature, to emphasize that their properties and interactions are dressed by the con-

¹¹Recall that the smoothing scale sets an effective cutoff of order $\sim \ell^{-1}$ on wavenumbers that participate in the integral.

densate and differ from their vacuum values. In our situation the background field values X^I describe one or more of these scalar condensates, and the fluctuations $\delta X_{\mathbf{p}}^I$ describe the quasiparticle cloud. The spike in power is produced by an abundant population of excitations in the quasiparticle cloud with wavenumbers $\sim \ell^{-1}$. We describe these as ‘fast’ or ‘peak’ excitations. Meanwhile, the longer-wavelength degrees of freedom of wavenumber $\lesssim L^{-1}$ can be coarse-grained to form an effective value for the background condensate. We describe modes in this region as ‘slow’.

Using this language we can give a spacetime interpretation of the convolution in (2.7). A peak-scale quasiparticle with momentum \mathbf{k} may strike the condensate, ejecting two particles with momenta $\mathbf{k} - \mathbf{p}$ and \mathbf{p} . (Here, we are continuing to use the convention introduced above that \mathbf{k} and \mathbf{p} label the fast and slow momenta, respectively.) The reverse process will also occur, in which two peak-scale quasiparticles with nearly opposite momenta \mathbf{k} , $\mathbf{p} - \mathbf{k}$ collide, producing a slow excitation that joins the coarse-grained condensate. Three-body exchange processes of this type typically describe the growth or decay of Bose–Einstein condensates in laboratory conditions; see, e.g., the book by Kamenev [66].

The properties of the newly-created condensate mode depend on the statistical distribution of the fast progenitors, which are (mostly) decorrelated from the coarse-grained background. The net effect is as if the long-wavelength condensate were coupled to a stochastic source of noise. We will see that the loops evaluate the auto- and cross-correlations of this noise source. They can be calculated explicitly within our framework, precisely because we prescribed that the δN formula including back reaction—Eq. (2.7)—should be smoothed on the scale ℓ . Had we instead chosen to smooth on the scale L , most information about the ℓ -scale modes would have been erased except for a few aggregate statistics. This is just the usual Wilsonian effect of integrating out ultraviolet modes. The missing information about the ℓ -scale modes would then have to be provided via counterterms, including stochastic counterterms to replicate the effect of the decorrelated noise. When properly defined and renormalized, these two approaches would agree on the final outcome. However, the ℓ -smoothed approach allows a much more explicit analysis to be given. We defer a discussion of whether it is actually more predictive than the L -smoothed approach to §5.

The conclusion is that spacetime processes described by the convolution in Eq. (2.7) correspond to redistribution of excitations within the quasiparticle cloud. The degree to which 3-body processes contribute to this redistribution is measured by the time dependent prefactor of the quadratic terms in an expression such as (2.1) or (2.2). There are similar contributions involving higher n -body processes which arise from the cubic and higher terms in these equations. The interpretation of these contributions parallels the discussion of 3-body interactions given here. Meanwhile, injection of new excitations into the cloud is described by the particle creation process discussed in §2.2.1.

Each available 3-body channel is described by tree-level S -matrix elements shown in Fig. 3. To evaluate the spacetime correlations they produce (up to normalization), we should compute the modulus-squared of the S -matrix element and sum over the bath of unobserved cloud states that source the interaction. The sum over cloud states implies that this is a loop-level calculation within the in–in formalism, even though each individual S -matrix process is at tree level. An exactly analogous loop appears when calculating the

In the language of the effective field theory of large-scale structure, the in–in loop of Fig. 4 is of ‘22-type’. This analysis shows that it can be interpreted using the toy model of Eqs. (1.5)–(1.6). Specifically, we may write (2.7) in a form that parallels (1.6),

$$\zeta_{\mathbf{p}} = \zeta_{L,\mathbf{p}}^{(1)} + \mathcal{S}_{\mathbf{p}}. \quad (2.13)$$

Each term has a counterpart in Eq. (1.6). The \mathbf{p}^{th} Fourier mode $\zeta_{\mathbf{p}}$ plays the role of $\overline{\zeta_L}$; the Gaussian field $\zeta_{L,\mathbf{p}}^{(1)}$ plays the role of the long-wavelength background ζ_L ,

$$\zeta_{L,\mathbf{p}}^{(1)}(t) \equiv \frac{\delta N(t)}{\delta X^J(t_*)} \left[\left\{ \delta X^J(\mathbf{x}, t_*) \right\}_{\ell} \right]_{\mathbf{p}}; \quad (2.14a)$$

and $\mathcal{S}_{\mathbf{p}}$ is a composite operator that should be regarded as an avatar for the sum $N^{-1} \sum_i S_i$,

$$\mathcal{S}_{\mathbf{p}} \equiv \frac{1}{2} \frac{\delta^2 N(t)}{\delta X^J(t_*) \delta X^K(t_*)} \int_{q \lesssim \ell^{-1}} \frac{d^3 q}{(2\pi)^3} \left[\left\{ \delta X^J(\mathbf{x}, t_*) \right\}_{\ell} \right]_{\mathbf{p}-\mathbf{q}} \left[\left\{ \delta X^K(\mathbf{x}, t_*) \right\}_{\ell} \right]_{\mathbf{q}}. \quad (2.14b)$$

Source excitations in the quasiparticle cloud that contribute to $\mathcal{S}_{\mathbf{p}}$ are decorrelated from the long-wavelength condensate and can be localized on a scale $\sim \ell$. In each of these quantities, as explained in the discussion following (2.7), extracting the Fourier mode \mathbf{p} is already tantamount to spatial averaging on the scale $L \sim p^{-1}$. The loop of Fig. 4 is therefore nothing more than an estimate of the $\mathcal{S}_{\mathbf{p}}$ autocorrelation $\langle \mathcal{S}_{\mathbf{p}} \mathcal{S}_{-\mathbf{p}} \rangle$, with the approximation of Gaussian statistics for the source excitations. It does not account for any inter-box correlation captured by the off-diagonal covariance $\langle S_i S_j \rangle$ for $i \neq j$ in Eq. (1.7). One could do so, if required, by including non-Gaussian effects. In summary, we expect the contribution from the 22-loop to be suppressed by the central-limit-like factor volume $N^{-1} = (\ell/L)^3$, just as its counterpart (1.8).

2.2.3 Loops in δN perturbation theory

Let us now systematically consider the types of loop that can appear. Each loop bears an interpretation analogous to the sum over cloud states in Fig. 4. In particular, the use of the term ‘loop’ should not be taken to indicate that the calculation involves quantum corrections, but rather an average over unobserved fluctuations regardless of their character.¹³

Correlation functions of $\zeta_{\mathbf{p}}$ are computed by taking expectation values of products of (2.7), with due care regarding the loop order at which these are calculated. (See, e.g., Refs. [77, 78].) We assign an order in the loop expansion to each product of δX^I , determined by the number of unconstrained momentum integrals they contain. It follows from combinatorial considerations that we can represent such products using Feynman-like diagrams constructed using the language of Fig. 4. As usual, there is an unconstrained momentum integral associated with each closed loop. These represent independent sums over excitations in

¹³In this context one may compare with the discussion of Ref. [76]. The discussion in §4 of that reference distinguished between what were called ‘C-Feynman’ and ‘Q-Feynman’ diagrams, with the C-Feynman diagrams roughly corresponding to what we describe as averages over classical stochastic structure. As pointed out there, the epithet *classical* strictly refers only to the time dependence of these modes; they do in fact arise from a vacuum fluctuation and carry factors of \hbar allowing the whole diagrammatic expansion to match with the in–in formalism.

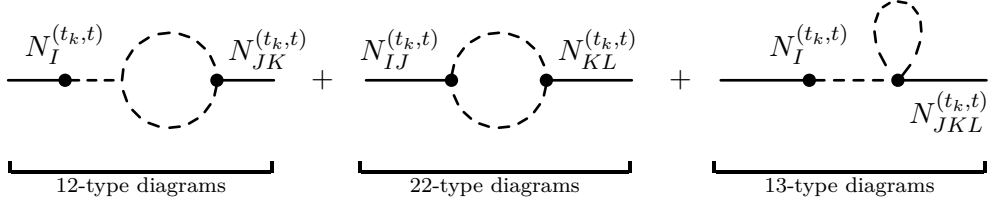


Figure 5: δN diagrams, in the language of Fig. 4, for one-loop corrections to the L -scale power spectrum due to ℓ -scale cloud modes. The unconstrained momentum integration implicit in each diagram, representing an average over unobserved cloud states, runs over scales near the short-scale power spectrum peak. The notation $N_I^{(t_*, t)}$, $N_{IJ}^{(t_*, t)}$ is introduced in Eqs. (2.15a)–(2.15b). In the diagrams we have set the initial time t_* to equal t_k ; see the discussion below Eq. (2.19).

the quasiparticle cloud. Notice that (as for vertices in any type of Feynman diagram) a given term in (2.7) may contribute at different loop orders in different correlation functions. For example, the quadratic term generates tree-level 112-type contributions to the bispectrum, but one-loop 22-type contributions to the power spectrum.

At one loop, the three possibilities are shown in Fig. 5. In these diagrams we have introduced a compact notation

$$N_I^{(t_*, t)} = \frac{\delta N(t)}{\delta X^I(t_*)}, \quad (2.15a)$$

$$N_{IJ}^{(t_*, t)} = \frac{\delta^2 N(t)}{\delta X^I(t_*) \delta X^J(t_*)}, \quad (2.15b)$$

with similar definitions for $N_{IJK}^{(t_*, t)}$ (and so on), as needed.

δX^I **correlators.**—Each diagram in Fig. 5 involves correlators of the δX^I fields. In linear perturbation theory these are free, Gaussian fields. Higher-order interactions and nonlinear evolution generate non-Gaussian contributions. We have already written down the two-point function for $\delta X_{\mathbf{k}_1}^I(t_*)$ in Eq. (2.10). We will also use the corresponding three-point function,

$$\langle \delta X_{\mathbf{k}_1}^I(t_*) \delta X_{\mathbf{k}_2}^J(t_*) \delta X_{\mathbf{k}_3}^K(t_*) \rangle \equiv (2\pi)^3 \delta(\mathbf{k}_1 + \mathbf{k}_2 + \mathbf{k}_3) \alpha^{IJK}(k_1, k_2, k_3; t_*). \quad (2.16)$$

$P^{IJ}(k_1; t_*)$ and $\alpha^{IJK}(k_1, k_2, k_3; t_*)$ are, respectively, second-order and fourth-order in powers of H/M_{Pl} . For free, massless fields in a nearly de Sitter spacetime we have, after dropping decaying modes,

$$P^{\phi\phi}(k_1; t_{k_1}) = \frac{H(t_{k_1})^2}{2k_1^3}, \quad (2.17)$$

where t_{k_1} is the horizon-crossing time for the wavenumber k_1 . In this paper we assume that Eq. (2.17) is a good approximation for the field fluctuations at horizon-crossing. We discuss this choice in the context of an explicit numerical study in Appendix A.

Tree-level.—The δN tree-level contribution comes from the product of linear terms in Eq. (2.7),

$$\langle \zeta_{\mathbf{p}} \zeta_{-\mathbf{p}} \rangle_{\text{tree}} \sim N_I^{(t_k, t)} N_J^{(t_k, t)} \langle \delta X_{\mathbf{p}}^I(t_k) \delta X_{-\mathbf{p}}^J(t_k) \rangle_{\text{tree}+1\text{-loop}}. \quad (2.18)$$

There is a subtlety with the δX two-point function appearing here. This term enters at tree-level within the δN expansion. However, in order to obtain a result that contains all contributions up to one-loop, the δX correlator should contain *both* tree-level and one-loop contributions.

One option is to evaluate these loops using a second application of the separate universe picture. This could be a fruitful approach if large contributions are expected from substructure that emerges between the horizon exit time t_p for the scale $L \sim 1/p$, and the corresponding exit time t_k for the scale $\ell \sim 1/k$. Specifically, it is at the time $t = t_k$ that we need to evaluate the correlation function.

In our present scenario, however, there are no large effects of this kind. At time t_k the enhanced modes on the scale ℓ have only just emerged from the horizon. There has not yet been time for scattering processes to have redistributed any power from small scales to large scales, so we do not expect a significant loop effect. Instead, the only source of back reaction is the particle creation event itself. This was considered in §2.2.1 and found to be negligible provided there is at least a modest hierarchy between the scales p and k . On this basis (here and in the remainder of this paper), we retain only the tree-level contribution to the δX two-point function in (2.18).

To close this section we give general expressions for each one-loop term in Fig. 5. In principle these can be applied to *any* model of inflation with an arbitrary number of fields. In §§3–4 we specialize these expressions to the case of a concrete 3-phase ultra-slow-roll model.

12-type loops.—Using a standard notation we label the three loop topologies as contributions of type 12, 22 (already introduced above), and 13.

First, consider the 12 loops. These arise from a product of the linear term in Eq. (2.7) with the quadratic term,

$$\langle \zeta_{\mathbf{p}} \zeta_{-\mathbf{p}} \rangle_{12} \sim N_I^{(t_k, t)} N_{JK}^{(t_k, t)} \int \frac{d^3 q}{(2\pi)^3} \langle \delta X_{\mathbf{p}}^I(t_k) \delta X_{-\mathbf{p}-\mathbf{q}}^J(t_k) \delta X_{\mathbf{q}}^K(t_k) \rangle_{\text{tree}}. \quad (2.19)$$

We have dropped the smoothing label $\{\{\dots\}\}_\ell$ on the perturbations $\delta X_{\mathbf{k}}^I$, partly to reduce clutter, and partly because none of the fields in this product include back-reaction from ℓ -scale effects. For the slow mode \mathbf{p} this follows from the discussion of §2.2.1. Meanwhile, the convolution is dominated by fast modes \mathbf{k} that are themselves associated with the scale ℓ . The convolution should still be cut off at $q \sim \ell^{-1}$, as in Eq. (2.7). Finally, in Eq. (2.19) and Fig. 5 we have set $t_* = t_k$, where t_k is the horizon exit time for modes contributing to the short-scale peak in the power spectrum.

Notice that (as explained above) it is important to set the smoothing lengthscale for the separate universe formula (2.7) to be no larger than the scale ℓ associated with the peak modes $\sim \mathbf{k}$. For this reason, one must choose the base time to be at least as late as the horizon exit time t_k , in order that these modes begin to evolve according to the classical superhorizon time dependence. If one chooses a larger smoothing length then the modes whose back-reaction we intend to compute will be erased.

The choice of smoothing scale $t_* = t_k$ has the consequence that we must *separately* account for the evolution of the $\delta X_{\mathbf{p}}$ mode between its horizon exit time and the time t_k . We

will see explicit examples in §4. The soft limit for the δX three-point function (and other soft limits needed for the remaining loop topologies) can generally be estimated using powerful factorization methods [45]; see Eq. (4.4).

The δX^I correlation function on the right-hand side of (2.19) would be exactly zero in a Gaussian approximation. It is present only when the cloud modes have long-short correlations that persist between the modes $p \sim L^{-1}$ and $k \sim \ell^{-1}$. The amplitude of these correlations is measured by the reduced bispectrum f_{NL} in a squeezed configuration, roughly $\sim f_{\text{NL}}(p, k, k)$. This evidently corresponds to the long-short correlation (1.9) in the toy model of §1.1, with f_{NL} playing the role of the correlation coefficient R . It follows that the short-scale power may add coherently over L -sized regions. The contribution from these modes is therefore not suppressed by the central-limit-like volume factor $N^{-1} = (\ell/L)^3 \sim (p/k)^3$.

If this is the case, how should we expect the correlation to behave when $p/k \rightarrow 0$? An estimate of this behaviour is critical, for two reasons. First, it will determine whether the back-reaction is significant. Second, on the basis of the decoupling principle, Fumagalli argued that one should expect the back-reaction (and therefore the loop) to vanish in the limit of an infinite hierarchy $p/k \rightarrow 0$ [29]. A similar argument was given by Tada *et al.* [31]; see also Firouzjahi [32]. In a single-field adiabatic model, the asymptotic squeezed limit of the ζ bispectrum is controlled by Maldacena’s consistency condition [46]. It has been argued that this is a gauge artefact that should be subtracted by moving to physically defined coordinates appropriate for a local observer [79–82]. This amounts to fixing our small-scale rulers so that, in each region, the peak is produced on a fixed physical scale, rather than a fixed comoving scale [81, 83]. If so, then when working on such a physically-defined hypersurface, the asymptotic squeezed limit of the reduced ζ -bispectrum would be zero, with the leading correction from gradients of order $(p/k)^2$ [80, 81], at least if there is a massless mode in the spectrum. (If all modes are massive then we expect stronger suppression.) This suggests that Eq. (2.19) may require corrections in order that the integral represents a sum over a suitable, physically-defined squeezed limit.

A general recipe to compute the necessary subtraction for any correlation function was given by Pajer *et al.* [81]. Their prescription involved an infrared regulator scale that was used to divide modes into a ‘soft’ part, which is effectively resummed into the new physical coordinates, and a ‘hard’ part. There does not yet appear to be a practical prescription for this subtraction that yields results manifestly independent of this infrared regulator. Nevertheless, it would seem plausible that, in a single-field adiabatic model, Eq. (2.19) scales like $(p/k)^2$ (or a steeper function of p/k) when $p/k \rightarrow 0$ at fixed k . If so, we should apparently conclude that the physical back-reaction on CMB-scale modes due to a spike of power associated with PBH-scale modes is exponentially small.¹⁴

In this situation it would be unclear whether the separate universe framework is ade-

¹⁴There are some ambiguities. For example, we should be free to compute the loop correction on any well-defined hypersurface and later translate to the physical hypersurface. The outcome of this calculation should be equivalent to performing the loop correction on the physical hypersurface from the outset by making subtractions to the three-point function in Eq. (2.19). (This neglects the effect of back-reaction on the definition of the physical hypersurface, which may be reasonable if the loop correction is smaller than the tree-level.) It is not clear that these operations commute.

quate to evaluate the loop, because we already expect gradient corrections to formulae such as (2.19). If we base the separate universe expansion near the horizon exit time for k then we would expect these gradients to be suppressed by $(p/k)^2$. They would therefore be the same order in gradients as the surviving terms from (2.19). Effects of this type at order $(p/k)^2$ have been reported by Tasinato using a large $|\eta|$ expansion [26], which could possibly be identified with these surviving contributions. However, the situation here is quite unclear.

On the other hand, if the model is *not* adiabatic, long–short correlations may survive, at least over some range of scales. For example, this may happen in inflationary models with multiple fields, if their isocurvature modes do not decay rapidly. The 12-loop (2.19) could then receive contributions from squeezed configurations. On physical grounds, one would still expect the soft limit of the correlation function to decay at least mildly as a function of p/k . This decay would be inherited by the loop, generating the expected decoupling as $p/k \rightarrow 0$.

In this paper we work with the separate universe formula (2.7), and the resulting 12-type loop, as they stand—with the understanding that the integrand of (2.19) (and similar loop contributions that depend on squeezed configurations of higher n -point functions) may require subtractions in order to define a physical squeezed limit. However, we defer a detailed analysis of how these squeezed limits should be handled to future work.

Just as for the 22-loops, the 12-loops have a particle interpretation. The topology depicted in Fig. 5 shows this must be related to the 22-loop; see Fig. 4. The major difference is that the 22-loop has the same interaction at both vertices, associated with conversion of two short-wavelength field fluctuations into a slow ζ mode. It correlates the volume-averaged field produced by this process with itself. In contrast, the 12-loop has different vertices. One of these is the same as the vertices occurring in the 22-loop, and is used to tie together two fast legs of the δX^I three-point function to produce a slow ζ . The other describes production of a slow δX^I mode which is re-interpreted directly as a slow ζ . It is this cross-correlation effect that allows it to evade volume suppression, as we have already seen in Eq. (1.9). The same conclusions would apply to a ζ -gauge calculation using the in–in formalism. Specifically, the 12- and 12-loops discussed here would both appear to be part of the in–in 22-loop (there being no 12-loop in the interaction picture).

22-type loops.—Some aspects of these loops have already been discussed in §2.2.2. They arise from the product of two quadratic terms in Eq. (2.7),

$$\langle \zeta_{\mathbf{p}} \zeta_{-\mathbf{p}} \rangle_{22} \sim N_{IJ}^{(t_k, t)} N_{KL}^{(t_k, t)} \int \frac{d^3 q}{(2\pi)^3} \int \frac{d^3 r}{(2\pi)^3} \langle \delta X_{\mathbf{q}}^I(t_k) \delta X_{\mathbf{p}-\mathbf{q}}^J(t_k) \delta X_{\mathbf{r}}^K(t_k) \delta X_{-\mathbf{p}-\mathbf{r}}^L(t_k) \rangle_{\text{tree}}. \quad (2.20)$$

The leading contribution comes from the disconnected part of this four-point correlation, representing a Gaussian approximation. We will see in §4 that it reproduces the expected shot-noise-like behaviour $\sim (p/k)^3$, described above. If desired, the connected contribution could also be kept, which would enter at two-loop order.

13-type loops.—These are generated by a product between the linear term in Eq. (2.7) and

the cubic term, which until now we have not written explicitly,

$$\langle \zeta_{\mathbf{p}} \zeta_{-\mathbf{p}} \rangle_{13} \sim N_I^{(t_k, t)} N_{JKL}^{(t_k, t)} \int \frac{d^3 q}{(2\pi)^3} \int \frac{d^3 r}{(2\pi)^3} \langle \delta X_{\mathbf{p}}^I(t_k) \delta X_{\mathbf{q}}^J(t_k) \delta X_{\mathbf{r}}^K(t_k) \delta X_{-\mathbf{p}-\mathbf{q}-\mathbf{r}}^L(t_k) \rangle_{\text{tree}} \quad (2.21)$$

The corresponding diagram (see Fig. 5) has a different topology to the 12- and 22-type loops. It constitutes a multiplicative renormalization of the power spectrum at wavenumber p , rather than a stochastic contribution from a decorrelated noise-like source. It represents a sum over S -matrix processes of the form

$$\langle \zeta_{\mathbf{p}} \zeta_{-\mathbf{p}} \rangle \sim \sum_{|\text{cloud}\rangle} \left(\text{---} \frac{\mathbf{p}}{\text{---}} \right) \left(\begin{array}{c} |\text{cloud}\rangle \\ \text{---} \text{---} \text{---} \text{---} \\ \text{---} \frac{\mathbf{p}}{\text{---}} \end{array} \right)^\dagger + \text{h.c.}, \quad (2.22)$$

where ‘+ h.c.’ indicates that we should add the Hermitian conjugate of the preceding term. The sum over cloud states $|\text{cloud}\rangle$ ties together two of the dashed legs in the diagram containing a four-point vertex, producing a loop. Roughly, the \mathbf{p} Fourier mode passes straight through the diagram; none of the decorrelated cloud excitations propagate into the final state.

In the ζ -gauge calculation performed using the in-in formalism, the 13-type diagram would correspond to the (topologically equivalent) diagram due to quartic-order ζ -interactions. This contribution has been calculated by Firouzjahi in Ref. [19] for a 3-phase ultra-slow-roll model with instantaneous transitions; see also the discussion in Ref. [32].

3 The 3-phase ultra-slow-roll model

The framework elaborated in §§1–2 can be applied to a wide range of scenarios. As an illustration, we consider a single-field model including a transient phase of ultra-slow-roll inflation [84–86]. This phase is both preceded and succeeded by conventional periods of slow-roll inflation. In this section we briefly review details of the ultra-slow-roll model and show how to describe the time evolution of its perturbations using the separate universe framework.

Scalar fluctuations are amplified during the ultra-slow-roll era. This produces a peak in the scalar power spectrum. By choosing the ultra-slow-roll phase to occur at the right time, the peak can be positioned on scales smaller than those constrained by CMB experiments. After horizon re-entry in the radiation era, these large perturbations may collapse to form primordial black holes [87]; for example, see the review by Sasaki *et al.* [88]. Such models are of interest because there is still a small mass window in which primordial black holes could account for a fraction (or even all) of the dark matter [4, 89, 90]. To trigger sufficient black hole formation, the small-scale power spectrum would need to be enhanced by roughly 10^7 relative to its value on CMB scales.

Similar multi-phase USR + SR scenarios have been discussed by Cai *et al.* [54], Kristiano & Yokoyama [8] and Firouzjahi & Riotto [23].

Background evolution.—We define the first three Hubble slow-roll parameters,

$$\epsilon \equiv -\frac{H'}{H}, \quad \eta \equiv \frac{\epsilon'}{\epsilon}, \quad \xi \equiv \frac{\eta'}{\eta}, \quad (3.1)$$

where a prime indicates a derivative with respect to the elapsed e-folding number, $N = \int^t H(t') dt'$. The inflationary phase is assumed to be supported by the potential energy $V(\phi)$ associated with a single scalar field ϕ . We also introduce V -type slow-roll parameters defined with respect to the potential,

$$\epsilon_V \equiv \frac{M_{\text{P}}^2}{2} \left(\frac{V_\phi}{V} \right)^2, \quad \eta_V \equiv M_{\text{P}}^2 \frac{V_{\phi\phi}}{V}. \quad (3.2)$$

Here, V_ϕ and $V_{\phi\phi}$ are the first and second derivatives of $V(\phi)$ with respect to ϕ . The V -type slow-roll parameters are not the same as the Hubble-type parameters defined in (3.1), but their order of magnitude is comparable when the slow-roll approximation is valid.

We suppose that $V(\phi)$ supports a period of slow-roll inflation while the largest observable scales leave the horizon. A slow-roll epoch (‘SR’) is characterized by the conditions $\epsilon = \dot{\phi}^2/(2H^2M_{\text{P}}^2) \ll 1$, and usually also $|\eta| = |\ddot{\phi}/(H\dot{\phi})| \ll 1$. At some later time we assume $V(\phi)$ flattens abruptly. In this phase there is no potential gradient to support the inflaton velocity, which therefore decays rapidly with $\eta \approx -6$. This epoch is described as *ultra-slow-roll inflation* (‘USR’). Finally, when the velocity has relaxed to a suitable value, there is a second phase of slow-roll inflation. We distinguish the two slow-roll phases using the labels ‘1’ and ‘2’. In particular, ϵ_1 and ϵ_2 denote the V -type ϵ parameter in the first and second slow-roll epochs,

$$\epsilon_1 = (\epsilon_V)_1, \quad \epsilon_2 = (\epsilon_V)_2. \quad (3.3)$$

We assume the second slow-roll epoch to be (eventually) terminated with $\epsilon \sim 1$, leading to a graceful exit.

The transitions between these phases are of particular importance. Kristiano & Yokoyama assumed an instant transition between ultra-slow-roll and the final slow-roll phase [8]. They used in–in methods to calculate the one-loop correction due to a (bulk) cubic interaction proportional to η' , which has a large δ -function spike in the limit of an instantaneous transition. Under certain assumptions, they found that the one-loop correction might become comparable to the tree-level. The same scenario featuring an instantaneous transition was also used by Firouzjahi [19, 32], leading to a similar conclusion. Riotto [18] and Firouzjahi [19, 32] suggested that the correction might be suppressed when the transition is smooth. (See also Firouzjahi & Riotto, Ref. [23]. We make a detailed comparison with this reference in §2.2 and §4.)

Franciolini *et al.* modelled the time evolution of η using an analytic function that allows for a smooth transition [25]. They found that, after fixing the final abundance of primordial black holes, the size of the one-loop correction is not significantly reduced by considering smooth evolution. Nevertheless, these numerical results show that the loop estimate given by Kristiano & Yokoyama is too large, even for models with instantaneous transitions. In Ref. [33], Davies *et al.* reached similar conclusions by numerically evaluating the one-loop term directly from a single-field potential yielding ultra-slow-roll.

In the following, we adopt the framework introduced by Cai *et al.* [54] to describe the transition from ultra-slow-roll to slow-roll, which we summarize below in §3.2. Our treatment will apply to instantaneous and smooth transitions. We discuss how the resulting one-loop corrections depend on the character of the transition in §4.

To proceed, we label the e-folding time at the start of the ultra-slow-roll phase by $N = N_s$, and use $t = t_s$ and $\tau = \tau_s$ to denote the same time in cosmic time and conformal time, respectively. We write the wavenumber leaving the horizon at this time as $k_s = (aH)|_{t=t_s}$. We take the transition at the end of ultra-slow-roll to occur at time $N = N_e$ (or $t = t_e$, $\tau = \tau_e$), and write the wavenumber leaving the horizon as k_e .¹⁵

In the following sections we use the δN formula to compute the tree-level ζ power spectrum for modes of order the CMB scale (§3.1), and those of order the peak scale (§3.2). In each case, we must select an initial time t_* at which to base the separate universe formula (2.2). In §§3.1–3.2 we take this to be the natural initial time, a little after horizon exit for the corresponding mode. However, when calculating loop corrections in §4 it will be necessary to set t_* equal to the horizon-crossing time for the peak modes, even when computing the power spectrum on CMB scales. In §3.3 we demonstrate that this calculation yields the same result as §3.1. This version of the argument will be critical for the discussion in §4.

3.1 CMB scales based at horizon exit

First, consider fluctuations on a scale that will be imprinted on the CMB, assumed to exit the horizon during the first slow-roll epoch. Throughout this section we continue to use the notation introduced in §2.2.2, in which \mathbf{p} labels the wavevector for a large-scale mode (here representing the CMB scale), and \mathbf{k} labels a wavevector near the short-scale peak. The corresponding horizon exit times are written t_p and t_k , respectively.

In this section the power spectrum will be computed up to tree level using the separate universe formula (2.2) based at the horizon exit time t_p .¹⁶ The analysis is standard, and we briefly recall only the major steps. During a slow-roll phase, the inflaton velocity is locked to the gradient of the potential. Introducing the momentum $\pi \equiv d\phi/dN$, this condition can be written

$$\pi = -M_{\text{P}}\sqrt{2\epsilon_1}. \quad (3.4)$$

We have used the relationship $3H^2M_{\text{P}}^2 \approx V$. If we further assume that ϵ_1 is approximately constant during the first slow-roll epoch then Eq. (3.4) can be integrated to obtain a formula for $N^{(t_p,t)}$,

$$N^{(t_p,t)} \approx \frac{1}{\sqrt{2\epsilon_1}} \frac{\phi(t_p) - \phi(t)}{M_{\text{P}}}, \quad (3.5)$$

¹⁵ In practice, when dealing with a smooth transition, it is necessary to introduce an additional criterion to identify the ultra-slow-roll phase. See the discussion in Appendix A.

¹⁶ In presentations of the separate universe method that invoke classical arguments, it is sometimes suggested that one should wait until a few e-folds *after* horizon exit before applying a formula such as Eq. (2.2). Ref. [43] argued, based on a direct analysis of the evolving correlation functions and *without* invoking a classical model, that to obtain the most accurate estimate one should begin the separate universe calculation exactly at horizon exit (here $t = t_p$), but drop decaying modes in the correlation functions of phase-space variables.

where $t > t_p$ is a time during the first slow-roll era. Note that the notation used here matches Eqs. (2.15a)–(2.15b). We are assuming ϕ rolls from large to small expectation values. If the opposite is true, a sign flip is needed in this expression.

Evolution up to end of first slow-roll epoch.—Eq. (3.5) measures the number of e-folds that elapse between two hypersurfaces on which ϕ assumes prescribed values $\phi(t_p)$ and $\phi(t)$. This is not strictly the quantity that appears in the δN formula (2.2), in which the final surface should be taken to have uniform density. In general $\rho = \dot{\phi}^2/2 + V$, and therefore hypersurfaces of uniform density do not coincide with hypersurfaces of fixed ϕ . However, during slow-roll inflation $\dot{\phi}^2/2$ is small compared with V . Therefore the difference is $O(\epsilon)$ and can be neglected if we aim only for expressions valid to leading order in the slow-roll parameters.

Outside the horizon, the perturbations begin to evolve like the background field. Variation of Eq. (3.4) shows that $\delta\pi$ becomes locked to the field fluctuation $\delta\phi$, with its amplitude suppressed by a slow-roll factor,

$$\delta\pi = \frac{\eta}{2}\delta\phi + \text{decaying}, \quad (3.6)$$

where η is given in Eq. (3.1), and ‘decaying’ represents a decaying mode that is exponentially suppressed on the slow-roll attractor.

We conclude that only the $\langle\phi\phi\rangle$ correlator is needed in the tree-level formula (2.18). The coefficient $N_\phi^{(t_p,t)}$ can be obtained from variation of (3.5) with respect to its initial condition $\phi(t_p)$, taking the final density—and hence $\phi(t)$ —to be fixed,

$$N_\phi^{(t_p,t)} \equiv \frac{\delta N(t)}{\delta\phi(t_p)} \approx \frac{1}{\sqrt{2\epsilon_1}} \frac{1}{M_{\text{P}}}. \quad (3.7)$$

One can reproduce the expected result by combining Eq. (2.17) for the spectrum of ϕ , Eq. (2.18) for the $\langle\zeta\zeta\rangle$ correlation function, and Eq. (3.7) for $N_\phi^{(t_p,t)}$, viz.,

$$\mathcal{P}_\zeta(p; t)_{\text{tree}} = \frac{1}{8\pi^2\epsilon_1} \frac{H(t_p)^2}{M_{\text{P}}^2}. \quad (3.8)$$

Evolution during ultra-slow-roll epoch.—After horizon-exit, \mathcal{P}_ζ becomes time-independent if the evolution is adiabatic. Alternatively, if isocurvature modes are present, it may evolve on a slow-roll timescale until the onset of the ultra-slow-roll phase. At that time a different analysis is required to determine its evolution.

During ultra-slow-roll the potential gradient is very shallow, so that $(\epsilon_V)_{\text{USR}}$ is extremely small. This can occur, for example, if the potential includes almost-stationary point of inflection (see, e.g., [91–93]), or a bump or dip [94, 95]. At the beginning of the ultra-slow-roll phase, the inflaton velocity is (comparatively) large, since it is controlled by $\epsilon_1 \gg (\epsilon_V)_{\text{USR}}$. The potential is no longer sufficient to support this velocity, so $\dot{\phi}$ must be balanced by the acceleration term rather than V' ,

$$\ddot{\phi} + 3H\dot{\phi} \approx 0. \quad (3.9)$$

Notice that the transition must be reasonably abrupt in order that $\dot{\phi}$ does not have time to smoothly relax to a value that can be supported by the new shallow gradient $(\epsilon_V)_{\text{USR}}$. If

that were to happen, Eq. (3.9) would no longer apply and we would merely have a phase of very shallow slow-roll inflation.

The solution to Eq. (3.9) can be written

$$\phi \approx A + Be^{-3H(t-t_0)} \approx A + Be^{-3(N-N_0)} \approx A + B'\sqrt{2\epsilon} \quad (3.10)$$

where A , B (and B') are constants of integration, and t_0 , N_0 label an arbitrary reference time. In the second approximate equality we have used $\Delta N \approx H\Delta t$, which follows because H is nearly constant. The final approximate equality uses $\epsilon \propto e^{-6Ht}$, which can be demonstrated using the first relation in (3.10).

The transition between slow-roll and ultra-slow-roll occurs on a hypersurface $\phi(t_s) = \text{const}$, determined by the position on the potential where the gradient rapidly decreases. Up to the transition point, the slow-roll attractor operates to lock the momentum fluctuation to the field fluctuation, as in (3.6). At the transition point, this typically makes $\delta\pi$ a few orders of magnitude smaller than $\delta\phi$. Meanwhile, if it is not extinguished, the decaying term is responsible for different regions of the universe entering the ultra-slow-roll phase with very slightly different values of the field momentum. However, it rapidly becomes negligible provided the horizon-exit time t_p occurs appreciably before the transition.

During ultra-slow-roll, Eq. (3.10) requires the momentum to decay exponentially, $\pi \propto e^{-3N}$. Inverting this relation, it follows that the number of e-folds that elapse during the ultra-slow-roll phase can be written

$$N^{(t_s,t)} \approx \frac{1}{3} \ln \frac{\pi_s}{\pi(t)}, \quad (3.11)$$

where, as explained above, t_s labels the start of the ultra-slow-roll phase and π_s is the value of the momentum at this time. If the decaying mode is present, it will contribute a small δN through variation in the initial and final momenta. To apply Eq. (3.11) to compute ζ , we should choose the final time t to lie on a hypersurface of fixed ϕ . These hypersurfaces practically coincide with slices of fixed density, because the kinetic energy is decaying exponentially.

We can now determine how \mathcal{P}_ζ evolves at the transition and during the ultra-slow-roll epoch. The number of elapsed e-folds $N^{(t_p,t)}$ should be broken into a slow-roll contribution $N^{(t_p,t_s)}$ from Eq. (3.5), and an ultra-slow-roll contribution $N^{(t_s,t)}$ from Eq. (3.11). These components join on the fixed surface $\phi(t_s) = \text{const}$. Therefore, the only contribution to δN from the slow-roll part is due to variation with respect to $\phi(t_p)$. Next, consider variation of the ultra-slow-roll part $N^{(t_s,t)}$. We first ignore the decaying mode of the momentum, so at the transition $\delta\pi_s$ would be determined by $\delta\phi_s$. During the ultra-slow-roll phase $\delta\pi$ would continue to be determined by Eq. (3.6). It follows that there is no late-time contribution from either the initial or final slices in (3.11). (Recall that $\phi(t_s)$ is fixed, and $\phi(t)$ is also fixed if the final slice has constant energy density.)

We now restore the decaying mode, which generates a contribution to δN from variation of (3.11) with respect to π , on both the initial and final hypersurface. This yields a *growing* contribution to $\langle\zeta\zeta\rangle$, which is proportional to $\pi^{-2}(t) = \epsilon^{-1}$. During an ultra-slow-roll phase this grows like e^{6N} . This growing contribution is very significant for modes that exit near

the transition, or during the ultra-slow-roll phase [54]. (See §3.2.) However, for modes such as \mathbf{p} that exit significantly before the transition, suppression of the decaying mode is very strong. In principle, its influence could be recovered if the ultra-slow-roll phase lasts for a sufficiently long time. However, in a model intended to produce a realistic abundance of primordial black holes, we typically expect only between 2 and 2.5 e-folds of ultra-slow-roll inflation [25].

The conclusion is that provided the horizon exit time t_p occurs more than a few e-folds before the transition, the decaying mode will be sufficiently extinguished that even the rapid e^{6N} enhancement during ultra-slow-roll cannot compensate for it. Therefore \mathcal{P}_ζ will practically not evolve during the whole ultra-slow-roll phase. It will also not evolve during the final slow-roll epoch, provided the evolution there is adiabatic. The conclusion is that $\mathcal{P}_\zeta(p)$ for the CMB mode is given by (3.8), with t now labelling a time during the second slow-roll epoch. Up to this point our analysis agrees with the discussion given in Cai *et al.* [54] and Firouzjahi & Riotto [23].

3.2 Peak scales based at horizon exit

Next, we calculate the tree-level power spectrum for a short-scale mode, \mathbf{k} , in the vicinity of the peak in the power spectrum. This mode is taken to cross during the ultra-slow-roll phase. The number of e-folds that elapse from horizon exit at $t = t_k$ up to some later time t —still assumed to be within the ultra-slow-roll epoch—is determined by Eq. (3.11) with the replacement $t_s \rightarrow t_k$,

$$N^{(t_k, t)} = \frac{1}{3} \ln \frac{\pi(t_k)}{\pi(t)}. \quad (3.12)$$

Unlike the CMB-scale mode \mathbf{p} , the $\delta\pi$ fluctuation at \mathbf{k} is independent of the field fluctuation. Therefore Eq. (3.12) yields a significant growing mode during the ultra-slow-roll phase, arising from variation in (3.12) between smoothed regions. To determine the final value of $\mathcal{P}_\zeta(k)$ we should follow the evolution of this mode until the dynamics become adiabatic. This requires a detailed description of the transition into the second slow-roll epoch. Following Ref. [54] we write the scalar field solution (3.10) during ultra-slow-roll in terms of the field and momentum expectation values ϕ_e , π_e (respectively) attained at time $t = t_e$, at the end of ultra-slow-roll. That yields

$$\phi(N) = \phi_e + \frac{\pi_e - \pi(N)}{3} \quad \text{and} \quad \pi(N) = \pi_e e^{-3(N-N_e)}. \quad (3.13)$$

We are not necessarily taking the transition into the second slow-roll phase to be abrupt, so it need not be meaningful to talk about a precise moment where the transition happens. For our purposes in this paper we assume it is possible to write down a condition that marks the division between ultra-slow-roll and slow-roll, at least to a reasonable approximation. (See the footnote 15 on p. 27.) Considering the exponential decay of the velocity during ultra-slow-roll, this condition must identify a practically unique value ϕ_e that does not vary from region to region. (If the phase of ultra-slow-roll inflation is extremely short, however, it may be necessary to allow for this possibility.)

To describe the subsequent slow-roll epoch we require information about the potential that supports it. Our analysis again follows Cai *et al.* [54]. Since $V(\phi)$ is assumed to be

fairly smooth, it can be represented near ϕ_e as a series,

$$V(\phi) \approx V_e \left[1 + (2\epsilon_2)^{1/2} \frac{\phi - \phi_e}{M_{\text{P}}} + \frac{1}{2} \eta_2 \left(\frac{\phi - \phi_e}{M_{\text{P}}} \right)^2 + \dots \right], \quad (3.14)$$

where $V_e \equiv V(\phi_e)$ is the fixed value of the potential on the transition hypersurface $\phi = \phi_e$. In this expression, $\epsilon_2 = (\epsilon_V)_2$ and $\eta_2 = (\eta_V)_2$ are taken to be roughly constant during the second slow-roll epoch, and to coincide with their values at $\phi = \phi_e$. We will use Eq. (3.14) only on the slow-roll side of the transition. The smoothness of this transition is quantified by the dimensionless parameter h [54]

$$h \equiv 6(2\epsilon_2)^{1/2} \frac{M_{\text{P}}}{\pi_e}. \quad (3.15)$$

This compares the actual inflation velocity at the end of the ultra-slow-roll epoch $\sim \pi_e$ to the natural value $\sim \epsilon_2^{1/2} M_{\text{P}}$ in the slow-roll phase. In the limit $h \rightarrow 0$, the transition becomes increasingly smooth. If the inflaton approaches the second slow-roll plateau with a velocity that matches the one on the second slow-roll attractor, $\pi_e = -(2\epsilon_2)^{1/2} M_{\text{P}}$, this corresponds to an instantaneous transition, described by $h = -6$.

The solutions for ϕ and π *after* the transition can be found by solving the slow-roll equation (3.4) using Eq. (3.14). The solutions matching ϕ_e, π_e , respectively, at the transition time $N = N_e$ can be written¹⁷

$$\begin{aligned} \phi(N) = \phi_e + \frac{2h\pi_e}{s^2 - 9} + \pi_e \frac{s - 3 - h}{s(s - 3)} \exp \left[\frac{s - 3}{2} (N - N_e) \right] \\ - \pi_e \frac{s + 3 + h}{s(s + 3)} \exp \left[-\frac{s + 3}{2} (N - N_e) \right], \end{aligned} \quad (3.16a)$$

$$\pi(N) = \pi_e \exp \left[-\frac{3}{2} (N - N_e) \right] \left[\cosh \frac{s(N - N_e)}{2} - \frac{3 + h}{s} \sinh \frac{s(N - N_e)}{2} \right], \quad (3.16b)$$

where s is defined to satisfy $s^2 \equiv 9 - 12\eta_2$. The final term in Eq. (3.16a) is subleading when N is at least modestly larger than N_e . Dropping this subleading contribution, the number of e-folds $N^{(t_e, t)}$ that elapse between hypersurfaces corresponding to $\phi = \phi_e$ and $\phi = \phi(t)$, can be found by inverting (3.16a),

$$N^{(t_e, t)} \approx \frac{2}{s - 3} \ln \left[\left(\phi(t) - \phi_e - \frac{12M_{\text{P}}(2\epsilon_2)^{1/2}}{s^2 - 9} \right) \frac{s(s - 3)}{\pi_e(s - 3 - h)} \right]. \quad (3.17)$$

The number of e-folds $N^{(t_k, t)}$ that elapse from horizon exit of the mode \mathbf{k} at time t_k , up to some practically uniform-density slice $\phi = \phi(t)$ during the second slow-roll era, should be obtained by summing (3.12) (with the replacement $t \rightarrow t_e$) and (3.17).

To use (2.2) to determine the time evolution of $\zeta_{\mathbf{k}}$, we vary $N^{(t_k, t)}$ with respect to the initial conditions at $t = t_k$. In doing so, we must keep ϕ_e and $\phi(t)$ fixed. Also, we are taking ϵ_2 and η_2 to be determined by ϕ_e , so these slow-roll parameters are also fixed. Only π_e will vary; it should be regarded as a function of the initial values $\phi(N_k)$ and $\pi(N_k)$ via

¹⁷There is a typo in Eq. (2.17) of Ref. [54], which is corrected in our Eq. (3.16b).

the solution for $\phi(N)$ in Eq. (3.13). This implies $\delta\pi_e/\delta\phi(N_k) = 3$, $\delta\pi_e/\delta\pi(N_k) = 1$. Taken together, these conditions mean that the only contribution from Eq. (3.17) comes from the factor $\pi_e(s - 3 - h)$ inside the logarithm. Hence we may write [23, 54]

$$N^{(t_k, t)} \asymp \frac{1}{3} \ln \frac{\pi(N_k)}{\pi_e} - \frac{2}{s-3} \ln \left| \frac{\pi_e}{M_{\text{P}}} (s - 3 - h) \right| \approx \frac{1}{3} \ln \frac{\pi(N_k)}{\pi_e} + \frac{1}{\eta_2} \ln \left[2\eta_2 \frac{\pi_e}{M_{\text{P}}} + 6(2\epsilon_2)^{1/2} \right]. \quad (3.18)$$

The symbol ‘ \asymp ’ is used to mean that this expression produces the same *derivatives* as the full formula for $N^{(t_k, t)}$, although it is not numerically equal. The second approximate equality follows by expanding s to lowest order in η_2 . Eq. (3.18) agrees with the expression Eq. (II.21) reported by Firouzjahi & Riotto [23], except that we do not have their first term representing the number of e-folds accumulated during the first slow-roll phase. This was discussed above in §3.1. However, it is not needed here: Eq. (2.7) requires that we base our separate universe formula at a time $t_* \sim t_k$, just a little later than the horizon exit time of the peak modes, which is already within the ultra-slow-roll phase. See §2.2 for more details.

Taking variations with respect to the ϕ and π fields at this time, we conclude

$$N_{\phi}^{(t_k, t)} = -\frac{1}{\pi_e} + \frac{3}{3M_{\text{P}}(2\epsilon_2)^{1/2} + \eta_2\pi_e} = \frac{1}{\pi_e} \left(-1 + \frac{6}{h + 2\eta_2} \right), \quad (3.19a)$$

$$N_{\pi}^{(t_k, t)} = \frac{1}{3\pi(N_k)} - \frac{1}{3\pi_e} + \frac{1}{3M_{\text{P}}(2\epsilon_2)^{1/2} + \eta_2\pi_e} = \frac{1}{3\pi_e} \left(\frac{\pi_e}{\pi(N_k)} - 1 + \frac{6}{h + 2\eta_2} \right). \quad (3.19b)$$

For both N_{ϕ} and N_{π} , we have re-introduced the smoothness parameter h in the second equality. This makes the dependence of the qualitative nature of the transition explicit.

Notice that, although our background model (3.18) agrees with Firouzjahi & Riotto [23], the derivatives Eq. (3.19a)–(3.19b) do not agree with the derivatives reported by these authors. Firouzjahi & Riotto reported $N_{\pi} \approx 0$ and gave an expression for N_{ϕ} —Eq. (II.24) of Ref. [23]—that agrees with our formula (3.7). This is because Ref. [23] always elected to base the separate universe formula at a time $t_* = t_p$ close to horizon exit for the CMB-scale **p**-mode. (See §2.2.) At this time the $\delta\pi$ mode can be neglected, as discussed above. The δN coefficients needed for our Eq. (2.7) are those of Eqs. (3.19a)–(3.19b).

If the transition is at least modestly smooth, the denominator of $6/(h + 2\eta_2)$ is small. Therefore this term gives the dominant contribution to both derivatives. If h is not significantly smaller than η_2 ,¹⁸ we find

$$N_{\phi}^{(t_k, t)} \approx \frac{6}{h\pi_e} \approx \frac{1}{M_{\text{P}}} \frac{1}{(2\epsilon_2)^{1/2}}. \quad (3.20)$$

A similar expression can be given for $N_{\pi}(t_k, t)$, but to calculate $\mathcal{P}_{\zeta}(k; t)$ for modes that cross the horizon during ultra-slow-roll we do not need it. For these modes, the field perturbation primarily populates the constant *A*-mode of Eq. (3.10). Accordingly, the momentum perturbation decays outside the horizon. It follows that the tree-level power spectrum Eq. (2.18) can be written

$$\mathcal{P}_{\zeta}(k; t)_{\text{tree}} = \left[N_{\phi}^{(t_k, t)} \right]^2 \mathcal{P}_{\phi\phi}(k; t_k) = \frac{1}{8\pi^2\epsilon_2} \frac{H(t_k)^2}{M_{\text{P}}^2} \quad (\text{assuming } t > t_e), \quad (3.21)$$

¹⁸For a discussion of the $h \ll 1$ expansion, see footnote 24 on p. 43.

where we have used (3.20).

We emphasize that (3.21) applies only after the transition into the second slow-roll epoch. At earlier times, \mathcal{P}_ζ is roughly given by $\mathcal{P}_\zeta \approx \mathcal{P}_{\phi\phi}/(2M_{\text{p}}^2\epsilon)$. This is rapidly growing, because the factor ϵ is decaying like e^{-6N} . The late-time value therefore should be evaluated when the dynamics become adiabatic. In this model, that occurs after the transition to the second slow-roll epoch, when $\epsilon \approx \epsilon_2$. This provides a qualitative explanation for the result of Eq. (3.21).

3.3 CMB scales based at exit time for peak scales

Finally, we demonstrate how to compute the tree-level power spectrum for the CMB-scale mode \mathbf{p} , but now using the separate universe formula (2.2) based at $t_* = t_k$, the horizon-crossing time for the peak-scale modes. According to (2.7) it is this arrangement that is required to compute the back-reaction from enhanced modes \mathbf{k} . Clearly, the answer must agree with our previous explicit calculation (3.8).

Eq. (3.7) shows that, for a mode \mathbf{p} that exits during the first slow-roll phase, $\zeta_{\mathbf{p}} = \delta\phi/(2M_{\text{p}}^2\epsilon)^{1/2}$. Since $\zeta_{\mathbf{p}}$ is conserved on superhorizon scales during this epoch, it follows that (to linear order) the growing mode of $\delta\phi$, evaluated at the transition $t = t_s$ into the ultra-slow-roll phase, can be written¹⁹

$$\delta\phi_{\mathbf{p}}(t_s) = \left(\frac{\epsilon(t_s)}{\epsilon(t_p)}\right)^{1/2} \delta\phi_{\mathbf{p}}(t_p). \quad (3.22)$$

After the transition, $\delta\phi$ evolves according to the solution (3.10). Assuming ϵ varies continuously, and matching smoothly across the transition, it follows that $\delta\phi$ will populate only the B -mode of this solution. Hence, at some time t during the ultra-slow-roll phase, we have

$$\delta\phi_{\mathbf{p}}(t) = \left(\frac{\epsilon(t)}{\epsilon(t_p)}\right)^{1/2} \delta\phi_{\mathbf{p}}(t_p) \quad (3.23a)$$

$$\delta\pi_{\mathbf{p}}(t) = \frac{\eta(t)}{2} \delta\phi_{\mathbf{p}}(t) \approx -3\delta\phi_{\mathbf{p}}(t). \quad (3.23b)$$

In the final step we have used $\eta \approx -6$, which is valid during ultra-slow-roll. This is very different to the behaviour of perturbations that exit in the ultra-slow-roll phase, described in §3.2. For an explicit numerical example, see Fig. 12. For those \mathbf{k} -scale modes, the field perturbation is primarily in the constant A -mode, and $\delta\pi$ rapidly becomes small. In contrast, for the \mathbf{p} -scale modes, the field perturbation is in the B -mode and $\delta\pi$ rapidly *grows* during the transition to ultra-slow-roll, becoming comparable to (in fact, slightly larger than) $\delta\phi$. It follows that we *cannot* neglect the momentum perturbation when the separate universe formula is based at $t = t_k$.

The power spectrum is readily computed from Eqs. (3.19a)–(3.19b). Working from Eq. (2.18) and substituting for $\delta\phi$, $\delta\pi$ using Eqs. (3.23a)–(3.23b),

$$\mathcal{P}_\zeta(p; t)_{\text{tree}} = \left[N_\phi^{(t_k, t)}\right]^2 \mathcal{P}_{\phi\phi}(p, t_k) + 2N_\phi^{(t_k, t)} N_\pi^{(t_k, t)} \mathcal{P}_{\phi\pi}(p, t_k) + \left[N_\pi^{(t_k, t)}\right]^2 \mathcal{P}_{\pi\pi}(p, t_k). \quad (3.24)$$

¹⁹Recall that in §3.1 we concluded the decaying mode could be safely dropped for modes that exit the horizon at least a few e-folds before the transition.

We have used $\mathcal{P}_{\pi\phi}(p, t_k) = \mathcal{P}_{\phi\pi}(p, t_k)$, which is approximately true because ϕ and π nearly commute outside the horizon. There is significant cancellation between the $\delta\phi$ and $\delta\pi$ terms in this expression. We find

$$\mathcal{P}_\zeta(p; t)_{\text{tree}} = \frac{1}{\pi(N_k)^2} \mathcal{P}_{\phi\phi}(p, t_k) = \frac{1}{2\epsilon(N_k)M_{\text{P}}^2} \frac{\epsilon(N_k)}{\epsilon(t_p)} \frac{H(t_p)^2}{4\pi^2} = \frac{1}{8\pi^2\epsilon(t_p)} \frac{H(t_p)^2}{M_{\text{P}}^2}. \quad (3.25)$$

In the final step we have used $\pi(N_k) = -M_{\text{P}}[2\epsilon(N_k)]^{1/2}$, which follows from (3.4) and (3.10). Since $\epsilon(t_p) \approx \epsilon_1$, this reproduces our earlier expression (3.8).

The primary conclusion from this analysis is that a correct outcome for the \mathbf{p} -scale mode requires inclusion of the momentum fluctuation when the separate universe expansion is based near the horizon exit time for the short modes. This calculation also provides a sanity-check of the δN expressions which we will use in §4 to calculate the one-loop corrections.

4 Case study: δN loops in the 3-phase ultra-slow-roll model

In this section, we apply the general formula (2.7) to compute the one-loop correction for the 3-phase ultra-slow-roll model of §3. In §4.1, §4.2 and §4.3 we give explicit expressions for the enhanced part of the 12-loop, 22-loop, and 13-loop, respectively, as defined in §2.2.3.

When using (2.7) to compute one-loop corrections, or correlation functions in general, we are obliged to carry out Wick contractions among the phase space fluctuations. These are best visualized using a diagrammatic expansion. In the case of the 3-phase model, the phase space coordinates X^I comprise a field value ϕ and its momentum π , and the corresponding diagrammatic representation is summarized in Fig. 6. In the following sections we use these diagrams to enumerate the contractions that contribute to each type of loop.

4.1 12-loop

The 12-type loop (2.19) was discussed in §2.2. It corresponds to the first diagram in Fig. 5. Here, we specialize it to the 3-phase model. In Eq. (2.19), the large-scale fluctuation $\delta X_{\mathbf{p}}^I(t_k)$ can be of either field or velocity type: they are both relevant and comparable at time t_k . (See Eqs. (3.23a)–(3.23b), which are valid for a large-scale mode during ultra-slow-roll.) The convolution integral runs over momenta $q \lesssim k$, where k continues to identify the peak scales. In this section, when making explicit estimates, we integrate loop momenta from the first mode leaving the horizon during ultra-slow-roll ($q = k_s$), up to the last such mode ($q = k_e$). Hence, the generic scale k can be interpreted as $k \sim k_e$, and likewise $t_k \sim t_{k_e}$.

The hierarchy $p \ll q$ implies that the momenta \mathbf{q} and $-\mathbf{p} - \mathbf{q}$ appearing in Eq. (2.19) correspond to peak scales. For these, the velocity auto- and cross-correlations become negligible soon after horizon crossing. Therefore we can neglect the velocity fluctuations. For an explicit numerical example, see the bottom panel of Fig. 12. It follows that the 12-type contribution to the $\langle \zeta \zeta \rangle$ correlation function can be written

$$\begin{aligned} \langle \zeta_{\mathbf{p}} \zeta_{-\mathbf{p}} \rangle_{12} &= N_{\phi\phi}^{(t_k, t)} \int_{k_s \lesssim q \lesssim k_e} \frac{d^3 q}{(2\pi)^3} \\ &\times \left(N_{\phi}^{(t_k, t)} \langle \delta\phi_{\mathbf{p}}(t_k) \delta\phi_{\mathbf{q}}(t_k) \delta\phi_{-\mathbf{p}-\mathbf{q}}(t_k) \rangle + N_{\pi}^{(t_k, t)} \langle \delta\pi_{\mathbf{p}}(t_k) \delta\phi_{\mathbf{q}}(t_k) \delta\phi_{-\mathbf{p}-\mathbf{q}}(t_k) \rangle \right). \quad (4.1) \end{aligned}$$

$$\begin{aligned}
\zeta_{\mathbf{p}}(t) &= \text{---} \bullet \text{---} \{ \delta\phi^{(t_k)} \}_{\ell}]_{\mathbf{p}} + \text{---} \bullet \circ \circ \circ \circ \bullet \{ \delta\pi^{(t_k)} \}_{\ell}]_{\mathbf{p}} \\
&+ \frac{1}{2!} \int \frac{d^3q}{(2\pi)^3} \frac{N_{\phi\phi}^{(t_k,t)}}{\text{---} \bullet \text{---}} \left\{ \begin{array}{l} \{ \delta\phi^{(t_k)} \}_{\ell}]_{\mathbf{q}} \\ \{ \delta\phi^{(t_k)} \}_{\ell}]_{\mathbf{p}-\mathbf{q}} \end{array} \right. + \frac{1}{2!} \int \frac{d^3q}{(2\pi)^3} \frac{N_{\pi\pi}^{(t_k,t)}}{\text{---} \bullet \circ \circ \circ \circ \bullet} \left\{ \begin{array}{l} \{ \delta\pi^{(t_k)} \}_{\ell}]_{\mathbf{q}} \\ \{ \delta\pi^{(t_k)} \}_{\ell}]_{\mathbf{p}-\mathbf{q}} \end{array} \right. + \dots \\
&+ \frac{1}{3!} \int \frac{d^3q_1}{(2\pi)^3} \int \frac{d^3q_2}{(2\pi)^3} \frac{N_{\phi\phi\phi}^{(t_k,t)}}{\text{---} \bullet \text{---}} \left\{ \begin{array}{l} \{ \delta\phi^{(t_k)} \}_{\ell}]_{\mathbf{q}_1} \\ \{ \delta\phi^{(t_k)} \}_{\ell}]_{\mathbf{q}_2} \\ \{ \delta\phi^{(t_k)} \}_{\ell}]_{\mathbf{p}-\mathbf{q}_1-\mathbf{q}_2} \end{array} \right. + \dots
\end{aligned}$$

Key

— long wavelength field $\zeta_{\mathbf{p}}$

-- field fluctuation $\delta\phi$

◦◦◦◦ momentum fluctuation $\delta\pi$

• contraction between the δN coefficients N_I, N_{IJ}, \dots , and fluctuations $X^I = \{\delta\phi, \delta\pi\}$

$N_{\phi}^{(t_k,t)}$ $\delta N(t)/\delta\phi(t_k)$ (similarly for higher-order derivatives)

$N_{\pi}^{(t_k,t)}$ $\delta N(t)/\delta\pi(t_k)$ (similarly for higher-order derivatives)

Figure 6: Diagrammatic form of the separate universe formula for $\zeta_{\mathbf{p}}$, Eq. (2.7), for a single-field model with a transient phase of ultra-slow-roll. The δN expansion has been based at the horizon-crossing time t_k of the peak-scale modes.

In the language of Fig. 6, this can be represented diagrammatically as

$$\langle \zeta_{\mathbf{p}} \zeta_{-\mathbf{p}} \rangle_{12} = \text{---} \bullet \text{---} \circ \circ \circ \circ \bullet \text{---} + \text{---} \bullet \circ \circ \circ \circ \bullet \text{---} \circ \circ \circ \circ \bullet \text{---} . \quad (4.2)$$

We can rewrite (4.1) in a more compact form by using Eq. (3.23b),

$$\langle \zeta_{\mathbf{p}} \zeta_{-\mathbf{p}} \rangle_{12} = N_{\phi\phi}^{(t_k,t)} \left(N_{\phi}^{(t_k,t)} + \frac{\eta}{2} N_{\pi}^{(t_k,t)} \right) \int_{k_s \lesssim q \lesssim k_e} \frac{d^3q}{(2\pi)^3} \langle \delta\phi_{\mathbf{p}}(t_k) \delta\phi_{\mathbf{q}}(t_k) \delta\phi_{-\mathbf{p}-\mathbf{q}}(t_k) \rangle . \quad (4.3)$$

The prefactor $N_{\phi}^{(t_k,t)} + \eta N_{\pi}^{(t_k,t)}/2$ appears frequently and is equal to the *total* field-space variation $\delta N^{(t_k,t)}/\delta\phi$ assuming the slow-roll attractor condition. As would be expected, in a single-field model on this attractor, we could (if we wished) eliminate the phase-space momentum $\delta\pi$.

The three-point correlation function appearing in (4.3) is in a squeezed configuration where $p \ll q$ and $|\mathbf{p} + \mathbf{q}| \simeq q$. It acts as a book-keeper of the hierarchy between large and

small scales. On physical grounds we expect it must (formally) vanish in the limit of an infinite separation where $p/k \rightarrow 0$. In this limit we expect that all back-reaction decouples and the 12-loop should vanish.

In Ref. [45] this squeezed three-point function was estimated using soft-limit arguments, with the outcome²⁰

$$\alpha^{IJK}(p, q_1, q_2; t_q) \simeq P^{IM}(p; t_q) P^{JK}_M(q; t_q) \quad \text{where } |\mathbf{q}_1| \sim |\mathbf{q}_2| \sim q \text{ and } p \ll q. \quad (4.4)$$

This result does not rely on the slow-roll approximation [45]. We expect that leading corrections to (4.4) are at relative order $(p/k)^2$ or higher. The quantity P^{IM} is the cross-power spectrum between X^I and X^M , and P^{JK}_M is defined to be the derivative

$$P^{JK}_M(q; t_q) \equiv \frac{\partial P^{JK}(q, t_q)}{\partial X^M(t_q)}. \quad (4.5)$$

In order to apply Eq. (4.4) we must push *back* the evaluation time for each fluctuation appearing in Eq. (4.3) from time t_k to the earlier time $t_q < t_k$. For the large-scale mode $\delta\phi_{\mathbf{p}}$, the linear time evolution is described by Eq. (3.23a). At the level to which we are now working, it should be supplemented by a quadratic correction. However, we drop this quadratic piece because it produces a result similar to the 22-loop and is therefore volume-suppressed, as explained in §2.2.2, and to be shown in detail in §4.2 below. Meanwhile, the peak-scale modes $\delta\phi_{\mathbf{q}}$ and $\delta\phi_{-\mathbf{p}-\mathbf{q}}$ are dominated by the constant ‘A-mode’ (again up to possible quadratic corrections that we drop). Therefore we may simply shift $\delta\phi_{\mathbf{q}}(t_k) \rightarrow \delta\phi_{\mathbf{q}}(t_q)$. It follows that

$$\langle \zeta_{\mathbf{p}} \zeta_{-\mathbf{p}} \rangle_{12} = N_{\phi\phi}^{(t_k, t)} \left(N_{\phi}^{(t_k, t)} + \frac{\eta}{2} N_{\pi}^{(t_k, t)} \right) \int_{k_s \lesssim q \lesssim k_e} \frac{d^3 q}{(2\pi)^3} \sqrt{\frac{\epsilon(t_k)}{\epsilon(t_q)}} \langle \delta\phi_{\mathbf{p}}(t_q) \delta\phi_{\mathbf{q}}(t_q) \delta\phi_{-\mathbf{p}-\mathbf{q}}(t_q) \rangle. \quad (4.6)$$

Eq. (4.6) clearly highlights the two ingredients necessary to obtain a non-vanishing 12-type loop correction. First, the small-scale modes $\delta\phi_{\mathbf{q}}$ and $\delta\phi_{-\mathbf{p}-\mathbf{q}}$ must *react* to the presence of the long-wavelength curvature perturbation. The nature of this reaction is encoded in the expression for the squeezed bispectrum. Specifically, the derivative (4.5) is non-vanishing only when the small-scale power spectrum depends on the background, which absorbs the contribution of the long mode $\zeta_{\mathbf{p}}$.

Second, one needs *non-linearity* in the mapping between the late-time, large-scale curvature perturbation $\zeta_{\mathbf{p}}(t)$ and the short scale field fluctuations. This requires $N_{\phi\phi}^{(t_k, t)} \neq 0$, which would generate a contribution to the *equilateral* bispectrum for momentum configurations of characteristic scale k . The conclusion is that the amplitude of the 12-type diagram depends on *two* distinct types of non-Gaussianity: one accounting for long–short mode coupling, and one measuring the non-linear interactions of the small-scale modes among themselves.

²⁰Note that Ref. [45] worked on the slow-roll attractor, so their Latin indices run over field-space labels only and exclude the momenta. However, their formulae are valid more generally. In the present case we are considering a single-field model, but with indices running over its field value and velocity.

Combining Eq. (4.4) and Eq. (4.6) yields

$$P_\zeta(p; t)_{12} = N_{\phi\phi}^{(t_k, t)} \left(N_\phi^{(t_k, t)} + \frac{\eta}{2} N_\pi^{(t_k, t)} \right) \int_{k_s \lesssim q \lesssim k_e} \frac{d^3 q}{(2\pi)^3} \sqrt{\frac{\epsilon(t_k)}{\epsilon(t_q)}} P^{\phi M}(p; t_q) P^{\phi\phi}_M(q; t_q). \quad (4.7)$$

As explained above, we use Eq. (2.17) to express the small-scale power spectrum $P^{\phi\phi}(q; t_q)$ as a function of $H(t_q)$ only. This is equivalent to the assumption that modes exiting the horizon during ultra-slow-roll were always in ultra-slow-roll, and will not reproduce the characteristic oscillations in the tree-level power spectrum at peak scales. These are due to a spike in η_V corresponding to the SR \rightarrow USR transition, which displaces the mode functions. (For an explicit numerical example see Fig. 10. A related discussion appears in Ref. [55].) Our treatment does not include the effect of these oscillations. We anticipate that they would typically boost the derivative (4.5). Therefore our results should be regarded as a minimal estimate for the one-loop correction produced within these models.

The estimates presented here, and in §§4.2–4.3 below, such as Eq. (4.7), account for the contribution to the loop from a band of modes whose amplitude is enhanced by ultra-slow-roll effects. They are intended to be comparable to estimates reported by other authors. In a realistic model one would have to understand how this enhanced band is connected to the broadband power spectrum at its high- and low-momentum boundaries.²¹ In particular, we shall not account for contributions from modes rising towards, or falling away from, a possible peak, which are typically present in realistic models. These modes are potentially implicated in cancellations that could reduce the size of the loop [14, 31, 32]. Accordingly, we caution that the results should be interpreted with care.

Due to the flatness of the potential during ultra-slow-roll, the derivative of $P^{\phi\phi}(q; t_q)$ with respect to ϕ is suppressed by $|V'/V| \ll 1$, and only the derivative with respect to π will contribute. Hence,

$$\frac{\partial H(t_q)^2}{\partial \pi(t_q)} \approx H(t_q)^2 \frac{\pi(t_q)}{3M_{\text{P}}^2} = -H(t_q)^2 \frac{[2\epsilon(t_q)]^{1/2}}{3M_{\text{P}}}. \quad (4.8)$$

Substitution in Eq. (4.7) yields

$$P_\zeta(p; t)_{12} = -N_{\phi\phi}^{(t_k, t)} \left(N_\phi^{(t_k, t)} + \frac{\eta}{2} N_\pi^{(t_k, t)} \right) \frac{[2\epsilon(t_k)]^{1/2}}{6M_{\text{P}}} \int_{k_s \lesssim q \lesssim k_e} \frac{d^3 q}{(2\pi)^3} P^{\phi\pi}(p; t_q) \frac{H(t_q)^2}{q^3}. \quad (4.9)$$

Using Eqs. (3.23a)–(3.23b), one can derive the 2-point correlations for the large-scale fluctuations during the ultra-slow-roll phase. They are

$$P^{\phi\phi}(p; t_q) = \frac{\epsilon(t_q)}{\epsilon(t_p)} \frac{H(t_p)^2}{2p^3}, \quad P^{\pi\pi}(p; t_q) = \frac{\eta^2}{4} P^{\phi\phi}(p; t_q), \quad P^{\phi\pi}(p; t_q) = P^{\pi\phi}(p; t_q) = \frac{\eta}{2} P^{\phi\phi}(p; t_q). \quad (4.10)$$

²¹In our explicit numerical examples, such as Fig. 10, this band forms a plateau and is not completed to a peak. This is because the dynamics of our 3-phase ultra-slow-roll model does not allow the power spectrum amplitude to reduce significantly even after the ultra-slow-roll phase has ended. However, our analytic formulae are more general than this scenario.

We have left factors of η explicit in order that they may be counted, but it should be remembered that $\eta \approx -6$ during ultra-slow-roll. We conclude that the amplitude of the 12-loop relative to the tree-level can be written

$$\begin{aligned} \Delta\mathcal{P}_\zeta(p; t)_{12} &\equiv \frac{\mathcal{P}_\zeta(p; t)_{12}}{\mathcal{P}_\zeta(p; t)_{\text{tree}}} \\ &= -N_{\phi\phi}^{(t_k, t)} \left(N_\phi^{(t_k, t)} + \frac{\eta}{2} N_\pi^{(t_k, t)} \right) \frac{\eta M_{\text{P}}}{6} [2\epsilon(t_k)]^{1/2} \frac{H^2}{2\pi^2} \int_{k_s}^{k_e} \frac{dq}{q} \epsilon(t_q), \end{aligned} \quad (4.11)$$

The quantity H represents the Hubble parameter during the ultra-slow-roll phase, which is nearly time-independent. From Eqs. (3.19a)–(3.19b) we note that

$$N_\pi^{(t_k, t)} = \frac{N_\phi^{(t_k, t)}}{3} + \frac{1}{3\pi(t_k)} = \frac{N_\phi^{(t_k, t)}}{3} - \frac{1}{3M_{\text{P}}[2\epsilon(t_k)]^{1/2}}. \quad (4.12)$$

When substituted in Eq. (4.11) this yields

$$\Delta\mathcal{P}_\zeta(p; t)_{12} = -N_{\phi\phi}^{(t_k, t)} \left[N_\phi^{(t_k, t)} \left(1 + \frac{\eta}{6} \right) [2\epsilon(t_k)]^{1/2} - \frac{\eta}{6M_{\text{P}}} \right] \frac{\eta M_{\text{P}}}{6} \frac{H^2}{2\pi^2} \int_{k_s}^{k_e} \frac{dq}{q} \epsilon(t_q). \quad (4.13)$$

For ultra-slow-roll models the contribution proportional to $N_\phi^{(t_k, t)}$ cancels and can be discarded. The remainder comes from the second term in square brackets. For a smooth transition, this term is smaller than the one associated with $N_\phi^{(t_k, t)}$; for an explicit numerical example, see the right panel in Fig. 8.

To perform the momentum integral we note that, during ultra-slow-roll, the time-dependence of the ϵ parameter has a simple expression when written in terms of the momenta,

$$\epsilon(t_q) = \epsilon(t_s) \left(\frac{k_s}{q} \right)^6. \quad (4.14)$$

This yields

$$\Delta\mathcal{P}_\zeta(p; t)_{12} = N_{\phi\phi}^{(t_k, t)} \left(\frac{\eta}{6} \right)^2 \frac{\epsilon(t_s)}{12\pi^2} H^2. \quad (4.15)$$

As has already been explained, $N_{\phi\phi}^{(t_k, t)}$ will contribute to the cubic non-linearity parameter (2.4b) evaluated on a peak-scale equilateral configuration, $f_{\text{NL}}^{\text{eq}}(k, k, k; t)$. In certain circumstances it actually provides the dominant contribution. Specifically, f_{NL} receives two contributions: one from the intrinsic bispectrum α^{IJK} of the phase-space fluctuations, and another from non-linear evolution on super-horizon scales. It is this non-linear effect that is encoded by the second derivative $N_{IJ}^{(t_k, t)}$ [39]. We distinguish these contributions by schematically writing $f_{\text{NL}} = f_{\text{NL}}^{(\alpha)} + f_{\text{NL}}^{(N_{IJ})}$. If the intrinsic bispectrum is small, then $f_{\text{NL}}^{(N_{IJ})}$ will be comparable to the total f_{NL} . For equilateral configurations evaluated on the peak scale, $f_{\text{NL}}^{(N_{IJ})}$ is

$$f_{\text{NL}}^{(N_{IJ})}(k; t) \approx \frac{5}{6} \frac{N_{\phi\phi}^{(t_k, t)}}{[N_\phi^{(t_k, t)}]^2} \equiv f_{\text{NL}}^{(N_{\phi\phi})}(k; t), \quad (4.16)$$

due to the fact that, over peak scales, the field fluctuation dominates the velocity fluctuation. Hence, using Eq. (3.19a) and its derivative, $f_{\text{NL}}^{(N_{\phi\phi})}$ can be written [54]

$$f_{\text{NL}}^{(N_{\phi\phi})}(k; t) = \frac{5}{2} \frac{[4\eta_2(\eta_2 - 3) + h^2 + 4\eta_2 h]}{(2\eta_2 + h - 6)^2}. \quad (4.17)$$

Both $N_{\phi}^{(t_k, t)}$ and $f_{\text{NL}}^{(N_{\phi\phi})}$ are constant over peak scales.²²

After substitution of Eqs. (4.16) and (3.21) in Eq. (4.15), we find

$$\Delta\mathcal{P}_{\zeta}(p; t)_{12} = \frac{2}{5} \left(\frac{\eta}{6}\right)^2 \epsilon(t_s) f_{\text{NL}}^{(N_{\phi\phi})}(\bar{k}; t) \mathcal{P}_{\zeta}(\bar{k})_{\text{tree}}. \quad (4.18)$$

We have written power spectrum, and the cubic nonlinearity parameter, in terms of a representative scale \bar{k} near the peak. In Eq. (4.18) we assume that p/k is finite, so the behaviour of the $p/k \rightarrow 0$ limit is no longer simple to extract.

In Eqs. (4.17)–(4.18), the evaluation time t of the correlation function $\langle \zeta_{\mathbf{p}} \zeta_{-\mathbf{p}} \rangle_{12}$ is taken to be during the final slow-roll phase, after the system has reached an adiabatic limit. In particular, the value of $f_{\text{NL}}^{(N_{\phi\phi})}(k; t)$ depends on the character of the USR→SR transition [54]. During the ultra-slow-roll phase we expect $f_{\text{NL}}^{(N_{\phi\phi})}(k; t) = \mathcal{O}(1)$ [97]. Later, for a sufficiently smooth transition, its amplitude decreases and becomes suppressed by a slow-roll parameter in the subsequent slow-roll phase [54]. If the transition is sudden then the evolution is more complicated and $f_{\text{NL}}^{(N_{\phi\phi})}$ may not be completely suppressed.

The physical meaning of each factor appearing in Eq. (4.18) can be understood as follows. First, the $(\eta/6)^2$ factor is due to the contribution of velocity fluctuations associated with the large-scale mode during ultra-slow-roll. Second, $\epsilon(t_s)$ acts as a book-keeper of the background evolution: for a perfectly de Sitter background ($\epsilon = 0$) the derivative in Eq. (4.8) vanishes, so the small-scale modes do not react to the large-scale mode $\zeta_{\mathbf{p}}$. Therefore the 12-type loop-correction is zero. Third, $f_{\text{NL}}^{(N_{\phi\phi})}(\bar{k}; t)$ accounts for non-linearity in the small-scale modes. Finally, $\mathcal{P}_{\zeta}(\bar{k})_{\text{tree}}$ tracks the growth of perturbations on small scales, locking the amplitude of the 12-type loop to the small-scale enhancement.

Let us now comment on the magnitude of the 12-type loop correction, subject to the caveats already given above. The calculation outlined here is general, meaning that Eq. (4.18) does not rely on assumptions about the character of the USR→SR transition. After substitution of $\eta = -6$ in Eq. (4.18) one sees that if $\mathcal{P}_{\zeta}(\bar{k})_{\text{tree}} \lesssim 10^{-2}$, the amplitude of $\Delta\mathcal{P}_{\zeta}(p; t)_{12}$ will be small, unless the equilateral non-Gaussianity on small scales is sufficiently large to overcome suppression by $\epsilon(t_s)$ and $\mathcal{P}_{\zeta}(\bar{k})_{\text{tree}}$. For models featuring a smooth transition, this expectation is not realistic [54]. On the other hand, for instantaneous transitions ($h = -6$) one can have $f_{\text{NL}}^{(N_{\phi\phi})}(\bar{k}; t) = \mathcal{O}(1)$, yielding a 12-type loop-correction that is less suppressed.

We can compare Eq. (4.18) with the result quoted by Firouzjahi & Riotto for their 12-loop [23]. Our answers both contain the amplitude factor $\mathcal{P}_{\zeta}(\bar{k})_{\text{tree}}$ and the nonlinearity parameter $f_{\text{NL}}^{(N_{\phi\phi})}(\bar{k}; t)$, which is η_s in Ref. [23]. The major differences are: (i) the $(\eta/6)^2$

²²Note that the total $f_{\text{NL}}^{\text{eq}}(k; t)$ is constant over peak scales for models featuring a non-attractor phase [96], as it is also for models where the small-scale enhancement is produced (on super-horizon scales) by multi-field effects [35].

correlation function individually. Instead, the separate universe formula will give the leading contribution in gradients for each type of loop. Gradient corrections to ζ , via Eq. (2.7), would generate corrections to *both* Eq. (4.18) and Eq. (4.23) at relative order $(p/k_s)^2$. Eq. (4.23) is therefore a reliable estimate of the leading contribution to the 22-loop, but we should recognize that it is subleading to the first gradient corrections to the 12-loop.

Recall that (4.23) is valid for any value of h . For a peak with amplitude $\mathcal{P}_\zeta(\bar{k})_{\text{tree}} = \mathcal{O}(10^{-2})$, it yields

$$\Delta\mathcal{P}_\zeta(p; t)_{22} = \mathcal{O}(10^4) \left[f_{\text{NL}}^{(N_{\phi\phi})}(\bar{k}; t) \right]^2 \left(\frac{p}{k_s} \right)^3. \quad (4.24)$$

Even a hierarchy as small as $p/k_s \sim 10^{-1.5}$ is already sufficient to cancel out the large $\mathcal{O}(10^4)$ prefactor. This type of loop correction is volume suppressed for instantaneous and smooth transitions.

4.3 13-loop

The 13-type loop was discussed from a general perspective in §2.2. It corresponds to the third diagram in Fig. 5. In the Gaussian approximation where we retain only disconnected contributions to the phase-space 4-point function in Eq. (2.21), the corresponding momentum configuration is of the “double-soft kite” type described in Ref. [98]. Therefore, as for the 12-loop, the 13-loop depends on a soft limit of δX correlations, which encode long–short mode couplings. The result is that the 13-loop is *not* automatically volume suppressed. The connected contributions to the 4-point function that have been dropped would generically involve only a single soft mode, but they enter at two-loop level and cannot consistently be retained at the accuracy to which we are working.

While peak-scale modes contribute only field fluctuations, the large-scale modes in Eq. (2.21) can be of either field or velocity type. Therefore we obtain

$$P_\zeta(p; t)_{13} = \frac{1}{3} N_I^{(t_k, t)} \left(N_{J\phi\phi}^{(t_k, t)} + N_{\phi J\phi}^{(t_k, t)} + N_{\phi\phi J}^{(t_k, t)} \right) P^{IJ}(p; t_k) \int \frac{d^3q}{(2\pi)^3} P^{\phi\phi}(q; t_k). \quad (4.25)$$

Using Eqs. (3.19a)-(3.19b) and (4.12), one can derive a relation between the third derivatives of N appearing in Eq. (4.25),

$$N_{\pi\phi\phi}^{(t_k, t)} = N_{\phi\pi\phi}^{(t_k, t)} = N_{\phi\phi\pi}^{(t_k, t)} = \frac{N_{\phi\phi\phi}^{(t_k, t)}}{3}. \quad (4.26)$$

This relationship is a specific property of the 3-phase ultra-slow-roll model *and* the precise choice of initial time. It does not apply in general.

Expanding the summation over J in Eq. (4.25), and using Eq. (4.26), we obtain²³

$$P_\zeta(p; t)_{13} = N_I^{(t_k, t)} N_{\phi\phi\phi}^{(t_k, t)} \left(P^{I\phi}(p; t_k) + \frac{1}{3} P^{I\pi}(p; t_k) \right) \int \frac{d^3q}{(2\pi)^3} P^{\phi\phi}(q; t_k). \quad (4.27)$$

²³Note that the second term in Eq. (4.27) was omitted in v1 of the arXiv version of this paper. The missing contribution has been added from v2 onwards.

In the language of Fig. 6, these four contributions can be visualized diagrammatically as

$$\begin{aligned} \langle \zeta_{\mathbf{p}} \zeta_{-\mathbf{p}} \rangle_{13} = & \text{---} \bullet \text{---} \text{---} \bullet \text{---} + \text{---} \bullet \text{---} \text{---} \bullet \text{---} \\ & \text{---} \bullet \text{---} \text{---} \bullet \text{---} + \frac{1}{3} \text{---} \bullet \text{---} \text{---} \bullet \text{---} \\ & + \frac{1}{3} \text{---} \bullet \text{---} \text{---} \bullet \text{---} \end{aligned} \quad (4.28)$$

Using Eq. (4.10), we find

$$P_{\zeta}(p; t)_{13} = N_I^{(t_k, t)} N_{\phi\phi\phi}^{(t_k, t)} \left(1 + \frac{\eta}{6}\right) P^{I\phi}(p; t_k) \int \frac{d^3 q}{(2\pi)^3} P^{\phi\phi}(q; t_k). \quad (4.29)$$

Eq. (4.29) shows that the 13-type loop vanishes for ultra-slow-roll evolution, where $\eta = -6$. However, it should be noted that absence of the 13-type loop is *not* a general property of models featuring a non-attractor phase. In the present case it depends not only on the condition $\eta = -6$, but also on Eq. (4.26) which relates the third derivatives of N . As already explained, this relation applies specifically when the δN calculation is based at a time during (or at the end of) the USR phase. If we were to base the δN formula at some later time during the final slow-roll phase, the 13-type loop need not vanish. This is expected because the total one-loop correction should be treated as a whole. We cannot usually break apart the different topologies and assign them a meaning invariant under changes in the calculational scheme.

Although the 13-loop will vanish in our scenario, it is instructive to continue the computation. This enables us to highlight the structural ingredients necessary to produce a result that is not volume suppressed. To this end, we isolate the vanishing prefactor $(1 + \eta/6)$ and retain η explicitly, but substitute $\eta = -6$ elsewhere. After further substitution of Eqs. (2.17) and (4.12), the 13-type loop correction relative to the tree level scalar power spectrum becomes

$$\begin{aligned} \Delta \mathcal{P}_{\zeta}(p; t)_{13} &\equiv \frac{\mathcal{P}_{\zeta}(p; t)_{13}}{\mathcal{P}_{\zeta}(p; t)_{\text{tree}}} \\ &= 2 \left(1 + \frac{\eta}{6}\right) N_{\phi\phi\phi}^{(t_k, t)} \left[N_{\phi}^{(t_k, t)} \left(1 + \frac{\eta}{6}\right) - \frac{\eta}{6 M_{\text{P}} [2\epsilon(t_k)]^{1/2}} \right] \epsilon(t_k) M_{\text{P}}^2 \left(\frac{H}{2\pi}\right)^2 \int_{k_s}^{k_e} \frac{dq}{q} \\ &= \left(1 + \frac{\eta}{6}\right) N_{\phi\phi\phi}^{(t_k, t)} \frac{|\eta| M_{\text{P}}}{6} [2\epsilon(t_k)]^{1/2} \left(\frac{H}{2\pi}\right)^2 \Delta N_{\text{USR}}. \end{aligned} \quad (4.30)$$

To obtain the last line we set $\eta = -6$ in the first term within square brackets. As in the case of the 12-loop, this term will vanish. Meanwhile, the momentum integral evaluates to $\ln(k_e/k_s)$, which approximately coincides with the duration of the ultra-slow-roll phase $\Delta N_{\text{USR}} = \mathcal{O}(1)$. Using Eqs. (3.19a) and (3.21), identifying the amplitude of the tree-level \mathcal{P}_{ζ}

on the small-scale plateau with its value at the peak scale, \bar{k} , and working in the limit of a smooth transition $h \rightarrow 0$, we find

$$\Delta\mathcal{P}_\zeta(p; t)_{13, h \rightarrow 0} = 2 \left(1 + \frac{\eta}{6}\right) N_{\phi\phi\phi}^{(t_k, t)} \frac{|\eta| M_{\text{P}}^3}{6} [2\epsilon(t_k)]^{1/2} \epsilon_2 \Delta N_{\text{USR}} \mathcal{P}_\zeta(\bar{k})_{\text{tree}}. \quad (4.31a)$$

Meanwhile, for an instantaneous transition with $h = -6$ we find

$$\Delta\mathcal{P}_\zeta(p; t)_{13, h=-6} = 8 \left(1 + \frac{\eta}{6}\right) N_{\phi\phi\phi}^{(t_k, t)} \frac{|\eta| M_{\text{P}}^3}{6} [2\epsilon(t_k)]^{1/2} \epsilon_2 \Delta N_{\text{USR}} \mathcal{P}_\zeta(\bar{k})_{\text{tree}}. \quad (4.31b)$$

The combination $|\eta|/6$ tracks the contribution of large-scale velocity fluctuations at time t_k . For consistency, we should regard this factor as equal to unity because our results formally apply only in the limit of ultra-slow-roll evolution where $\eta = -6$.

Excluding the vanishing factor $(1 + \eta/6)$, the remaining terms in Eqs. (4.31a)–(4.31b) clearly exhibit the essential ingredients needed to synthesize a non-vanishing 13-contribution. First, non-linear interactions among small-scale modes are again required. In this case, these interactions are measured by the third derivative $N_{\phi\phi\phi}^{(t_k, t)}$. Second, the slow-roll parameters $\epsilon(t_k)$ and ϵ_2 act as book-keepers for the dependence on the background dynamics, as $\epsilon(t_s)$ does for the 12-loop in Eq. (4.18). On a perfectly de Sitter background, the 13-loop vanishes. Third, the duration of the USR phase, $\Delta N_{\text{USR}} \sim \ln(k_e/k_s)$, measures the number of small-scale modes that contribute in the loop integral. Finally, $\mathcal{P}_\zeta(\bar{k})_{\text{tree}}$ locks the amplitude of the 13-loop to the enhancement of the small scales, as it does for the 12 loop (4.18).

While Eqs. (4.31a)–(4.31b) are very useful to understand the physical interpretation of the 13-loop, they depend on the character of the USR→SR transition. For this reason, in the following we revert to the last line of Eq. (4.30). The third derivative $N_{\phi\phi\phi}^{(t_k, t)}$ can be expressed (approximately) in terms of the dimensionless non-linearity parameter g_{NL} , defined in Eq. (2.5),

$$g_{\text{NL}}(k; t) \approx \frac{25}{54} \frac{N_{\phi\phi\phi}^{(t_k, t)}}{[N_{\phi}^{(t_k, t)}]^3}, \quad (4.32)$$

due to the fact that only field fluctuations contribute on peak scales. Employing Eq. (3.19a) and its derivatives, we find

$$g_{\text{NL}}(k, t) = \frac{25}{3} \frac{h^3 + 6h^2\eta_2 + 12(h-2)\eta_2^2 + 8\eta_2^3}{(2\eta_2 + h - 6)^3}. \quad (4.33)$$

It is suppressed for a smooth USR→SR transition for which $\eta_2 \ll 1$ and $h \ll 1$,²⁴ and is scale invariant across the peak. We therefore identify it with a representative value $g_{\text{NL}}(\bar{k}; t)$ on the fiducial scale \bar{k} . Using (3.21) and (4.32) in Eq. (4.30), we obtain

$$\Delta\mathcal{P}_\zeta(p; t)_{13} = \left(1 + \frac{\eta}{6}\right) \frac{54}{25} g_{\text{NL}}(\bar{k}; t) \frac{|\eta|}{6} [N_{\phi}^{(t_k, t)} M_{\text{P}}] [2\epsilon(t_k)]^{1/2} \Delta N_{\text{USR}} \mathcal{P}_\zeta(\bar{k})_{\text{tree}}. \quad (4.34)$$

²⁴ Note that expanding Eqs. (4.17) and (4.33) for $h \ll 1$ requires careful consideration. Specifically, both h and η_2 are small and the final result is sensitive to the order in which the expansions for $h \ll 1$ and $\eta_2 \ll 1$ are performed. This subtlety was not discussed in Ref. [54]. The result reported there, $f_{\text{NL}} \approx -5\eta_2/6$, was obtained by first expanding Eq. (4.17) for $h \ll 1$ and then for $\eta_2 \ll 1$. While it is important to obtain a precise result, this does not affect the discussion in the main text. In both cases f_{NL} and g_{NL} are either slow-roll suppressed (since $\eta_2 \ll 1$), or suppressed due to the smoothness of the transition ($h \ll 1$).

Eq. (4.34) applies to any type of transition. Specialising to the case of a smooth transition using Eq. (3.20) yields

$$\Delta\mathcal{P}_\zeta(p;t)_{13,h\rightarrow 0} = \left(1 + \frac{\eta}{6}\right) \frac{54}{25} g_{\text{NL}}(\bar{k};t) \frac{|\eta|}{6} \left(\frac{\epsilon(t_k)}{\epsilon_2}\right)^{1/2} \Delta N_{\text{USR}} \mathcal{P}_\zeta(\bar{k})_{\text{tree}}, \quad (4.35)$$

where $g_{\text{NL}}(\bar{k};t) \ll 1$.

While neither the 12- and 13-type loop corrections are volume-suppressed, the 12-diagram is the only non-vanishing correction with this property in our scenario. Note that the 13-type diagram corresponds topologically to the one produced by quartic ζ -interactions within the in–in formalism. In Ref. [19], Firouzjahi calculated the loop-level contribution from both cubic and quartic interactions, and found that for $h = -6$ they have the same sign and are equal. Understanding the reason for this mismatch will require a careful understanding of how to interpret the separate universe calculation within the in–in framework. We leave this for future work.

Before closing, let us compare our final expression (4.35) for the 13-type diagram with the corresponding result Eq. (III.46) obtained by Firouzjahi & Riotto [23]. While we obtain a vanishing 13-type loop, their result is nonzero. For our case, the 13-loop vanishes only if one includes all relevant contributions. In particular, see Eqs. (4.27)-(4.29), where the first and second term cancel. Inspection of the non-vanishing factors in Eq. (4.35) shows that we recover the dependence on the duration of the ultra-slow-roll epoch found by Firouzjahi & Riotto. However, our expressions differ due to the factors $|\eta|/6$ and $[\epsilon(t_k)/\epsilon_2]^{1/2}$, which are present in Eq. (4.35) but do not appear in Eq. (III.46). (Note that the η_s^2 factor in Eq. (III.46) corresponds to $g_{\text{NL}}(\bar{k};t)$. However, this is different to our $g_{\text{NL}}(\bar{k};t)$ because it is evaluated at a different time). As for the 12-type contribution, we believe that these differences are due to different implementations of the δN calculation (§2.2).

5 The smoothing scale as a Wilsonian cutoff

We now return to the question raised below Eq. (2.7) on p. 15. How does the analysis change if we choose to smooth on the scale L immediately after the ℓ -size boxes emerge from the horizon?

5.1 The separate universe framework as an effective field theory

At the outset, it is already clear that the smoothing scale functions as a Wilsonian cutoff. Indeed, the separate universe framework can be interpreted as an almost-textbook application of the logic of effective field theories. Moving the smoothing lengthscale from ℓ (relatively, an ultraviolet scale) to L (relatively, an infrared scale) corresponds to integrating out degrees of freedom. There are no long-range effects mediated by the modes between L and ℓ , so their influence should appear local from the perspective of the L -size regions. Therefore we expect that it can be captured by a renormalization of local operators. It is this renormalization that allows different versions of the computation, performed with different smoothing scales, to agree. The smoothing/renormalization process erases most detailed information about the modes between L and ℓ . Only a limited quantity of aggregated information is retained,

carried by the renormalized operators. As in any effective theory, if we choose to work up to a specified accuracy in the ratio $\ell/L = p/k \ll 1$, then only a finite number of operators need be renormalized.

In this section we outline the main steps in the renormalization procedure. Our discussion applies quite generally and does not depend on specific properties of the 3-phase ultra-slow-roll model. However, the precise choice of counterterms is model-dependent. In order to give an explicit discussion it is helpful to work in the context of the momentum dependence carried by the 12- and 22-type loops, see Eqs. (4.18) and (4.23). It was explained in §4.3 that the 13-type loop vanishes for the specific scenario of §§3–4. However, our discussion will include suitable counterterms to renormalize its contribution in a scenario where it is present.

Counterterms.—Concretely, suppose we smooth on the scale L just after the time t_k corresponding to horizon exit of the mode $k \sim \ell^{-1}$. We are then committed to working with the smoothed fields $\{\{\delta X^I(\mathbf{x}, t)\}\}_L$, which correspond to the volume-averaged fields calculated in §2.2.1.

Smoothing on this scale averages over injection of energy due to particle creation at the horizon, but then *erases the newly-injected modes*. The ζ -field smoothed on the same scale is $\{\{\zeta(\mathbf{x}, t)\}\}_L$. It is given by Eq. (2.2), and its Fourier modes satisfy (2.7) with the replacement $\ell \rightarrow L$. In particular, the base time $t_* = t_k$ in Eq. (2.7) is not changed. However, the modes between p and k are now missing from the convolution integral in the quadratic part of (2.7). This happens because the δX fields in (2.1) and (2.2) are smoothed before forming nonlinear products, as emphasized in §2.2.

There are several consequences. First, consider the δN tree-level term in Eq. (2.18).²⁵ This includes a spatial average over particle creation, no matter where the cutoff is positioned. If we work with the cutoff at ℓ , these effects are explicitly included via the analysis of §2.2.1. On the other hand, if we work with the cutoff at L the same effect is incorporated into the definition of the smoothed δX fields, and there is no loop to include. The situation is different for the 12-, 22-, and 13-type loops (2.19)–(2.21). These are dramatically modified. With the cutoff set to the lengthscale L , each loop integral now has a cutoff of order p . All information about nonlinear interactions among the peak-scale modes, responsible for cascading power into the deeper infrared modes, is absent.

How can the final two-point function for $\{\{\zeta\}\}_L$ be made to agree with that already calculated for $\{\{\zeta\}\}_\ell$? Consider the 12- and 13-type loops, Eqs. (4.18) and (4.35). Their p -dependence is the same as the tree-level power spectrum. We introduce a quadratic counterterm, which for simplicity we express in terms of ζ . The counterterm action has the form

$$S_{\text{ct}} = \int_{-\infty}^{\infty} dt \int \frac{d^3 q_1}{(2\pi)^3} \frac{d^3 q_2}{(2\pi)^3} (2\pi)^3 \delta(\mathbf{q}_1 + \mathbf{q}_2) a(t)^3 M_{\text{P}}^2 \delta_{\text{ct}}(t) \mathcal{O}_{\mathbf{q}_1}(t) \mathcal{Q}_{\mathbf{q}_2}(t), \quad (5.1)$$

where $\mathcal{O}_{\mathbf{q}}(t)$ and $\mathcal{Q}_{\mathbf{q}}(t)$ symbolically stand for $\zeta_{\mathbf{q}}(t)$ or one of its derivatives, each possibly carrying tensor indices under 3-dimensional rotations that we have suppressed. The normal-

²⁵To be clear, by “ δN tree-level” we mean that this term is at tree-level in the δN expansion. As explained in §2.2.3, the $\langle \delta X \delta X \rangle$ correlation function that appears in it should be computed to one-loop level.

ization factor of M_{P}^2 appears in explicit calculations and guarantees that ζ is projected out of the path integral in a limit where gravity is decoupled via $M_{\text{P}} \rightarrow \infty$. It is introduced here by hand so that δ_{ct} has the expected mass dimension if (5.1) is expressed in terms of a canonically normalized field $\delta\phi$. The kernel $\delta_{\text{ct}}(t)$ should have mass dimension $2 - \dim(\mathcal{O}) - \dim(\mathcal{Q})$. It may be an explicit function of time, but does not depend on the momenta $\mathbf{q}_1, \mathbf{q}_2$. It is the analogue of a Wilson coefficient. Its amplitude and time evolution should depend only on properties of the short modes. From this perspective, as for any Wilson coefficient, Eq. (5.1) represents a factorization of physics associated with the different scales p and k . We treat δ_{ct} as if it were a one-loop term in the loop expansion; its tree-level graphs should be included along with the one-loop contributions described above. The counterterm insertion in the two-point function corresponds to the diagram

$$\langle \zeta_{\mathbf{q}_1} \zeta_{\mathbf{q}_2} \rangle^{\text{ct}} \supset \frac{\tau}{\mathbf{q}_1 \times \mathbf{q}_2}$$

where the cross denotes the counterterm vertex. In the simplest case where $\mathcal{O}_{\mathbf{q}}$ and $\mathcal{Q}_{\mathbf{q}}$ are scalar operators, this diagram gives a contribution to the two-point function that is schematically of the form

$$\langle \zeta_{\mathbf{p}} \zeta_{-\mathbf{p}} \rangle_{\eta}^{\prime \mathcal{O}\mathcal{Q}} = i \psi_p^{\zeta}(\eta)^2 \int_{-\infty}^{\eta} \frac{d\tau}{H^4(\tau)\tau^4} M_{\text{P}}^2 \delta_{\text{ct}}(\tau) \psi_p^{\mathcal{O}*}(\tau) \psi_p^{\mathcal{Q}*}(\tau) + \text{c.c.}, \quad (5.2)$$

where η is the conformal time of evaluation, τ is the time at the counterterm vertex, and ‘+c.c.’ indicates that we should add the complex conjugate of the preceding term. Recall that the prime ‘ \prime ’ attached to the correlation function indicates that the conventional factor $(2\pi)^3$ and the momentum conservation δ -function are not written. The symbol ‘ \ast ’ denotes complex conjugation. We have written the mode functions of the operators ζ , \mathcal{O} and \mathcal{Q} for momentum \mathbf{p} as ψ_p^{ζ} , $\psi_p^{\mathcal{O}}$, $\psi_p^{\mathcal{Q}}$, respectively. The Wronskian normalization for these mode functions implies that ψ_p^{ζ} can be written as $(2p^3)^{-1/2}$ multiplied by a dimensionless time-dependent function, and $\psi_p^{\mathcal{O}}$ and $\psi_p^{\mathcal{Q}}$ inherit their normalization from ψ_p^{ζ} .

In this section we are working to lowest order in the slow-roll expansion, and we assume that each time integral is dominated by contributions around horizon exit. This means that a (physical) time or space derivative applied to $\zeta_{\mathbf{p}}$ can be estimated as roughly $\sim (p/a)\zeta_{\mathbf{p}}$, because there is no other scale in the problem. The analysis becomes technically more involved when one includes time evolution of the background, but is not conceptually different.

For example, if $\mathcal{O} = \mathcal{Q} = \dot{\zeta}$, then one can check that $(\psi_p^{\zeta})^2 \sim \mathcal{P}_{\zeta}(p)p^{-3}$ and $\psi_p^{\mathcal{O}}\psi_p^{\mathcal{Q}} \sim \mathcal{P}_{\zeta}(p)p^{-1}/a^2$. This counterterm preserves the shift symmetry of the ζ action and respects conservation of ζ outside the horizon [99–102]. The corresponding kernel δ_{ct} has dimension 0. Hence, the counterterm contribution to the two-point function can be estimated as

$$\langle \zeta_{\mathbf{p}} \zeta_{-\mathbf{p}} \rangle_{\eta}^{\prime \dot{\zeta}^2} \simeq \mathcal{P}_{\zeta}(p, \eta) \frac{i}{p^4} \int_{-\infty}^{\eta} \frac{d\tau}{H(\tau)^2 \tau^2} M_{\text{P}}^2 \delta_{\text{ct}}(\tau) \mathcal{P}_{\zeta}(p, \tau) \times \dots, \quad (5.3)$$

where ‘ \dots ’ denotes time-dependent factors that we have not written explicitly. If δ_{ct} contains no characteristic timescales different to $1/p$ then the vertex integral can be estimated on

dimensional grounds as

$$i \int_{-\infty}^{\eta} \frac{d\tau}{\tau^2} \delta_{\text{ct}}(\tau) \times \dots \sim pC, \quad (5.4)$$

where C is some dimensionless constant determined by δ_{ct} . We conclude

$$\langle \zeta_{\mathbf{p}} \zeta_{-\mathbf{p}} \rangle_{\eta}^{\zeta^2} \simeq \frac{C}{p^3} \mathcal{P}(p, \eta). \quad (5.5)$$

Evidently, the counterterm is just a renormalization of the ζ kinetic term.²⁶ In a model with isocurvature modes one could also have a mass counterterm ζ^2 generated by $\mathcal{O} = \mathcal{Q} = \zeta$. For this operator the power counting for p works in a similar way. However, the time integral can be infrared divergent which complicates the analysis.

5.2 12- and 13-loop counterterms

Clearly Eq. (5.5) has p -dependence matching the tree-level ζ power spectrum, and therefore can be used to absorb the 12- and 13-type loops. Moreover, this can be done while respecting the universality criterion that δ_{ct} depends only on properties of the short modes. The conclusion of this discussion is that, if we insist on setting the smoothing scale equal to L , we should add a counterterm $\sim \zeta^2$ of the form (5.1) with δ_{ct} *chosen* to have the correct amplitude and time dependence to reproduce the explicit results (4.18) and (4.35).

In practice, from the perspective of the separate universe framework with an L -scale cutoff, this amplitude and time dependence is not predictable because it depends on detailed information about the behaviour of modes above the cutoff that we have intentionally erased from our model. In the L -smoothed version of the theory, we have no choice other than to accept the presence of the counterterm and attempt to fit its amplitude and time dependence by comparison with observation. This is exactly the same as the renormalization procedure required in the effective field theory of large scale structure [10, 12, 13, 103, 104]. The counterterm is needed only for modes that are softer than k , and at times later than their horizon exit time t_k .

It follows that in the L -smoothed version of the theory, the back-reaction for peak-scale modes can be accommodated but *is not predicted* because we have no adequate rationale to estimate its time dependence. This time dependence is critical to evaluate the significance of any back-reaction. By comparison, in the ℓ -smoothed version, detailed information about the interactions and behaviour of the peak-scale modes is retained. It is then true that explicit computation of the loops, as in Eqs. (4.18), (4.23) and (4.35), supplies a predictive estimate of the back-reaction from these modes. However, we cannot conclude from this that the ℓ -smoothed theory is predictive as a whole, because the back-reaction from peak scales cannot be measured separately. Specifically, we should recognize that the ζ^2 operator will already receive renormalizations from all scales that were integrated out in the smoothing procedure, i.e. modes $\gg k$. Eqs. (4.18) and (4.35) are therefore degenerate with further unknown renormalizations associated with deeper ultraviolet modes [105], and this conclusion applies to both the ℓ - and L -smoothed versions of the analysis. It is these renormalizations

²⁶For simplicity we have phrased the discussion in terms of ζ^2 . However, at the order to which we are working, one could equally well express the analysis in terms of the counterterm $\zeta \partial^2 \zeta / a^2$.

that compensate for the explicit ultraviolet cutoff dependence $q \lesssim k_e$ of the loop integrals reported in §4. Clearly, the final correlation functions must be independent of any such arbitrary cutoff scale.²⁷

The practical outcome is that the one-loop shift represented by Eqs. (4.18) and (4.35) is not directly observable, and should not be used to draw conclusions about any putative breakdown of the loop expansion. Only the *running* of the one-loop correction can be observed separately [106].

There is a possible exception for the specific scenario considered here. Deeply subhorizon modes do not feel the curvature of spacetime and approximately restore the Lorentz symmetry that is spontaneously broken by the background. One would therefore expect loop contributions from these modes to renormalize the Lorentz-invariant kinetic operator $\partial^a \phi \partial_a \phi$ rather than $\dot{\zeta}^2$ or $\zeta \partial^2 \zeta / a^2$ separately. This could provide a possible rationale to regard running generated, e.g., by Eq. (4.18) (or more refined estimates of the same loops) as the largest contribution. This would be interesting to pursue, but we leave a detailed analysis for future work.

The soft three-point function appearing in the 12-loop (4.3) or the (double) soft four-point function in the 13-loop (4.25) will have subleading contributions proportional to powers of $(p/k)^2$. As has been explained, if the $O(p/k)^0$ contribution should be subtracted to isolate the physical correlations then the order $(p/k)^2$ term will be the leading contribution. This momentum dependence can be absorbed by higher-derivative counterterms for ζ . If we take $\mathcal{O} = \mathcal{Q} = \ddot{\zeta}$ in (5.1) then we expect $\psi_p^{\mathcal{O}} \psi_p^{\mathcal{Q}} \sim \mathcal{P}_\zeta(p) p / a^4$. Also, δ_{ct} should now have mass dimension -2 , which we expect can be associated with a suppression $\sim 1/k^2$ by the ‘heavy’ scale that has been integrated out. In the counterterm (5.1) this should appear as the corresponding *physical* scale k/a . Therefore we write $\delta_{\text{ct}} = \tilde{\delta}_{\text{ct}} / (k/a)^2$, with $\tilde{\delta}_{\text{ct}}$ taken to be dimensionless. It follows that we can estimate the contribution from this operator to the ζ two-point function,

$$\langle \zeta_{\mathbf{p}} \zeta_{-\mathbf{p}} \rangle_{\eta}^{\prime, \ddot{\zeta}^2} \simeq \mathcal{P}_\zeta(p, \eta) \frac{i}{p^3} \int_{-\infty}^{\eta} \frac{d\tau}{H(\tau)^2 \tau^2} \frac{M_{\text{P}}^2}{k^2} \tilde{\delta}_{\text{ct}}(\tau) \mathcal{P}_\zeta(p, \tau) p \times \dots \quad (5.6)$$

The estimate for the time integral is the same as above, viz., $i \int_{-\infty}^{\eta} d\tau \tau^{-2} \tilde{\delta}_{\text{ct}}(\tau) \times \dots \sim p C'$. [In this expression, C' is a different constant to the quantity C appearing in (5.4).] Hence,

$$\langle \zeta_{\mathbf{p}} \zeta_{-\mathbf{p}} \rangle_{\eta}^{\prime, \ddot{\zeta}^2} \simeq \frac{C'}{p^3} \frac{p^2}{k^2} \mathcal{P}_\zeta(p, \eta). \quad (5.7)$$

As expected, this has the correct momentum dependence to match the order $(p/k)^2$ term from the 12- and 13-type loops. Higher powers of p/k can be handled in exactly the same way, by introducing increasingly irrelevant operators (in the technical sense) built from higher derivatives of ζ , and suppressed by higher powers of k/a .

²⁷One might wonder how the infrared cutoff scale is compensated (as it also must be). As explained in footnote 3 on p. 5, this can be absorbed into a sufficiently precise definition of the expectation value that is being computed.

5.3 22-loop counterterm

A similar analysis can be given for the 22-loop, although the kinematic structure of this loop produces differences. In this section we provide only a sketch of the renormalization procedure, leaving a complete analysis to future work.

It was explained in §2.2.2 that, from the perspective of the long mode \mathbf{p} , the 22-loop can be regarded as injection of uncorrelated noise. We therefore expect the counterterm needed to absorb the 22-loop to have a stochastic character. To model it, we introduce an auxiliary field ξ coupled to ζ . The precise interaction must be chosen to reproduce the momentum dependence of (4.23). (See, e.g., Refs. [59, 64].) Its contribution to the ζ two-point function involves the insertion of a ξ line,

$$\langle \zeta_{\mathbf{q}_1} \zeta_{\mathbf{q}_2} \rangle_{\eta}^{\xi\xi} \supset \frac{\tau}{\mathbf{q}_1} \text{---} \text{ZZZZ} \text{---} \frac{\nu}{\mathbf{q}_2}$$

The auxiliary field has an imaginary action that can be regarded as a probability distribution on $\xi_{\mathbf{q}}$. Working in a Gaussian approximation, the variance of this measure would determine the noise correlator $\langle \xi_{\mathbf{q}_2} \xi_{\mathbf{q}_1} \rangle$. Therefore, when used in an effective equation of motion, $\xi_{\mathbf{q}}$ can be regarded as a stochastic variable. Alternatively, we can attempt to integrate out ξ to produce an effective counterterm involving only the long-wavelength field $\zeta_{\mathbf{p}}$. This is a Hubbard–Stratonovitch transformation [107, 108]. However, it does not yet seem clear what type of counterterms would be produced.

6 Discussion

In this paper we have reconsidered the evaluation of loop corrections to the large-scale primordial power spectrum. We are motivated by scenarios in which there is a peak in the power spectrum on short scales, but the general framework we have assembled is not specific to this case. The same framework could be used to evaluate back-reaction in many scenarios—including those where the short-scale power is broadly distributed over a range of scales rather than being concentrated in the vicinity of a peak. However, in this case the connection to the toy model of §1.1 becomes substantially more complicated. Instead of a single mosaic of ℓ -sized boxes, we would need to deal with a distribution of box sizes. Moreover, if the power spectrum no longer has a significant blue tilt these boxes would develop complex spatial correlations. One would therefore have to track all relevant correlation lengths. The necessary information is embedded within the higher-order correlation functions, for which a suitable prescription would have to be given.

6.1 Advantages of the separate universe framework

This toy model is a useful source of intuition regarding the types of back-reaction that can occur, and their dependence of the scale hierarchy $p/k \ll 1$. In particular, it emphasizes that the back-reaction effects being computed are *classical*. For this reason the separate universe framework provides a very convenient method with which to perform loop computations. The complexities of the in-in formalism are not needed, and may even prove to be an unhelpful

distraction. Concretely, one can regard a formula such as Eq. (2.7) as a more complete version of the toy-model spatial average (1.6). We argue that the separate universe framework offers a number of important simplifications when compared with alternative frameworks.

First, the time dependence of each correlation function can be evaluated accurately, even accounting for transitions between different eras—such as the transition between ultra-slow-roll and ordinary slow-roll, discussed in §3. This is critical in order to obtain reliable estimates for the magnitude of each loop. The same thing can be done using in–in, but one needs the time dependence of the propagator to be valid to arbitrarily late times. This is possible, but is not always easy to achieve, for example if one uses the slow-roll approximation to solve for the mode functions [43].

Second, a separate universe expression such as (2.7) makes explicit how the different back-reaction effects add coherently (or fail to do so) over the large L -size box. Correlations depending on a soft limit of a δX correlation function, such as the 12-loop (2.19) and the 13-loop (2.21), can add coherently. This is one of our primary results: loop contributions *can* be present without volume suppression. The same conclusion (with some differences of detail) was reached by Riotto [14]. The unsuppressed parts are the 12- and 13-type diagrams in Fig. 5. For the specific 3-phase ultra-slow-roll model of §3 we focus on the effect of modes populating a small-scale plateau in the tree-level \mathcal{P}_ζ . In this approximation we find that the 12-loop is always suppressed, regardless of the character of the transition from ultra-slow roll to the final slow-roll phase, and that the 13-type loop vanishes. Meanwhile, the 22-type loop is volume suppressed. Therefore the total large-scale, one-loop correction is small relative to the tree-level power spectrum. This conclusion applies for models with both smooth and instantaneous transitions. Of course, it must be equally possible to arrive at the same understanding using the in–in approach. The δN version should be regarded merely as a reorganization of the calculation that makes these conclusions more manifest. For example, in the δN calculation it is clear that the 22-loop (2.20) should be suppressed by the central-limit volume factor $N^{-1} = (p/k)^3$. This is substantially harder to see in a direct in–in calculation, where the outcome depends on cancellations between diagrams with different vertices and is afflicted by technicalities involving boundary terms.

Third, in the δN calculation it is straightforward to see how powerful factorization principles, such as the Maldacena limit [14, 31] or the soft factorization formulae developed in Ref. [45], can be used to evaluate the soft limits needed for the loop integrands. These factorizations are not at all easily visible within pure in–in perturbation theory. Further, the appearance of soft limits in these integrands emphasizes that one should be concerned about subtractions that may be necessary to isolate physical correlations, as opposed to correlations that are merely gauge artefacts. Many authors have suggested that, in a single-field, adiabatic model, the physical correlations in the squeezed limit decay like $(p/k)^2$ [79–82].²⁸ If this is the case, then the order $(p/k)^0 \sim 1$ contribution to an integral over a soft limit such as (2.19) would apparently be subtracted. This would make such loop corrections exponentially small, because the surviving contribution would presumably be of order $(p/k)^2 \ll 1$. This is at the same order in p/k as the loop contributions found by Tasinato using a large $|\eta|$ expansion [26],

²⁸For a dissenting view, see Matarrese *et al.* [109].

and provides one possible interpretation of those terms. However, if that is the case, it is not clear why the calculation of Ref. [26] would not capture the $O(1)$ contribution from the Maldacena factorization in the squeezed limit.

If soft limit subtractions make the loop of order $(p/k)^2$, then unfortunately we would be obliged to conclude that the separate universe formula is *not* adequate to evaluate it. This is because a formula such as (2.19) should be corrected by gradient effects. In a model with two scales (here, p and k) it is possible for these corrections to scale like $(p/k)^2$ [55]. We would therefore be unable to capture these effects accurately, unless one included the first gradient corrections to the separate universe framework. A formalism for doing so was elaborated by Tanaka & Sasaki [110, 111]. Whether or not one chooses to pursue this possibility, because the surviving one-loop term that does *not* depend on a soft limit is the incoherent 22-loop which is suppressed by a volume factor, we would still be able to conclude that the one-loop corrections are negligible in a single-field, adiabatic model. This is already sufficient for models with a short-scale peak that are relevant for primordial black hole formation, because two-loop terms would presumably be negligible even if they are not volume suppressed. Nevertheless, as a point of principle, it would be very valuable to extend the conclusion to all orders in the loop expansion.

A similar discussion applies to the 13-loop (2.21). In the Gaussian approximation to the 4-point function used in this paper, the integral in (2.21) reduces to a double-soft limit involving the insertion of two soft δX modes into the hard δX two-point function. If all limits of this kind are subtracted then one must conclude that a loop contribution that is *not* volume suppressed would require the presence of at least one isocurvature mode. In models containing such modes, the leading loop effects would return to lowest order in p/k , and therefore the formulae presented in §2 could be used to evaluate their magnitude.

It is not yet entirely clear how these considerations should be applied to the loop contributions of §2.2.3 and in particular how any subtraction should be implemented in a way that is independent of any infrared regulator scale. It is also unclear how (or whether) the subtraction operation commutes with computation of the loop integrals. We believe that both of these issues require an adequate resolution before we are in a position to evaluate squeezed contributions to each loop. However, we leave these issues for future work.

In the main text of the paper, we have not performed explicit subtractions. This enables comparison of our results with previous estimates that have been reported in the literature.

6.2 The role of nonlinear couplings

The appearance of soft limits clarifies how the loop depends on nonlinear mode couplings. Previous discussions have generally emphasized the dependence of the one-loop correction on powers of $|\eta| \sim 6$ —see the $(\Delta\eta)^2 = |\eta|^2$ factor in the final result of Ref. [8]—because this determines whether the effect is significant. We have argued above that this emphasis can obscure the fact a soft limit is involved, with possible nontrivial scaling as $p/k \rightarrow 0$. In our analysis, some of these powers of η are proxies for a nonlinear coupling—either a soft limit of a higher-order correlation function such as $\langle \delta X^I \delta X^J \delta X^K \rangle$, or a higher-order time-dependent coefficient such as N_{IJ} .

Each loop involves at least one of these two types of nonlinearity. They reflect different aspects of the physics. Coefficients such as N_{IJ} or N_{IJK} reflect the nonlinear dependence of ζ on the early-time δX fluctuations. This type of nonlinearity is responsible for the interactions that allow short-wavelength modes at the base time t_* to cascade power into long-wavelength infrared modes at a later time, but says nothing about whether this power can add up coherently over a large volume. When these coefficients appear in a contribution to ζ , they organize themselves into combinations such as $N_{IJ}N^I N^J/(N^K N_K)^2$ or $N_{IJK}N^I N^J N^K/(N^L N_L)^3$ that can be recognized as the dominant contribution to the reduced bispectrum $f_{\text{NL}}(k_1, k_2, k_3)$, or a higher nonlinearity parameter such as g_{NL} , when these parameters are large [39, 112, 113]. These nonlinearity parameters are evaluated for an equilateral momentum configuration $k_i \sim k$ with characteristic scale k corresponding to the short-scale modes, and at a time equal to the time of evaluation of the loop. One can regard each such parameter as a measure of the nonlinearity of the short-scale modes among themselves. (We emphasize that nothing is being said about the *shape* of the correlations, only that the nonlinearity parameter is evaluated on an equilateral *configuration*.) If these parameters are significantly suppressed, the loop is likewise significantly suppressed.²⁹ This conclusion is likewise difficult to see from a direct in-in calculation, where it is obscured by the time integrations that appear at each vertex of the loop.

On the other hand, soft limits of correlation functions such as $\langle \delta X^I \delta X^J \delta X^K \rangle$ measure the coupling between long- and short-wavelength modes. This is an independent effect, responsible for allowing power cascaded from short-wavelength modes to add up coherently over large regions. We can interpret the corresponding physics, as follows. Transfer of power from small to large scales can depend only on local environmental conditions in each ℓ -scale box. To generate a coherent effect, the local environment must first *react* to the presence of the long mode. This biases nearby boxes to behave in a correlated way, effectively tracing the skeleton laid down by the long-wavelength modes. It is this correlated reaction to the presence of the long mode that allows *back*-reaction onto the long mode itself.

The long-short coupling corresponds to a nonlinearity parameter evaluated in a squeezed momentum configuration. In our framework the nonlinearity parameters that appear are usually not related to f_{NL} , g_{NL} , etc., in a simple way, because the soft limit involves δX correlations functions rather than those of ζ . (The relation may be more direct in a single-field model.) In principle it is possible to have one type of nonlinearity without the other, especially where the underlying correlations have significant scale dependence. However, as we have emphasized in §§2–4, *both* types of nonlinearity are needed to generate large loop contributions that are not suppressed by central-limit-like effects. The 22-type loop involves only short-scale nonlinearities and therefore depends on the square of the equilateral-mode f_{NL} evaluated on the corresponding scales. However, the 12- and 13-type loops involve both types of nonlinearity.

This complex structure, involving nonlinear parameters evaluated on equilateral and

²⁹When the reduced bispectrum $f_{\text{NL}}(k_1, k_2, k_3)$ becomes sufficiently small, one must distinguish between the combination $N_{IJ}N^I N^J/(N^K N_K)^2$ and the equilateral configuration of the reduced bispectrum. There is a difference from the intrinsic non-Gaussianity of the δX fluctuations. It is the combination $N_{IJK}N^I N^J N^K/(N^L N_L)^3$ that controls the amplitude of the loop.

squeezed configurations of higher-order correlation functions, is again not easily visible in the pure in-in framework. There, the different contributions to each nonlinear parameter are broken up between many interaction vertices and must be reassembled to obtain a full picture. In the separate universe framework we can deal with these correlations as a single entity from the outset.

6.3 The Wilsonian EFT description

In §5 we have shown how to relate loop calculations in the separate universe framework when the smoothing scale is varied. To calculate back-reaction from the peak, our preferred prescription (see §2.2) involves smoothing on the scale $\ell \sim 1/k$ associated with substructure generated by the peak in the power spectrum. This version of the calculation involves explicit loop contributions, described in §2.2.2. The loops have a natural cutoff at the smoothing scale ℓ . If, instead, we choose to smooth on a larger scale, some or all of the peak-scale modes are removed from our effective description. This depopulates the degrees of freedom available to circulate in the loops. Eventually, they become merely vestigial when the smoothing scale is sufficiently large that no peak modes remain. The effects they previously described must instead be absorbed into renormalization of local operators in the ζ effective description. This is the usual outcome from varying the cutoff (in a Wilsonian sense) in any effective theory.

In §5 we argued that effects from the 12-type loop (which are not volume suppressed) can be absorbed into a renormalization of the ζ kinetic operator $\dot{\zeta}^2$. The same discussion applies to the 13-type loop, which shares the same momentum dependence. Corrections at higher orders in $(p/k)^2$ can be absorbed into higher-derivative operators that are suppressed by the ‘heavy’ scale k associated with the peak. The resulting effective description, including loops, organizes itself into an expansion in powers of the small parameter $p/k \ll 1$. It furnishes a very convenient tool with which to understand the significance of back-reaction in this model. However, its utility depends on a separation of scales between the short peak modes $\sim k$ and the long CMB modes $\sim p$. The peak does not need to be monochromatic, but it must be sufficiently well separated from the modes whose effective description we are trying to find.

The 3-phase ultra-slow-roll model was used to calculate explicit estimates for the loop contributions in §4. The EFT analysis raises the interesting possibility that one could perhaps even dispense altogether with a dynamical model for the short-scale modes, instead accounting for their influence through parameters of the effective description. The primary difficulty one would encounter in this approach is to relate the EFT parameters to the height and width of the short-scale spike, which would be needed to relate the back-reaction to phenomenological considerations such as the abundance of primordial black holes.

6.4 Degeneracy with UV counterterms

Taken together with the discussion in §6.3, the conclusion of §5 is that local counterterms are needed to compensate for the dependence of each loop integral on the smoothing scale. The smoothing scale functions as a natural cutoff on each integral, although (of course) we

can impose a lower cutoff by hand if we wish. In this section we denote the cutoff by Λ . In the language of §4 the cutoff scale is the upper limit of integration, $\Lambda = k_e$.

Provided Λ is much larger than any wavenumber of interest, we expect that changes in its value can be absorbed by adjusting the coefficients of local operators. These are the counterterms. In flat space one can see this as follows. (In the following, q and p temporarily label 4-vectors.) Consider a wavenumber q contributing to the loop near the cutoff. We focus on the two-point function, so there is only one relevant wavenumber, p , and assume a Wick rotation to Euclidean signature. By assumption $q \gg p$, and therefore we can Taylor expand the loop integrand as a series in p/q . The series expansion is regular if there are no infrared singularities for $p \rightarrow 0$. It follows that the entire integral can also be expressed as a series in p^2 . This is exactly the behaviour that would be produced by insertion of one or more local operators built from the fields and their derivatives, as many as are needed to reproduce the terms in the series.³⁰ Contributions that are *not* an analytic function of p^2 , and which therefore are not degenerate with insertion of local operators, must come from the region of the integral where $q \sim p$ and the Taylor expansion in p^2 does not apply. Any such nonanalytic pieces cannot be modified by unknown ultraviolet effects and constitute reliable low-energy predictions of the model. For more details, see (e.g.) the classic papers by Donoghue [114, 115].

A similar argument can be applied to the loop integrands encountered in cosmology. Moreover, this argument explains why it is meaningful to compute loop corrections in an effective field theory at all. By construction, the ultraviolet behaviour of the effective description is intentionally different to the original parent theory. This is certainly true for the separate universe framework, which predicts entirely fictitious subhorizon behaviour because gradients are neglected. But in any field theory, the loops run over all momenta. Therefore one might worry that there are relevant effects, generated by the contribution of subhorizon quanta, that could be captured using the in-in formalism but could never be reproduced by loops based on the δN formula.³¹ The resolution is that, if such effects are present, they can only renormalize the coefficients of local operators.

Clearly, the necessity to include these counterterms complicates the interpretation of loop integrals such as those computed in §4. By choosing a suitable cutoff we were able to retain sufficient dynamical information about the short scale modes to obtain reliable estimates of the back-reaction effect. This procedure led to our final expressions for the 12-, 22- and 13-type loops, Eqs. (4.18), (4.23) and (4.35). Also, in §5 we demonstrated explicitly that at least the 12- and 13-type loops had momentum dependence, aside from the normalization $1/p^3$, that is analytic in p and could be absorbed into a renormalization of ζ^2 . (We have now reverted to our usual notation in which \mathbf{p} is a CMB-scale wavenumber and p is its magnitude.) Clearly this is a consequence of the large hierarchy p/q between the

³⁰For simplicity, and because it is the case we need, the discussion in this paragraph has been framed as if there is only one loop momentum q . This implicitly restricts to one-loop contributions. However, the argument can be generalized to higher loops.

³¹Of course, the usual cosmological framework based on a local quantum field theory description of the matter fields, and a semiclassical gravitational field, can itself only be an effective description. Therefore we should not give unwarranted deference its ultraviolet predictions. The same argument applies to loops computed using in-in, just with the cutoff at a higher (subhorizon) scale.

mode \mathbf{p} of interest and the modes \mathbf{k} that form the peak. We should expect almost the entire loop correction to \mathbf{p} , from modes of order \mathbf{k} , to be degenerate with counterterms. Only if \mathbf{p} is changed to be of order the peak scale should we expect the loop to produce significant nonanalytic terms.

Unfortunately, this means that our results (4.18) and (4.35) must be combined with unknown ultraviolet contributions before they are used to predict observables. By themselves, their meaning is ambiguous. There are limited circumstances in which it may be possible to extract meaningful information. First, if logarithmic running is present then this can be regarded as unambiguous, because the logarithm is nonanalytic and cannot be compensated by ultraviolet contributions. This strategy could be used to obtain a prediction from the renormalization of the $\dot{\zeta}^2$ kinetic term. The running predicted in this way would have to compete with running from other unknown sources, but a variant of the usual argument about cancellation of ultraviolet effects would apply. Either the running from unknown ultraviolet effects is small, in which case the contribution from the loop is dominant, or else it is large, in which case we expect running at least as large as the low-energy prediction. Either way, absent an unexpected tuning, the low-energy value gives a *lower bound* on the expected behaviour.

Second, if the leading contribution enters at higher order in p/k (perhaps because we are working in a model for which the contributions at $(p/k)^0$ are not physical and must be subtracted) then the loop renormalizes a higher-derivative operator such as $M_{\text{p}}^2 \delta_{\text{ct}} \ddot{\zeta}^2$, where the Wilson coefficient δ_{ct} would be suppressed by the heavy scale $(k/a)^2$ as explained in §5. In this case there is a rationale to regard the loop contribution obtained by integrating over the peak as the largest part of δ_{ct} . Contributions from quanta lying deeper in the ultraviolet would presumably be suppressed by an even larger scale.

These considerations have not yet been applied to loop computations based on the separate universe framework. In this paper we present our results in a form that can easily be compared with previous expressions reported in the literature. However, before it is possible to evaluate the significance of one-loop corrections in this model (and others), there is clearly a critical need to develop measures of the loop effect that are insensitive to ultraviolet effects. We hope to return to this in future work.

Acknowledgments

The authors are grateful to Chris Byrnes for very helpful comments and questions. LI would like to thank Matteo Braglia, Andrew Gow, Joseph Jackson, Alfredo Urbano and David Wands for many interesting discussions. LI was supported by a Royal Society funded postdoctoral position for much of this work and acknowledges current financial support from the STFC under grant ST/X000931/1. DJM is supported by a Royal Society University Research Fellowship. DS was supported by STFC grants ST/X001040/1 and ST/X000796/1.

A Numerical results for a 3-phase ultra-slow-roll model

In this Appendix we give explicit numerical results for a 3-phase ultra-slow-roll model of the type discussed in §3. This is one example of a model with a smooth USR to SR transition,

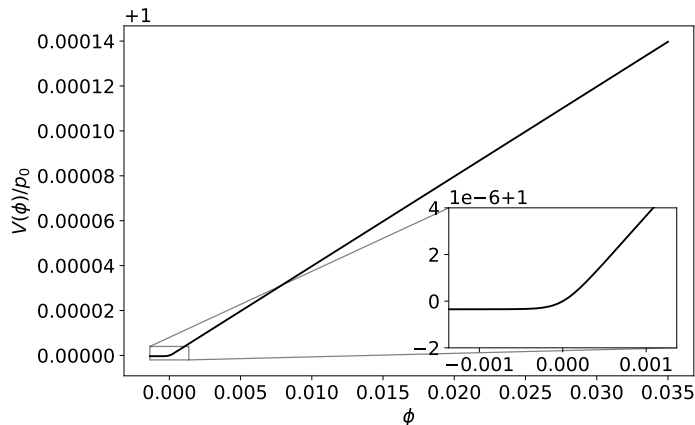


Figure 7: Shape of the (normalized) toy-model potential in Eq. (A.1). The x-axis range corresponds to the values that the inflaton, ϕ , acquires in the 20 e-folds following the horizon crossing of the CMB scale. The inset panel shows the potential shape at the transition between the two constant slope regions.

which allows us to compare the analytical results of §3 with numerical counterparts calculated from an explicit inflationary potential. The results discussed in this Appendix are obtained by using the public code `PyTransport` [116–118].

We employ a single-field inflationary model, with potential

$$\frac{V(\phi)}{p_0} = p_1 + p_2 \left[\ln(\cosh p_3 \phi) + (p_3 + p_4) \phi \right]. \quad (\text{A.1})$$

The parameters are

$$p_0 = 4 \times 10^{-12}, \quad (\text{A.2a})$$

$$p_1 = 1, \quad (\text{A.2b})$$

$$p_2 = 5 \times 10^{-7}, \quad (\text{A.2c})$$

$$p_3 = 4 \times 10^3, \quad (\text{A.2d})$$

$$p_4 = 2. \quad (\text{A.2e})$$

The potential in Eq. (A.1) features two regions with constant slope, separated by a smooth transition region, see Fig. 7. In this sense, it can be regarded as a smoothed version of the Starobinsky potential [119]. We note that this should not be considered as a realistic model of inflation, see e.g. the evolution of ϵ in the left panel of Fig. 8, rather as a toy-model providing a simple realisation for the 3-phase ultra-slow-roll dynamics.

Our fiducial background evolution is obtained by setting the initial condition $\phi_{\text{in}} = 0.075$ and SR initial velocity. We stop the background evolution at e-folding time $N_{\text{end}} = 30$, and identify the large-scale mode p as the one crossing the horizon 20 e-folds before the end of inflation, $\Delta N_p \equiv N_{\text{end}} - N_p = 20$. In realistic models p cannot be the CMB mode, 0.05 Mpc^{-1} , as we would expect $\Delta N_p \in [50, 60]$ in this case [7, 120], as well as a larger separation of scales between the CMB and peak scales. Nevertheless, for the purpose of the current numerical

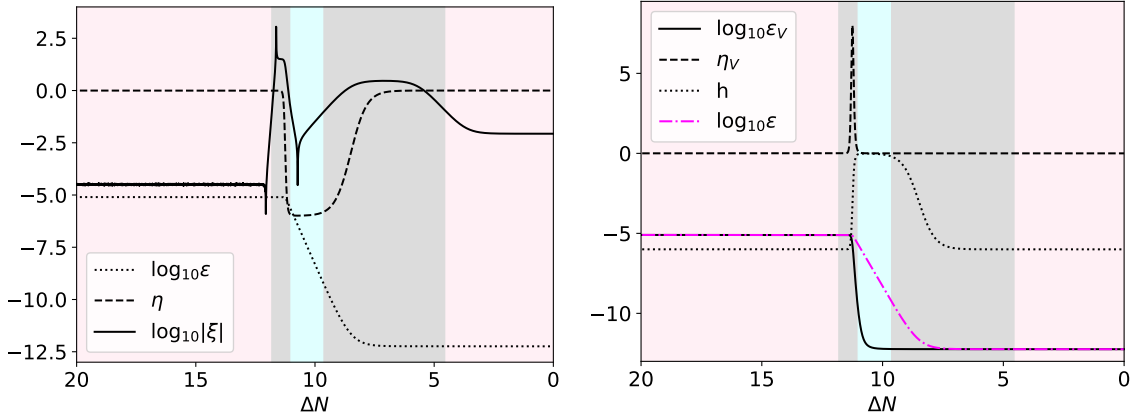


Figure 8: Slow-roll parameters evolution. **Left panel:** Evolution for the first three Hubble slow-roll parameters against $\Delta N \equiv N_{\text{end}} - N$. **Right panel:** Evolution of the first two potential slow-roll parameters, ϵ_V and η_V , against ΔN . We also include the time evolution of the h parameter, see Eq. (3.15), and $\log_{10} \epsilon$. In both panels, times corresponding to SR, USR evolution and transitions between the two are highlighted in pink, blue and gray respectively. We define the transitions times as the times when $|\xi|$ crosses 0.1 (see the left panel).

calculations, this choice of large-scale mode is acceptable, as (i) $p/\bar{k} \simeq 10^{-5} \ll 1$, coherent with our working assumption of a large separation of scales between the large-scale mode p and the peak scales; (ii) ζ_p is approximately constant on super-horizon scales. With this in mind, we will refer to p as the CMB scale.

We represent in the left panel of Fig. 8 the evolution of the first three Hubble slow-roll parameters, see Eq. (3.1), against $\Delta N \equiv N_{\text{end}} - N$. The time-evolution of ϵ , η and ξ shows the sequence of SR \rightarrow USR \rightarrow SR phases. We choose to define the times at which the SR \rightarrow USR and USR \rightarrow SR transitions occur as the times when $|\xi|$ becomes larger than 0.1³². This choice in turn identifies the start and end of the USR phase, therefore fixing the values of N_s and N_e respectively. In the first SR phase, ϵ , η and ξ are small and the inflaton slowly rolls down its potential. During this first SR phase, the CMB scale crossed the horizon, $\Delta N_p = 20$. During the subsequent USR phase, ϵ decreases as a^{-6} and $\eta \simeq -6$. During the USR \rightarrow SR transition, η decreases in magnitude and ϵ becomes constant again. The time-evolution of ϵ shows that the potential (A.1) doesn't yield to the end of inflation (happening when $\epsilon = 1$), which explains why we artificially stop the background numerical evolution, after the system has evolved back to SR.

In the right panel of Fig. 8 we display the potential slow-roll parameters ϵ_V and η_V , see

³²This choice is arbitrary (within reason), e.g. one could instead define the transition times as the times when $|\xi|$ becomes larger than 0.05. The choice of transition times will in turn influence the value of h , see Eq. (3.15). For a smooth transition, as it is for the potential (A.1) (see the evolution of η in the left panel of Fig. 8), $h \rightarrow 0$. For the time-evolution of $h(N)$, see the right panel of Fig. 8. In order to employ the analytic results derived in Ref. [54] to describe the dynamics of our toy model, we need therefore to select a transition time such that $h \rightarrow 0$. This is the case for the criterion $|\xi| \geq 0.1$, which yields $h \simeq -0.2$. The choice $|\xi| \geq 1$ instead leads to $h \simeq -2$, which is clearly not appropriate if we want to apply the analytic results of Ref. [54].

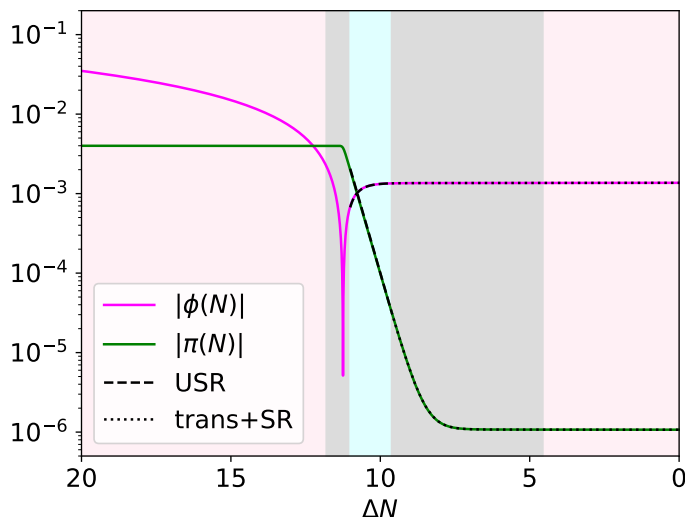


Figure 9: Numerical evolution of $|\phi(N)|$ and $|\pi(N)|$ against ΔN . The black dashed and dotted lines represent the analytic solutions derived in §3.2 for the USR and USR→SR transition and following SR phase respectively. Times corresponding to SR, USR evolution and transitions between the two are highlighted in pink, blue and gray respectively.

Eq. (3.2), against ΔN . The parameter η_V displays a spike during the SR→USR transition, a feature common to potentials supporting a USR phase. We note that ϵ and ϵ_V are very close to one another during slow roll [121], while $\epsilon \gg \epsilon_V$ during USR. In the same panel, we also represent the time-evolution of $h(N) \equiv 6\sqrt{2\epsilon_V}/\pi$, whose value at the end of the USR phase, h , see Eq. (3.15), defines the character of the USR→SR transition. For our choice of N_e , we have $h \simeq -0.2$, consistent with a smooth transition [54].

In Fig. 9, we compare the numerical solutions for the inflaton evolution and its velocity, $|\phi(N)|$ and $|\pi(N)|$, with the analytical expressions derived in §3.2, see Eqs. (3.13) (black, dashed lines) and Eqs. (3.16a)-(3.16b) (black, dotted lines). Fig. 9 shows an excellent agreement between numerical results and analytical expressions.

The numerical, tree-level scalar power spectrum, $\mathcal{P}_\zeta(k)_{\text{tree}}$, is shown in Fig. 10—note that here we use k to indicate a generic comoving wavenumber, while in the main text it usually refers to the peak scales. The behavior of $\mathcal{P}_\zeta(k)_{\text{tree}}$ can be understood in terms of the super-horizon ($k \ll aH$) evolution of the curvature perturbation,

$$\zeta(N)_{k \ll aH} = c_1 + c_2 \int dN \exp\left(-\int dN' [3 - \epsilon(N') + \eta(N')]\right), \quad (\text{A.3})$$

where the first solution is often referred to as the *growing* mode and the second one as the *decaying* mode. During SR inflation ($\epsilon, \eta \ll 1$), the second solution quickly decays and therefore the curvature perturbation is constant on super-horizon scales. On the other hand, during USR, in which case $\epsilon \ll 1$ and $\eta = -6 < -3$, the decaying mode grows exponentially, and ζ is no longer constant on super-horizon scales. For a large-scale mode that crossed the horizon long before the onset of the USR phase, the decaying mode is so small at that time that its exponential growth during USR is not appreciable. This is the case, e.g., for the

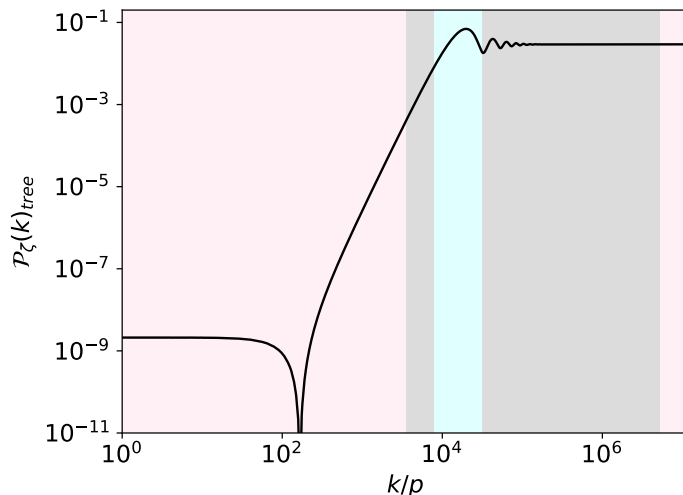


Figure 10: Tree-level, dimensionless scalar power spectrum, $\mathcal{P}_\zeta(k)_{\text{tree}}$, calculated for the potential (A.1). The CMB mode, with comoving wavenumber p , is defined by $\Delta N_p = 20$. We shade regions of $\mathcal{P}_\zeta(k)_{\text{tree}}$ for comoving wavenumbers that crossed the horizon during the SR, USR phases, and transition between these, in pink, blue and gray respectively. The transition times are defined as in Fig. 8. The amplitude at the peak is $\mathcal{P}_\zeta(\bar{k})_{\text{tree}} \simeq 0.07$.

CMB mode p . While modes corresponding to the portion of $\mathcal{P}_\zeta(k)_{\text{tree}}$ growing as k^4 also crossed the horizon during SR, they did so close to the onset of the USR phase, such that the exponential growth of the decaying mode is appreciable at these scales.

Modes crossing during the USR phase correspond to the peak in the scalar power spectrum, which is characterized by oscillations. These are due to the localized spike in $V_{\phi\phi}$ just before the onset of USR, see the plot of η_V in the right panel of Fig. 8. For an analytic treatment of these oscillations in a related model see, e.g., [122]. The δN calculation in §3.2, see Eq. (3.21), yields $\mathcal{P}_\zeta(\bar{k})_{\text{tree}} \approx 0.027$, which is of the same order of magnitude as the numerical value $\mathcal{P}_\zeta(\bar{k})_{\text{tree}} \approx 0.07$. The discrepancy between the δN and numerical results is due to the use of Eq. (2.17) in the δN calculation, i.e. the oscillations in the power spectrum are not taken into account. For more details, see Fig. 11 and the discussion below.

We note that on very small scales the peak in $\mathcal{P}_\zeta(\bar{k})_{\text{tree}}$ does not decrease in amplitude, as expected within realistic models, but rather settles into a plateau.

In Fig. 11 we represent the e-folding evolution around horizon-crossing of $\mathcal{P}^{\phi\phi}$ for the CMB mode p (left panel) and for six peak-scale modes (right panel). We compare these with the horizon-crossing value predicted for massless, non-interacting fields on de Sitter, see Eq. (2.17), which we use in the analytical calculations of §3 and §4. The results in the left panel show that working with Eq. (2.17) is justified when considering the CMB mode p , as $\mathcal{P}^{\phi\phi}(p)$ evolves towards $H(t_p)^2/(2\pi)^2$ soon after horizon crossing. On the other hand, $\mathcal{P}^{\phi\phi}$ for peak scales oscillates around $H(t_{\bar{k}})^2/(2\pi)^2$, resulting into the $\mathcal{P}_\zeta(\bar{k})_{\text{tree}}$ oscillations seen in Fig. 10. Since the numerical values of $\mathcal{P}^{\phi\phi}$ soon after horizon crossing are approximately of the same order of magnitude as $H(t_{\bar{k}})^2/(2\pi)^2$, we employ Eq. (2.17) in §4. Nevertheless, the results in the right panel of Fig. 11 flag up the limitations of analytical approximations

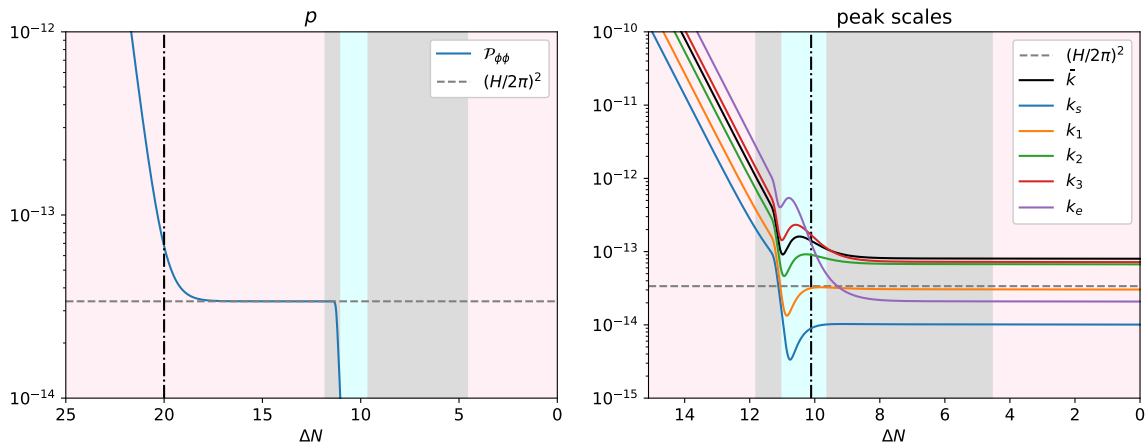


Figure 11: Field fluctuations around horizon-crossing. **Left panel:** Evolution of $\mathcal{P}^{\phi\phi}$ for the CMB mode p against $\Delta N \equiv N_{\text{end}} - N$. The horizon-crossing time of the CMB mode is highlighted with a vertical, dot-dashed, black line. The value of $H^2/(2\pi)^2$ at horizon crossing is represented with a dashed, gray line. **Right panel:** Evolution of $\mathcal{P}^{\phi\phi}$ for the peak scale, \bar{k} , and 5 more peak scales, $k_s \leq k \leq k_e$, against $\Delta N \equiv N_{\text{end}} - N$. Each scale considered crossed the horizon at a different time between N_s and N_e . In particular, we highlight the horizon-crossing time of \bar{k} with a dot-dashed, black line. The dashed, gray line represents the value of $H^2/(2\pi)^2$ when \bar{k} crossed the horizon. We expect this value to be the same for $k_s \leq k \leq k_e$ since $H \simeq \text{const}$ during USR. In both panels we highlight times corresponding to SR, USR evolution and transitions between the two in pink, blue and gray respectively.

(for a related discussion, see Ref. [55]). In particular, the use of Eq. (2.17) implies that the effect of the oscillations at peak scales is not included in the analytical calculation of §4.

In Fig. 12 we display the evolution of the field, velocity correlators and field-velocity cross-correlators for the CMB mode p and the peak scale mode \bar{k} .

First, let us comment on the evolution of the correlators around the time of horizon crossing. Both for the CMB and peak scale modes, the $\mathcal{P}^{\pi\pi}$, $\mathcal{P}^{\phi\pi}$ and $\mathcal{P}^{\pi\phi}$ correlators decay soon after horizon crossing, leaving $\mathcal{P}^{\phi\phi}$ as the only sizeable correlator at this time. This shows with a numerical example what discussed in §3. We also note that the $\mathcal{P}^{\pi\pi}$, $\mathcal{P}^{\phi\pi}$ and $\mathcal{P}^{\pi\phi}$ correlators for the large-scale mode p (see the top, left panel of Fig. 12), reach a constant value at about $\Delta N = 14$. This is due to the fact that, at that time, the decaying mode ($\mathcal{P}^{\pi\pi} \propto (k/aH)^4$ and $\mathcal{P}^{\phi\pi}, \mathcal{P}^{\pi\phi} \propto (k/aH)^2$) becomes smaller than the growing mode. The latter can be obtained from Eq. (3.6), yielding $\delta\pi_p(t) = -\eta \delta\phi_p(t)/2$, valid on super-horizon scales during SR.

On the other hand, when the δN calculation of $\mathcal{P}_\zeta(p)_{\text{tree}}$ is initialized during the USR phase, see §3.3, all correlators must be taken into account. This is due to the fact that during USR the correlators $\mathcal{P}^{\phi\phi}$, $\mathcal{P}^{\pi\pi}$, $\mathcal{P}^{\phi\pi}$ and $\mathcal{P}^{\pi\phi}$ are all of comparable magnitude, i.e. one *cannot* neglect the velocity perturbations. In particular, the numerical results displayed in the top-right panel show an excellent agreement with the analytical expressions (4.10).

As discussed below Eq. (A.3), the large separation between the horizon-crossing of the

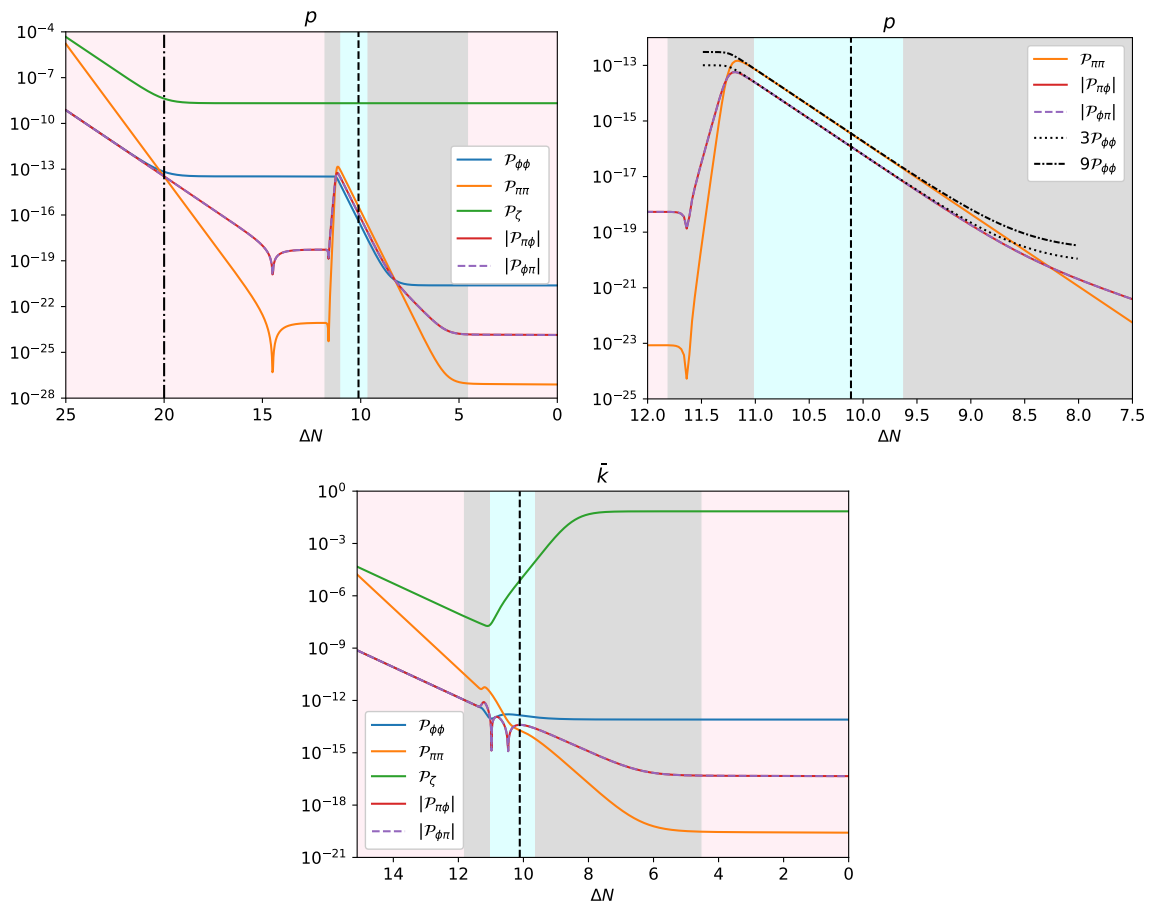


Figure 12: E-folding evolution of the field, velocity and curvature perturbation dimensionless correlators and field-velocity cross-correlators for the CMB mode p (top line) and peak scale \bar{k} (bottom line). The top right panel allows us to zoom into the USR and transition regions. Here, we represent the CMB dimensionless correlators $\mathcal{P}^{\pi\pi}(p)$, $\mathcal{P}^{\phi\pi}(p)$ and $\mathcal{P}^{\pi\phi}(p)$, and compare their numerical solutions with the analytical approximations in Eq. (4.10). In each panel we highlight times corresponding to SR, USR evolution and transitions between the two in pink, blue and gray respectively. We signal the horizon crossing time of the CMB (peak) scale with a vertical, dot-dashed (dashed), black line.

p mode and the onset of USR makes the super-horizon evolution of $\zeta_p(N)$ not appreciable, as shown by the numerical solution to $\mathcal{P}_\zeta(p; N)_{\text{tree}}$ in the top-left panel. On the other hand, $\mathcal{P}_\zeta(\bar{k}; N)_{\text{tree}}$ grows from the onset of the USR phase, settling to a constant value when the system has evolved back to SR, see the bottom panel.

Before closing, let us comment on non-Gaussianity. The numerical results for the e-folding evolution of the non-linearity parameter f_{NL} , see Eq. (2.4b), are displayed in Fig. 13. In particular, we consider f_{NL} in the equilateral configuration $k_1 = k_2 = k_3 = \bar{k}$. As expected for a model featuring a smooth transition from USR to SR, while f_{NL} is sizeable soon after horizon crossing, it then decreases during the transition, acquiring a slow-roll suppressed value in the subsequent SR phase [54].

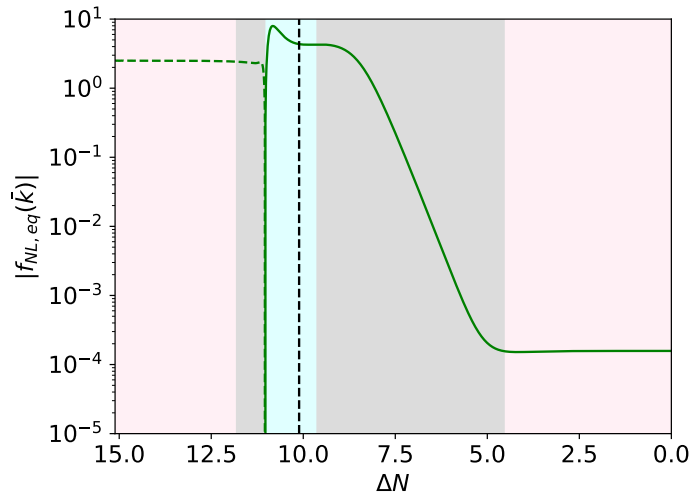


Figure 13: Evolution of $|f_{\text{NL}}|$ equilateral for the peak scale ($k_1 = k_2 = k_3 = \bar{k}$) against $\Delta N \equiv N_{\text{end}} - N$. Positive (negative) $|f_{\text{NL}}|$ is represented with a continuous (dashed) line. The black, dashed vertical line marks the horizon crossing time of \bar{k} . We highlight times corresponding to SR, USR evolution and transitions between the two in pink, blue and gray respectively.

References

- [1] B. Carr and F. Kuhnel, *Primordial Black Holes as Dark Matter: Recent Developments*, *Ann. Rev. Nucl. Part. Sci.* **70** (2020) 355 [[2006.02838](#)].
- [2] A. M. Green and B. J. Kavanagh, *Primordial Black Holes as a dark matter candidate*, *J. Phys. G* **48** (2021) 043001 [[2007.10722](#)].
- [3] P. Villanueva-Domingo, O. Mena and S. Palomares-Ruiz, *A brief review on primordial black holes as dark matter*, *Front. Astron. Space Sci.* **8** (2021) 87 [[2103.12087](#)].
- [4] S. Bird, I. Cholis, J. B. Muñoz, Y. Ali-Haïmoud, M. Kamionkowski, E. D. Kovetz et al., *Did LIGO detect dark matter?*, *Phys. Rev. Lett.* **116** (2016) 201301 [[1603.00464](#)].
- [5] A. Hall, A. D. Gow and C. T. Byrnes, *Bayesian analysis of LIGO-Virgo mergers: Primordial vs. astrophysical black hole populations*, *Phys. Rev. D* **102** (2020) 123524 [[2008.13704](#)].
- [6] G. Franciolini, I. Musco, P. Pani and A. Urbano, *From inflation to black hole mergers and back again: Gravitational-wave data-driven constraints on inflationary scenarios with a first-principle model of primordial black holes across the QCD epoch*, *Phys. Rev. D* **106** (2022) 123526 [[2209.05959](#)].
- [7] PLANCK collaboration, *Planck 2018 results. X. Constraints on inflation*, *Astron. Astrophys.* **641** (2020) A10 [[1807.06211](#)].
- [8] J. Kristiano and J. Yokoyama, *Ruling Out Primordial Black Hole Formation From Single-Field Inflation*, [2211.03395](#).
- [9] J. I. Kapusta and C. Gale, *Finite-temperature field theory: Principles and applications*, Cambridge Monographs on Mathematical Physics. Cambridge University Press, 2011, [10.1017/CBO9780511535130](#).

- [10] J. J. M. Carrasco, M. P. Hertzberg and L. Senatore, *The Effective Field Theory of Cosmological Large Scale Structures*, *JHEP* **09** (2012) 082 [[1206.2926](#)].
- [11] J. J. M. Carrasco, R. Kallosh, A. Linde and D. Roest, *Hyperbolic geometry of cosmological attractors*, *Phys. Rev. D* **92** (2015) 041301 [[1504.05557](#)].
- [12] E. Pajer and M. Zaldarriaga, *On the Renormalization of the Effective Field Theory of Large Scale Structures*, *JCAP* **08** (2013) 037 [[1301.7182](#)].
- [13] A. A. Abolhasani, M. Mirbabayi and E. Pajer, *Systematic Renormalization of the Effective Theory of Large Scale Structure*, *JCAP* **05** (2016) 063 [[1509.07886](#)].
- [14] A. Riotto, *The Primordial Black Hole Formation from Single-Field Inflation is Not Ruled Out*, [2301.00599](#).
- [15] S. Choudhury, M. R. Gangopadhyay and M. Sami, *No-go for the formation of heavy mass Primordial Black Holes in Single Field Inflation*, [2301.10000](#).
- [16] S. Choudhury, S. Panda and M. Sami, *No-go for PBH formation in EFT of single field inflation*, [2302.05655](#).
- [17] J. Kristiano and J. Yokoyama, *Response to criticism on "Ruling Out Primordial Black Hole Formation From Single-Field Inflation": A note on bispectrum and one-loop correction in single-field inflation with primordial black hole formation*, [2303.00341](#).
- [18] A. Riotto, *The Primordial Black Hole Formation from Single-Field Inflation is Still Not Ruled Out*, [2303.01727](#).
- [19] H. Firouzjahi, *One-loop corrections in power spectrum in single field inflation*, *JCAP* **10** (2023) 006 [[2303.12025](#)].
- [20] H. Motohashi and Y. Tada, *Squeezed bispectrum and one-loop corrections in transient constant-roll inflation*, *JCAP* **08** (2023) 069 [[2303.16035](#)].
- [21] S. Choudhury, S. Panda and M. Sami, *Quantum loop effects on the power spectrum and constraints on primordial black holes*, [2303.06066](#).
- [22] S. Choudhury, S. Panda and M. Sami, *Galileon inflation evades the no-go for PBH formation in the single-field framework*, [2304.04065](#).
- [23] H. Firouzjahi and A. Riotto, *Primordial Black Holes and Loops in Single-Field Inflation*, [2304.07801](#).
- [24] H. Firouzjahi, *Loop Corrections in Gravitational Wave Spectrum in Single Field Inflation*, [2305.01527](#).
- [25] G. Franciolini, A. Iovino, Junior., M. Taoso and A. Urbano, *One loop to rule them all: Perturbativity in the presence of ultra slow-roll dynamics*, [2305.03491](#).
- [26] G. Tasinato, *A large $|\eta|$ approach to single field inflation*, [2305.11568](#).
- [27] S.-L. Cheng, D.-S. Lee and K.-W. Ng, *Power spectrum of primordial perturbations during ultra-slow-roll inflation with back reaction effects*, *Phys. Lett. B* **827** (2022) 136956 [[2106.09275](#)].
- [28] S.-L. Cheng, D.-S. Lee and K.-W. Ng, *Primordial perturbations from ultra-slow-roll single-field inflation with quantum loop effects*, [2305.16810](#).
- [29] J. Fumagalli, *Absence of one-loop effects on large scales from small scales in non-slow-roll dynamics*, [2305.19263](#).

- [30] S. Maity, H. V. Ragavendra, S. K. Sethi and L. Sriramkumar, *Loop contributions to the scalar power spectrum due to quartic order action in ultra slow roll inflation*, [2307.13636](#).
- [31] Y. Tada, T. Terada and J. Tokuda, *Cancellation of quantum corrections on the soft curvature perturbations*, [2308.04732](#).
- [32] H. Firouzjahi, *Revisiting Loop Corrections in Single Field USR Inflation*, [2311.04080](#).
- [33] M. W. Davies, L. Iacconi and D. J. Mulryne, *Numerical 1-loop correction from a potential yielding ultra-slow-roll dynamics*, [2312.05694](#).
- [34] K. Inomata, M. Braglia, X. Chen and S. Renaux-Petel, *Questions on calculation of primordial power spectrum with large spikes: the resonance model case*, *JCAP* **04** (2023) 011 [[2211.02586](#)].
- [35] L. Iacconi and D. J. Mulryne, *Multi-field inflation with large scalar fluctuations: non-Gaussianity and perturbativity*, *JCAP* **09** (2023) 033 [[2304.14260](#)].
- [36] J. Fumagalli, S. Bhattacharya, M. Peloso, S. Renaux-Petel and L. T. Witkowski, *One-loop infrared rescattering by enhanced scalar fluctuations during inflation*, [2307.08358](#).
- [37] A. A. Starobinsky, *Multicomponent de Sitter (Inflationary) Stages and the Generation of Perturbations*, *JETP Lett.* **42** (1985) 152.
- [38] M. Sasaki and E. D. Stewart, *A General analytic formula for the spectral index of the density perturbations produced during inflation*, *Prog. Theor. Phys.* **95** (1996) 71 [[astro-ph/9507001](#)].
- [39] D. H. Lyth and Y. Rodriguez, *The Inflationary prediction for primordial non-Gaussianity*, *Phys. Rev. Lett.* **95** (2005) 121302 [[astro-ph/0504045](#)].
- [40] D. Seery and J. E. Lidsey, *Primordial non-Gaussianities from multiple-field inflation*, *JCAP* **09** (2005) 011 [[astro-ph/0506056](#)].
- [41] D. J. Mulryne, *Transporting non-Gaussianity from sub to super-horizon scales*, *JCAP* **09** (2013) 010 [[1302.3842](#)].
- [42] D. Seery, D. J. Mulryne, J. Frazer and R. H. Ribeiro, *Inflationary perturbation theory is geometrical optics in phase space*, *JCAP* **09** (2012) 010 [[1203.2635](#)].
- [43] M. Dias, R. H. Ribeiro and D. Seery, *The δN formula is the dynamical renormalization group*, *JCAP* **10** (2013) 062 [[1210.7800](#)].
- [44] C. Burrage, R. H. Ribeiro and D. Seery, *Large slow-roll corrections to the bispectrum of noncanonical inflation*, *JCAP* **07** (2011) 032 [[1103.4126](#)].
- [45] Z. Kenton and D. J. Mulryne, *The squeezed limit of the bispectrum in multi-field inflation*, *JCAP* **10** (2015) 018 [[1507.08629](#)].
- [46] J. M. Maldacena, *Non-Gaussian features of primordial fluctuations in single field inflationary models*, *JHEP* **05** (2003) 013 [[astro-ph/0210603](#)].
- [47] D. H. Lyth, *The curvature perturbation in a box*, *JCAP* **12** (2007) 016 [[0707.0361](#)].
- [48] D. Seery, *Infrared effects in inflationary correlation functions*, *Class. Quant. Grav.* **27** (2010) 124005 [[1005.1649](#)].
- [49] R. Paris and D. Kaminski, *Asymptotics and Mellin-Barnes Integrals*, Encyclopedia of mathematics and its applications. Cambridge University Press, 2001.
- [50] S. Friot, D. Greynat and E. De Rafael, *Asymptotics of Feynman diagrams and the Mellin-Barnes representation*, *Phys. Lett. B* **628** (2005) 73 [[hep-ph/0505038](#)].

- [51] I. Dubovyk, J. Gluza and G. Somogyi, *Mellin-Barnes Integrals: A Primer on Particle Physics Applications*, *Lect. Notes Phys.* **1008** (2022) pp. [2211.13733].
- [52] A. A. Starobinsky, *STOCHASTIC DE SITTER (INFLATIONARY) STAGE IN THE EARLY UNIVERSE*, *Lect. Notes Phys.* **246** (1986) 107.
- [53] Y. Tada and V. Vennin, *Statistics of coarse-grained cosmological fields in stochastic inflation*, *JCAP* **02** (2022) 021 [2111.15280].
- [54] Y.-F. Cai, X. Chen, M. H. Namjoo, M. Sasaki, D.-G. Wang and Z. Wang, *Revisiting non-Gaussianity from non-attractor inflation models*, *JCAP* **05** (2018) 012 [1712.09998].
- [55] J. H. P. Jackson, H. Assadullahi, A. D. Gow, K. Koyama, V. Vennin and D. Wands, *The separate-universe approach and sudden transitions during inflation*, 2311.03281.
- [56] M. Dias, J. Elliston, J. Frazer, D. Mulryne and D. Seery, *The curvature perturbation at second order*, *JCAP* **02** (2015) 040 [1410.3491].
- [57] M. Dias, J. Frazer and D. Seery, *Computing observables in curved multifield models of inflation—A guide (with code) to the transport method*, *JCAP* **12** (2015) 030 [1502.03125].
- [58] V. Vennin and A. A. Starobinsky, *Correlation Functions in Stochastic Inflation*, *Eur. Phys. J. C* **75** (2015) 413 [1506.04732].
- [59] M. Gell-Mann and J. B. Hartle, *Classical equations for quantum systems*, *Phys. Rev. D* **47** (1993) 3345 [gr-qc/9210010].
- [60] R. P. Feynman and F. L. Vernon, Jr., *The Theory of a general quantum system interacting with a linear dissipative system*, *Annals Phys.* **24** (1963) 118.
- [61] R. Feynman, A. Hibbs and D. Styer, *Quantum Mechanics and Path Integrals*, Dover Books on Physics. Dover Publications, 2010.
- [62] A. O. Caldeira and A. J. Leggett, *Path integral approach to quantum Brownian motion*, *Physica A* **121** (1983) 587.
- [63] A. O. Caldeira and A. J. Leggett, *Quantum tunneling in a dissipative system*, *Annals Phys.* **149** (1983) 374.
- [64] E. Calzetta and B.-L. Hu, *Stochastic behavior of effective field theories across threshold*, *Phys. Rev. D* **55** (1997) 3536 [hep-th/9603164].
- [65] E. Calzetta and B. L. Hu, *Stochastic dynamics of correlations in quantum field theory: From Schwinger-Dyson to Boltzmann-Langevin equation*, *Phys. Rev. D* **61** (2000) 025012 [hep-ph/9903291].
- [66] A. Kamenev, *Field Theory of Non-Equilibrium Systems*. Cambridge University Press, 2023.
- [67] K. N. Ananda, C. Clarkson and D. Wands, *The Cosmological gravitational wave background from primordial density perturbations*, *Phys. Rev. D* **75** (2007) 123518 [gr-qc/0612013].
- [68] D. Baumann, P. J. Steinhardt, K. Takahashi and K. Ichiki, *Gravitational Wave Spectrum Induced by Primordial Scalar Perturbations*, *Phys. Rev. D* **76** (2007) 084019 [hep-th/0703290].
- [69] K. Kohri and T. Terada, *Semianalytic calculation of gravitational wave spectrum nonlinearly induced from primordial curvature perturbations*, *Phys. Rev. D* **97** (2018) 123532 [1804.08577].
- [70] G. Domènech, *Scalar induced gravitational waves review*, 2109.01398.

- [71] A. Ota, M. Sasaki and Y. Wang, *One-loop tensor power spectrum from an excited scalar field during inflation*, *Phys. Rev. D* **108** (2023) 043542 [2211.12766].
- [72] C. Chen, A. Ota, H.-Y. Zhu and Y. Zhu, *Missing one-loop contributions in secondary gravitational waves*, *Phys. Rev. D* **107** (2023) 083518 [2210.17176].
- [73] S. Melville and E. Pajer, *Cosmological Cutting Rules*, *JHEP* **05** (2021) 249 [2103.09832].
- [74] H. Goodhew, S. Jazayeri, M. H. Gordon Lee and E. Pajer, *Cutting cosmological correlators*, *JCAP* **08** (2021) 003 [2104.06587].
- [75] J. Collins, *Foundations of perturbative QCD*, vol. 32. Cambridge University Press, 11, 2013, 10.1017/9781009401845.
- [76] D. H. Lyth and D. Seery, *Classicality of the primordial perturbations*, *Phys. Lett. B* **662** (2008) 309 [astro-ph/0607647].
- [77] D. Seery, *One-loop corrections to a scalar field during inflation*, *JCAP* **11** (2007) 025 [0707.3377].
- [78] D. Seery, *One-loop corrections to the curvature perturbation from inflation*, *JCAP* **02** (2008) 006 [0707.3378].
- [79] T. Tanaka and Y. Urakawa, *Dominance of gauge artifact in the consistency relation for the primordial bispectrum*, *JCAP* **05** (2011) 014 [1103.1251].
- [80] P. Creminelli, G. D’Amico, M. Musso and J. Norena, *The (not so) squeezed limit of the primordial 3-point function*, *JCAP* **11** (2011) 038 [1106.1462].
- [81] E. Pajer, F. Schmidt and M. Zaldarriaga, *The Observed Squeezed Limit of Cosmological Three-Point Functions*, *Phys. Rev. D* **88** (2013) 083502 [1305.0824].
- [82] R. de Putter, O. Doré and D. Green, *Is There Scale-Dependent Bias in Single-Field Inflation?*, *JCAP* **10** (2015) 024 [1504.05935].
- [83] Y. Tada and V. Vennin, *Squeezed bispectrum in the δN formalism: local observer effect in field space*, *JCAP* **02** (2017) 021 [1609.08876].
- [84] W. H. Kinney, *Horizon crossing and inflation with large eta*, *Phys. Rev. D* **72** (2005) 023515 [gr-qc/0503017].
- [85] K. Dimopoulos, *Ultra slow-roll inflation demystified*, *Phys. Lett. B* **775** (2017) 262 [1707.05644].
- [86] C. Pattison, V. Vennin, H. Assadullahi and D. Wands, *The attractive behaviour of ultra-slow-roll inflation*, *JCAP* **08** (2018) 048 [1806.09553].
- [87] B. J. Carr and S. W. Hawking, *Black Holes in the Early Universe*, *Monthly Notices of the Royal Astronomical Society* **168** (1974) 399.
- [88] M. Sasaki, T. Suyama, T. Tanaka and S. Yokoyama, *Primordial black holes—perspectives in gravitational wave astronomy*, *Class. Quant. Grav.* **35** (2018) 063001 [1801.05235].
- [89] G. Bertone and T. Tait, M. P., *A new era in the search for dark matter*, *Nature* **562** (2018) 51 [1810.01668].
- [90] N. Bartolo, V. De Luca, G. Franciolini, A. Lewis, M. Peloso and A. Riotto, *Primordial Black Hole Dark Matter: LISA Serendipity*, *Phys. Rev. Lett.* **122** (2019) 211301 [1810.12218].
- [91] J. Garcia-Bellido and E. Ruiz Morales, *Primordial black holes from single field models of inflation*, *Phys. Dark Univ.* **18** (2017) 47 [1702.03901].

- [92] C. Germani and T. Prokopec, *On primordial black holes from an inflection point*, *Phys. Dark Univ.* **18** (2017) 6 [1706.04226].
- [93] G. Ballesteros and M. Taoso, *Primordial black hole dark matter from single field inflation*, *Phys. Rev. D* **97** (2018) 023501 [1709.05565].
- [94] V. Atal, J. Garriga and A. Marcos-Caballero, *Primordial black hole formation with non-Gaussian curvature perturbations*, *JCAP* **09** (2019) 073 [1905.13202].
- [95] S. S. Mishra and V. Sahni, *Primordial Black Holes from a tiny bump/dip in the Inflaton potential*, *JCAP* **04** (2020) 007 [1911.00057].
- [96] M. W. Davies, P. Carrilho and D. J. Mulryne, *Non-Gaussianity in inflationary scenarios for primordial black holes*, 2110.08189.
- [97] M. H. Namjoo, H. Firouzjahi and M. Sasaki, *Violation of non-Gaussianity consistency relation in a single field inflationary model*, *EPL* **101** (2013) 39001 [1210.3692].
- [98] Z. Kenton and D. J. Mulryne, *The Separate Universe Approach to Soft Limits*, *JCAP* **10** (2016) 035 [1605.03435].
- [99] V. Assassi, D. Baumann and D. Green, *Symmetries and Loops in Inflation*, *JHEP* **02** (2013) 151 [1210.7792].
- [100] L. Senatore and M. Zaldarriaga, *On Loops in Inflation*, *JHEP* **12** (2010) 008 [0912.2734].
- [101] G. L. Pimentel, L. Senatore and M. Zaldarriaga, *On Loops in Inflation III: Time Independence of zeta in Single Clock Inflation*, *JHEP* **07** (2012) 166 [1203.6651].
- [102] L. Senatore and M. Zaldarriaga, *The constancy of ζ in single-clock Inflation at all loops*, *JHEP* **09** (2013) 148 [1210.6048].
- [103] D. Baumann, A. Nicolis, L. Senatore and M. Zaldarriaga, *Cosmological Non-Linearities as an Effective Fluid*, *JCAP* **07** (2012) 051 [1004.2488].
- [104] L. F. de la Bella, D. Regan, D. Seery and S. Hotchkiss, *The matter power spectrum in redshift space using effective field theory*, *JCAP* **11** (2017) 039 [1704.05309].
- [105] C. P. Burgess, S. P. Patil and M. Trott, *On the Predictiveness of Single-Field Inflationary Models*, *JHEP* **06** (2014) 010 [1402.1476].
- [106] A. Durakovic, P. Hunt, S. P. Patil and S. Sarkar, *Reconstructing the EFT of Inflation from Cosmological Data*, *SciPost Phys.* **7** (2019) 049 [1904.00991].
- [107] R. L. Stratonovich, *On a Method of Calculating Quantum Distribution Functions*, *Soviet Physics Doklady* **2** (1957) 416.
- [108] J. Hubbard, *Calculation of Partition Functions*, *Phys. Rev. Lett.* **3** (1959) 77.
- [109] S. Matarrese, L. Pilo and R. Rollo, *Resilience of long modes in cosmological observables*, *JCAP* **01** (2021) 062 [2007.08877].
- [110] Y. Tanaka and M. Sasaki, *Gradient expansion approach to nonlinear superhorizon perturbations*, *Prog. Theor. Phys.* **117** (2007) 633 [gr-qc/0612191].
- [111] Y. Tanaka and M. Sasaki, *Gradient expansion approach to nonlinear superhorizon perturbations. II. A Single scalar field*, *Prog. Theor. Phys.* **118** (2007) 455 [0706.0678].
- [112] D. Seery and J. E. Lidsey, *Non-Gaussianity from the inflationary trispectrum*, *JCAP* **01** (2007) 008 [astro-ph/0611034].

- [113] C. T. Byrnes, M. Sasaki and D. Wands, *The primordial trispectrum from inflation*, *Phys. Rev. D* **74** (2006) 123519 [[astro-ph/0611075](#)].
- [114] J. F. Donoghue, *Leading quantum correction to the Newtonian potential*, *Phys. Rev. Lett.* **72** (1994) 2996 [[gr-qc/9310024](#)].
- [115] J. F. Donoghue, *General relativity as an effective field theory: The leading quantum corrections*, *Phys. Rev. D* **50** (1994) 3874 [[gr-qc/9405057](#)].
- [116] M. Dias, J. Frazer, D. J. Mulryne and D. Seery, *Numerical evaluation of the bispectrum in multiple field inflation—the transport approach with code*, *JCAP* **12** (2016) 033 [[1609.00379](#)].
- [117] J. W. Ronayne and D. J. Mulryne, *Numerically evaluating the bispectrum in curved field-space— with PyTransport 2.0*, *JCAP* **01** (2018) 023 [[1708.07130](#)].
- [118] D. J. Mulryne and J. W. Ronayne, *PyTransport: A Python package for the calculation of inflationary correlation functions*, *J. Open Source Softw.* **3** (2018) 494 [[1609.00381](#)].
- [119] A. A. Starobinsky, *Spectrum of adiabatic perturbations in the universe when there are singularities in the inflation potential*, *JETP Lett.* **55** (1992) 489.
- [120] A. R. Liddle and S. M. Leach, *How long before the end of inflation were observable perturbations produced?*, *Phys. Rev.* **D68** (2003) 103503 [[astro-ph/0305263](#)].
- [121] A. R. Liddle, P. Parsons and J. D. Barrow, *Formalizing the slow roll approximation in inflation*, *Phys. Rev. D* **50** (1994) 7222 [[astro-ph/9408015](#)].
- [122] J. Martin and L. Sriramkumar, *The scalar bi-spectrum in the Starobinsky model: The equilateral case*, *JCAP* **01** (2012) 008 [[1109.5838](#)].